МІНІСТЕРСТВО ОСВІТИ І НАУКИ УКРАЇНИ
ДВНЗ «УЖГОРОДСЬКИЙ НАЦІОНАЛЬНИЙ УНІВЕРСИТЕТ»

НАУКОВИЙ ВІСНИК
УЖГОРОДСЬКОГО УНІВЕРСИТЕТУ

СЕРІЯ
«ФІЗИКА»

Науковий журнал

Випуск 54
2023

УЖГОРОД
2023

ISSN 2415-8038

Засновником журналу Науковий вісник Ужгородського університету. Серія «Фізика»
є ДВНЗ «Ужгородський національний університет», фізичний факультет
та Закарпатське фізичне товариство

Рекомендовано до друку та поширення
через мережу Інтернет Вченою Радою
ДВНЗ «Ужгородський національний університет»
(протокол № 11 від 18 грудня 2023 р.)

Свідоцтво про державну реєстрацію
друкованого засобу масової інформації
Серія КВ № 7972 від 09 жовтня 2003 р.

Журнал входить до переліку наукових фахових видань України
Категорія: Б. Науки: фізико-математичні. Спеціальності: 104 – Фізика та астрономія,
105 – Прикладна фізика та наноматеріали
(наказ Міністерства освіти і науки України від 11 липня 2019 р. № 975)

Журнал представлено у міжнародних наукометричних базах даних,
репозитаріях та пошукових системах: Google Scholar, BASE, НБУ ім. В. І. Вернадського,
Crossref, Scopus, OpenAIRE, WorldCat

Науковий вісник Ужгородського університету. Серія «Фізика» : наук. журн. / [редкол.:
В. М. Різак (голов. ред.) та ін.]. – Ужгород : ДВНЗ «УжНУ», 2023. – Вип. 54. – 106 с.

Адреса редакції:
ДВНЗ «Ужгородський національний університет»
88000, вул. Волошина, 54, м. Ужгород
Закарпатська область, Україна
тел/факс: (03122) 3-20-24
E-mail: info@physics.uz.ua
www: https://physics.uz.ua/uk

MINISTRY OF EDUCATION AND SCIENCE OF UKRAINE
UZHHOROD NATIONAL UNIVERSITY

SCIENTIFIC HERALD
OF UZHHOROD UNIVERSITY

SERIES
“PHYSICS”

Scientific Journal

Issue 54
2023

UZHHOROD
2023

ISSN 2415-8038

The journal Scientific Herald of Uzhhorod University. Series “Physics” is founded
by Faculty of Physics, Uzhhorod National University
and Transcarpathian Physical Society

Recommended for printing and distribution
via the Internet by the Academic Council
of Uzhhorod National University
(Minutes No. 11 of December 18, 2023)

Certificate of state registration
of the print media
Series KV No. 7972 of October 09, 2003

The journal is included in the list of scientific professional publications of Ukraine
Category: B. Branch of Sciences: Physics and Mathematics. Specialties: 104 – Physics
and Astronomy, 105 – Applied Physics and Nanomaterials
(order of the Ministry of Education and Science of Ukraine of July 11, 2019 No. 975)

The journal is presented international scientometric databases, repositories
and scientific systems: Google Scholar, BASE, VNLU, Crossref, Scopus, OpenAIRE, WorldCat

Rizak V.M., et al. Scientific Herald of Uzhhorod University. Series “Physics”. Issue 54. Uzhhorod:
Uzhhorod National University; 2023. 106 p.

The address of editorial board:
Uzhhorod National University
88000, 54 Voloshyn Str., Uzhhorod
Transcarpathian region, Ukraine
Tel./fax: (03122) 3-20-24
E-mail: info@physics.uz.ua
www: https://physics.uz.ua/en

НАУКОВИЙ ВІСНИК УЖГОРОДСЬКОГО УНІВЕРСИТЕТУ.
СЕРІЯ «ФІЗИКА»
ВИПУСК 54

Редакційна колегія

SCIENTIFIC HERALD OF UZHHOROD UNIVERSITY.
SERIES "PHYSICS"
ISSUE 54

Editorial Board

НАУКОВИЙ ВІСНИК УЖГОРОДСЬКОГО УНІВЕРСИТЕТУ.
СЕРІЯ «ФІЗИКА»
ВИПУСК 54

ЗМІСТ

В. В. Заводянний

Іонні мемристивні ефекти нанометрового масштабу в оксидах металів:
розуміння процесу зміни валентності 9

Ш. А. Зейналов, Ф. Ш. Керімов, С. І. Сафарова, С. Г. Садигова, Т. П. Мусаєв

Вплив фталіміду на процес електричного старіння поліетилену високого тиску 18

А. А. Абдувайтов, Г. Іманова, Д. А. Ташмухамедова, Х. Х. Болтаєв, Б. Е. Умірзаков

Вплив імплантації іонів Mg^+ та подальшого відпалу на склад,
електронну структуру, емісійні та оптичні властивості CdF_2 27

Г. Н. Саргсян, А. М. Сільвейстр, М. В. Лисий, М. О. Моклюк, Г. П. Саргсян

Поява стоячих хвильових структур у реакційному середовищі
під час дифузійного розвитку ланцюгової реакції 36

С. Ш. Ташпулатов, Д. А. Бахріддінова, Ш. Н. Нутфулаєва, Л. Н. Нутфулаєва, М. С. Мумінова

Дослідження впливу гідротермічної обробки текстильних матеріалів
на їх фізико-механічні властивості та розробка інноваційної технології 47

В. В. Заводянний, М. М. Волошин, В. О. Зубенко, Р. В. Телюта, С. О. Квітка

Кристалічна структура пірованадата $BaMnV_2O_7$ 67

А. Сатибалдиєв, С. Бердибекова, А. Аттокуров, Ж. Ігамбердієва

Теорія струн та теорія Всього: огляд досліджень 80

Ш. А. Зейналов, Ф. Ш. Керімов, С. І. Сафарова, Б. Г. Гараджаєв, Г. С. Джафарова

Вплив фенолформальдегідної смоли на механічну міцність
і структуру поліетилену низької щільності 96

SCIENTIFIC HERALD OF UZHHOROD UNIVERSITY.
SERIES "PHYSICS"
ISSUE 54

CONTENTS

V. Zavodyannyi

Ionic memristive effects on the nanometre scale in metal oxides:
Understanding the process of valence change 9

S. Zeynalov, F. Kerimov, S. Safarova, S. Sadygova, T. Musaev

Influence of the phthalimide on the process
of electrical aging of the high-pressure polyethylene 18

A. Abduvayitov, G. Imanova, D. Tashmukhamedova, K. Boltaev, B. Umirzakov

The influence of implantation of Mg^+ ions and subsequent annealing
on the composition, electronic structures, emission and optical properties of CdF_2 27

G. Sargsyan, A. Silveistr, M. Lysyi, M. Mokliuk, H. Sargsyan

The appearance of standing wave structures in the reaction medium during
the diffusion development of the chain reaction process 36

S. Tashpulatov, D. Bakhriddinova, S. Nutfullaeva, L. Nutfullaeva, M. Muminova

Examination of the influence of hydrothermal treatment of textile materials
on their physical and mechanical properties and development of innovative technology 47

V. Zavodyannyi, M. Voloshyn, V. Zubenko, R. Teliuta, S. Kvitka

Crystal structure of barium manganese vanadate $BaMnV_2O_7$ 67

A. Satybaldyev, S. Berdibekova, A. Attokurov, Z. Igamberdieva

String theory and theory of everything: Review research 80

S. Zeynalov, F. Kerimov, S. Safarova, B. Garajaev, G. Jafarova

Effect of phenol-formaldehyde resin on mechanical durability
and structure of low-density polyethylene 96

Scientific Herald of Uzhhorod University
Series "Physics"

Journal homepage: https://physics.uz.ua/en
Issue 54, 9–17
Received: 30.08.2023. Revised: 15.11.2023. Accepted: 18.12.2023

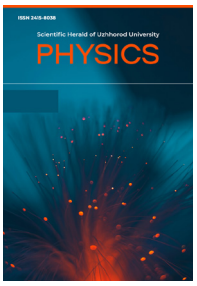

UDC 538.9.537.5:620
PACS: 81.07.-b
DOI: 10.54919/physics/54.2023.09

Ionic memristive effects on the nanometre scale in metal oxides: Understanding the process of valence change

Victor Zavodyannyi*
PhD in Physical and Mathematical Sciences, Associate Professor
Kherson State Agrarian and Economic University
25031, 5/2 Universytetskyi Ave., Kropyvnytskyi, Ukraine
https://orcid.org/0000-0002-8224-8215

Abstract

Relevance. The relevance of the study is due to the great potential of memristive effects, which are manifested in the change of material resistance under the influence of an external electric field and ionic fluxes.

Purpose. The aim is to analyse and study the mechanisms of ionic memristive effects, with a detailed consideration of the process of changing the valence of metal cations.

Methodology. The work was based on the study of nanometre-sized metal oxides TiO_2 and ZrO_2. The materials were obtained by synthesis by chemical deposition using high-purity precursors.

Results. The obtained results open up wide opportunities for the practical use of ionic membrane effects. The study of ionic memristive effects in TiO_2 and ZrO_2-based films has shown that the change in resistance occurs due to various mechanisms, including ionic migration, electrochemical reactions, and defect reorganization. Under the influence of an external electric field, a change in the resistance of both materials is observed. In TiO_2, the resistance decreases with increasing voltage, while in ZrO_2, an increase in resistance is observed. During additional experiments in the temperature range of 25-200°, it was found that temperature significantly affects the ionic membrane effects. With its increase, a noticeable increase in the intensity of these effects in both materials is observed.

Conclusions. The use of X-ray diffractometry and infrared spectroscopy revealed that changes in the valence of metal cations in both films occur under the influence of an electric field. The analysis of changes in the X-ray and infrared spectra showed the presence of modifications in the crystal and molecular structure in response to the electric field. In particular, the change in the positions and intensity of the peaks indicates a restructuring of the bonds in the crystal lattice. The paper proposes new studies to expand the understanding of these effects and to consider possible ways to improve membrane devices. The study of ionic memristive effects in TiO_2 and ZrO_2 is of great practical importance for the development of electronics and the creation of new generations of memristors and neuromorphic systems.

Keywords: radiation safety; ionising radiation; collective dose; exposure dose rate; gamma photons; drills; neutron energy

Suggested Citation:
Zavodyannyi V. Ionic memristive effects on the nanometre scale in metal oxides: understanding the process of valence change. *Sci Herald Uzhhorod Univ Ser Phys.* 2023;(54):9–17. DOI: 10.54919/physics/54.2023.09

*Corresponding author

Introduction

With the rapid development of nanotechnology and nanomaterials, the study of the electrical properties of materials on the n of the mechanism of valence change in these materials. An important aspect is the understanding of the process of changing the valence of metal cations, which can form the basis for the development of new memristors and electronic devices with the ability to learn and adapt.

The nanometre-scale ionic memristive effects in metal oxides are related to the resistive switching behaviour of materials based on these oxides used in memristors. The valence change mechanism is a bipolar resistive switching mechanism that plays a key role in such devices. In this mechanism, the movement of oxygen ions within the oxide semiconductor can change the resistance of the memristor with a change in valence. In the work of D.Y. Shovkoplyas & S.B. Tugay [1] describe in detail the mechanism of the membrane functioning, which is explained as the electromigration of oxygen ions under the influence of alternating electric fields. This mechanism is the main reason for the occurrence of an ambiguous current-voltage dependence in the contacts of a metal electrode with complex transition metal oxides. The most effective materials are films based on platinum and tantalum oxide.

According to the research of V.V. Shamaev *et al.* [2], the concentration of oxygen vacancies in such materials becomes very heterogeneous as they approach the surface. For example, yttrium-barium cuprate forms a thin, undersupplied layer in this region that has the properties of an antiferromagnetic dielectric. Since the change in metal valence is directly related to the change in resistance, it is interesting to note that the electrical resistance of the film decreases with the formation of oxygen vacancies. Thus, in the work of D.V. Zalevskii [3] studied ZnO films. As a result, the energy distance between the last filled and the first unoccupied levels decreases by two orders of magnitude. At this time, an internal electric field is formed in the direction of vacancy stacking. The potential distribution becomes linear with a pronounced difference along the direction of the vacancy filament, i.e. an internal bias voltage is formed. This conductive effect increases with the increase in the density of oxygen vacancies up to a certain concentration.

The method of producing films from metal oxides also plays a significant role in research, and I.M. Khodakovskii [4] introduced a technique for generating nanostructures through localized probe oxidation of conductive materials, such as semiconductor substrates and extremely thin metal films, which is equally essential in this context. During the experiment, the valence of the surface changes, and it is able to undergo oxidation when a positive voltage shift is applied to it relative to the probe. Y.O. Kravchenko [5] also found an uneven distribution of elements in the cross-section of the coatings, which is due to radiation-stimulated processes and oxidation of the surface layer. Understanding the process of valence change in nanometre-scale ionic memristor effects in metal oxides is important for the development of high-performance applications in computing, digital and analogue circuits, including neuromorphic networks. For example, a titanium oxide-based memristor uses the drift of oxygen vacancies for switching, as pointed out by A.V. Lemeshko *et al.* [6] in their article. One of the important tasks in the development of neuromorphic systems is the effective implementation of these components.

Therefore, the main goal is to study and analyse ionic memristive effects, with a special emphasis on the process of changing the valence of metal cations. The study of ionic memristive effects in metal oxides allows better understanding the process of valence change and its impact on the electrical properties of memristive devices. A deep understanding of this process is important for the development of new materials, device architectures and systems that are characterized by high efficiency and long service life. The research and development of ionic memristive effects represent a significant challenge in science and technology that can significantly impact the future of modern electronics and nanotechnology. Understanding these phenomena opens up new opportunities for creating highly efficient and intelligent electronic systems that can adapt to the needs of modern society.

Materials and Methods

A comprehensive analysis of modern scientific works and literature sources on ionic membrane effects and their manifestation in nanometre metal oxides was carried out. In order to clarify the current state of research in this area, the basic information was identified and the key areas that have already been studied in previous studies were established. An experimental approach was used. In the course of the experiment conducted in 2023, nanometre-sized metal oxides, in particular titanium (TiO_2) and zirconium (ZrO_2), were used as objects for studying ionic membrane effects. The samples of materials were synthesized by the chemical deposition method using high-purity precursors. For the synthesis of TiO_2 and ZrO_2 films, the precursors $Ti(OC_3H_7)_4$ and $Zr(OC_4H_9)_4$ were used, respectively. Acetylacetone was added as a complexing agent to stabilize the zirconium butoxide solution in a 1:1 ratio. The addition of the stabilizer helped to avoid aggregation of the nanoparticles and ensured a homogeneous particle size distribution. Acetylacetone was also added to the $Ti(OC_3H_7)_4$ solution in a 1:1 ratio. Under vigorous stirring, a 1 n solution of HNO3 in isopropanol was added to the already stabilized solutions dropwise to hydrolyse the substances before

the formation of films. The prepared clear solutions were separately applied to the previously cleaned glass substrates to obtain TiO_2 and ZrO_2 films. The films were left for one hour at room temperature to complete hydrolysis and then subjected to successive heat treatments at 100, 300, and 600°C. This method made it possible to obtain nanometre films with high purity and determine their structural and electrical properties. After the synthesis, the samples were washed from excess reagents and dried in a controlled humidity atmosphere. The synthesized materials were obtained in the form of thin films with a thickness of approximately 100 nm. Additionally, the films were subjected to vacuum treatment for final drying and achieving the desired properties and structure.

The structure and physical properties of the materials were characterized by X-ray diffraction (XRD) using a Bruker D8 Advance diffractometer (Germany). To determine the surface morphology and structure of the samples, a scanning electron microscope (SEM) Hitachi S-4800 (Japan) was used. For electrical measurements, an Autolab PGSTAT302N Potentiostat (Metrohm Autolab, the Netherlands) with the ability to change the applied voltage and record the current was used. To study the influence of temperature on ionic membrane effects, a series of experiments were conducted in which the changes in current and voltage were monitored at temperature changes from 25 to 200°C. The measurements were carried out in an atmosphere of controlled humidity and temperature. In parallel with the experiments, computer modelling was carried out using COMSOL Multiphysics. The specialized software was used to perform numerical simulations of ion fluxes and their effect on the valence of cations in metal oxides. To further understand the behaviour of ions in the structure of materials, the data obtained from the experiments was subjected to statistical and mathematical analysis. The combination of methods helped in the qualitative study of ionic membrane effects in nanometre-sized metal oxides.

Results

The memristive effect is a phenomenon where the resistance of a material changes from its pre-fixed values when subjected to an external voltage or current shift [7]. One of the most important aspects is the interaction between cations and anions in the crystal structure of the metal oxide. When an external voltage is applied to a material, it can affect the arrangement of the Jordan bonds and the placement of cations. The mechanisms behind membrane effects can vary, but the main ones include ionic migration, electrochemical reactions, oxide decomposition, and defect reorganization. One of them is a change in the configuration of defects in the crystal structure of the material. When the voltage in the material is shifted, ions (metal cations) can move in the crystal structure. This leads to a change in the configuration of defects and the valence of metal ions, i.e., it is accompanied by the movement of ions in the crystal lattice of the material [8]. As a result of these processes, the electrical conductivity of the material changes, which is manifested as a membrane effect.

TiO_2 and ZrO_2 films with a thickness of approximately 100 nm were subjected to detailed characterization. Experiments have shown that under the influence of an external electric field, the resistance of both materials changes. For TiO_2, a decrease in resistance is observed with increasing voltage, while for ZrO_2, an increase in resistance is observed (Table 1).

Table 1. Measured resistance and voltage values for TiO_2 and ZrO_2 films

	TiO_2			ZrO_2		
Resistance	500 Ω	200 Ω	100 Ω	500 Ω	1000 Ω	2000 Ω
Voltage	2.0 V	2.2 V	2.5 V	2.5 V	3.2 V	3.8 V
	2.5 V	2.7 V	3.0 V	3.0 V	3.7 V	4.3 V
	3.0 V	3.2 V	3.5 V	3.5 V	4.2 V	4.8 V

Source: compiled by the author

From the data for TiO_2, it was found that with an increase in voltage, there is a noticeable decrease in resistance, which indicates a change in the structure and conductivity of the material under the influence of an electric field. Conversely, in the case of ZrO_2, there was observed a rise in resistance when subjected to an electric field. This characteristic suggests a distinct response to an external stimulus, which could be attributed to specific aspects of its electronic structure or its interaction with ions within the studied context. Under the influence of an external electric field, materials exhibit ionic membrane effects, which are accompanied by changes in the valence of metal cations. This means that under the influence of an electric field, ions move in the material, changing their valence, which affects the electrical properties of the material and causes the memristive effect.

Additional experiments in the temperature range of 25-200°C showed that temperature significantly affects the ionic membrane effect, as shown in Figure 1. In particular, an increase in temperature led to a noticeable increase in the intensity of the ionic memristive effects in both films. This can be explained by the fact that a higher temperature promotes more active

ion movement processes in the material, which facilitates ionic migration and leads to more pronounced effects of metal cation valence changes [9]. It is worth noting that high temperatures promote greater migration of defects in the crystal structure of the material, which can affect the efficiency of membrane switching.

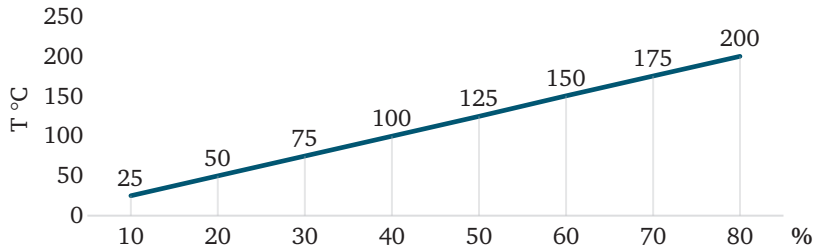

Figure 1. Graph of dependence of the intensity of ionic memristive effects on temperature
Source: compiled by the author

The change in the valence of metal ions is an important mechanism behind the memristive time-dependent characteristic of materials. In this case, the change in valence occurs due to the transfer of metal ions (cations) through the thin oxide film. When exposed to an electric field or current, metal ions can move in the crystal structure of the material [10]. This effect is based on the interaction between the metal oxide and the electrodes, which changes as a result of the applied electric field or current. When the electric field or current is reversed, metal ions are transferred from one metal electrode to another through the oxide film. This leads to a change in metal valence, as metal ions can have different degrees of oxidation. For example, the valence of one metal can change from zero (as a metal) to positive (as an oxide) or negative (as a reduced form). The process of changing the metal's valence is accompanied by a change in the electrical conductivity of the membrane. When metal ions are transferred through the oxide film, they change the location and structure of the film, which affects the electronic structure and conductivity of the system.

Each metal has different degrees of oxidation that affect its chemical properties. In materials that contain titanium (Ti) or zirconium (Zr), these metals can exist in different oxidation states or valencies. For example, in the case of titanium (TiO_2), titanium can have several oxidation states, including Ti(II), Ti(III), Ti(IV), etc. This means that each atom of titanium or zirconium can interact with the oxide matrix by ionic migration, changing its number of charges. When an electric field or current is applied, the titanium or zirconium ions can move in the crystal structure of the material. As a result, a single atom can lose or gain electrons, which changes its number of charges and, accordingly, its degree of oxidation. When an electric field or current is applied, the ions can switch between these different states, which affects the electronic structure and conductivity of the material. In metal oxides, metal ions can have different valences, such as Ti^{3+}/Ti^{4+} or Cr^{3+}/Cr^{6+}. These changes in valence can occur due to the interaction of ions with defects, as well as changes in the environment of the oxide ions. For example, vacancies in the oxide ion network can change the valence of a metal ion or create an ionic residue. Such changes in valence promote ion migration, which provides conductivity in metal oxides. In the absence of an electrical stimulus, there is an equilibrium between the different valence states, but when an external stimulus such as a voltage is applied, a difference in ion valences can occur, resulting in a change in the conductivity of the material.

The change in the resistance of materials under the influence of an electric field occurs due to ionic membrane effects, which affect the interaction of charged particles in the material. In the case of titanium oxide TiO_2, with an increase in voltage, there is an active reorganization of the probabilities of ion passage in the crystal structure, which leads to a decrease in resistance. For zirconium oxide ZrO_2, changes in the electronic structure and interactions of ions under the influence of the field are likely to cause an increase in resistance. These phenomena are associated with the movement of ions in the crystal matrix and their influence on the configuration and conductivity of the material. Metal oxides, such as titanium, chromium, zirconium, and others, are popular materials for membrane devices. They are known for their high stability, low resistance, and efficient switching, making them attractive for electronics applications.

Using X-ray diffractometry and infrared spectroscopy, changes in the valence of metal cations in both materials under the influence of an electric field were revealed. X-ray diffractometry allows determining the location of atoms in the crystal lattice and defining their distances. Infrared spectroscopy provides information on the interactions of atoms and groups of atoms in the sample. The analysis also revealed changes in the location of the peaks, which indicate changes in the distances between the atoms in the crystal lattice. This indicates that under the influence of an electric field, the valence of metal cations in both materials

changes. This indicates that the processes associated with ionic migration and changes in the configuration of defects in the crystal structure are active under the influence of an external electrical stimulus.

A comparative analysis of the ionic membrane effects for TiO_2 and ZrO_2 has been carried out. It was found that the nature and intensity of the effect depends on the chemical composition and on the intra-atomic structure of the crystal lattice, as well as on the location and mobility of ions in the material. In the case of TiO_2, the regions of decreasing resistance were more active than the regions of increasing resistance. This indicates the important role of oxygen vacancies and cationic interstices in the mechanisms of the membrane effect for this material [11]. In ZrO_2, on the contrary, the dominant influence of the regions of increased resistance is observed. This may be due to the peculiarities of the movement of oxygen ions in the structure of this material. Such a detailed analysis showed that the properties of ionic membrane effects strongly depend on the characteristics of a particular material and can be controlled by influencing its chemical composition and crystal structure. In addition to the comparative analysis of the ionic memristive effects in TiO_2 and ZrO_2, a detailed study of the influence of other parameters, such as temperature and ion concentration in the electrolyte, on the nature and intensity of these effects was carried out. It was found that the ionic membrane effects in TiO_2 and ZrO_2 films manifest themselves differently depending on the experimental parameters, such as temperature and time of exposure to the electric field. Changes in the valence of metal cations occur not only under the influence of external stimuli, but also depending on the crystal structure of the material and its chemical composition. In addition, additional analyses of the structural and electronic properties of both materials under the influence of an electric field were carried out, which allowed gaining a deeper understanding of the mechanisms that determine the ionic membrane effects in these metal oxides.

The obtained results indicate that the process of changing the valence of metal cations in TiO_2 and ZrO_2 materials involves ionic migration. Under the influence of an external electric field, metal cations are transferred through the oxide film, which leads to a change in their redox state. As a result, the electronic structure of the material and its electrical conductivity change. In particular, the TiO_2 material shows a decrease in resistance with increasing voltage, indicating a change in the valence of titanium cations. In the case of ZrO_2, an increase in resistance is observed, indicating a change in the valence of zirconium cations. This process is based on the transfer of metal ions through the oxide film, which occurs under the influence of an external electric field.

These studies indicate the great potential of using ionic memristive effects in the creation of high-performance and low-energy electronic devices and artificial intelligence systems [12-14]. It has also been found that ionic memristive effects can be used to create low-power, high-speed memory elements and logic gates, which opens up new opportunities for the development of modern electronic devices. Understanding these mechanisms is key to the development of new electronic devices and systems that use ionic memristive effects. The effect of conductivity change can be used to create memristors that are unstable charge storage devices. For example, when a voltage is applied to a memristor, ions can migrate from one electrode to another and thereby change the degree of conductivity of the material. When the current is switched off, the voltage stops affecting the memristor, but the changed state of conductivity can be saved. This makes it possible to store information in memristive materials. Additional research in this area could expand the understanding and use of these effects in modern technologies.

Discussion

One of the key findings of the study is the different nature of the membrane effects in TiO_2 and ZrO_2. In particular, a decrease in resistance in TiO_2 and an increase in ZrO_2 were observed with increasing voltage. This indicates the importance of the chemical composition and crystal structure of the material for these effects, which are the basis of membrane devices. The essence of these devices is their ability to display multiple resistance values and switch between them, which is known as resistive switching. In another study conducted by C. Singh & N. Ray [15] looked at metal oxides such as HfO_x, TaO_x, and TiO_x, which have shown promise in memristive devices. During this experiment, various resistive switching mechanisms were evaluated, including filament formation and breakage, as well as barrier-type memristors. The results were very encouraging for NiO and TaO-based memristors. Given the use of metal oxides as the main components, such memristors have the potential to be the first in line for future alternatives to current technology, offering unique advantages. Comparing the results of the authors of this study with those of C. Singh & N. Ray [15], some similarities can be noted, especially in the context of titanium oxide (TiO_x). The experimental data in both studies demonstrate that TiO_x shows promise in membrane devices. At the same time, the importance of the chemical composition and crystal structure of the material for resistive switching is also indicated.

The results indicate different mechanisms underlying the membrane effects. An important aspect is ionic migration, which can cause changes in the valence of metal cations and, consequently, changes

in electrical conductivity. The mechanism of switching of resistive storage devices with a change in valence has long been recognized, and it is caused by the ionic movement of oxygen vacancies, which leads to a change in the valence of metal cations, as can be seen from the results of the study. In the work of A. Kindsmüller *et al.* [16] used hard X-ray, photoelectron emission microscopy (PEEM) to analyse local valence changes in $Pt/ZrO_x/Ta$ membrane devices. The use of hard X-rays allowed obtaining information from deep layers, providing chemical data on buried components. By extracting X-ray photoelectron spectra from different parts of the PEEM images, it was demonstrated that zirconium dioxide in the working area of the device decreases compared to the neighbouring area, which confirms the change in valence in the ZrO_x film during electroforming. The change in valence in zirconium oxide-based films in this study can also be noted. In addition, the authors observed a decrease in the degree of oxidation of tantalum (Ta) in the low resistance state. This observation challenges the existing model because the conventional understanding is that the internal oxygen redistribution between ZrO_x and the Ta electrode during switching should result in the oxidation of the Ta layer in the low-resistance state. However, it is noteworthy that Ta actively participates in the switching process within devices, involving the release and re-incorporation of oxygen into the ZrO_x/TaO_x double layer during switching. This is supported by the degradation of the high-resistance state observed during endurance measurements conducted in a vacuum. Additional experiments at different temperatures confirmed the importance of ionic migration for the membrane effects. Increasing temperature promotes more active ionic movement, which increases the intensity of these effects. However, not only temperature changes have a significant impact. For example, in the work of K. Nagashima *et al.* [17] demonstrate how the environment affects memristive switching at the nanoscale using an open-top planar device. Planar-type devices such as NiO_x and CoO_x exhibited memristive behaviour under atmospheric pressure, while planar-type TiO_{2-x} devices did not exhibit memristive switching, even in the same environment. The change in ambient pressure and the use of a SiO_2 passivation layer in the case of planar TiO_{2-x} devices led to the manifestation of memristive behaviour. Thus, the results indicate that the thermodynamic interaction with the environment crucially affects the occurrence of memristive switching due to changes in the stability of the non-stoichiometry. Since this effect becomes more important for smaller devices with a higher specific surface area, adaptation of the environmental influence by means of appropriate passivation is important for high-density devices.

Based on the results obtained, several promising areas for further research are possible. This could include expanding the range of materials used, analysing the influence of various parameters (e.g. pressure, temperature), and investigating the impact of memristive effects on specific additional applications. The results open up prospects for the use of memristive effects in various technologies, such as neural networks, mnemonics, and energy-efficient memories. S. Tappertzhofen *et al.* [18] focuses on the dynamics of filaments, nanoparticles, and clusters in a switching material. Furthermore, this highlights the progress made in employing voltage and current-based techniques like cyclic voltammetry to discern electrochemical reactions involved in resistive switching. It's emphasized that cations play a pivotal role in the switching process across various device types, a fact substantiated by the results. It is worth noting that these fundamental physical processes can potentially pave the way for a novel spectrum of energy-efficient electro-optical applications centered around ultrafast programmable memristive devices. The reference to S. Saylan *et al.* [19] offers insights into the development of HfO_2-based memristive systems featuring a p-silicon bottom electrode, which are designed to be compatible with complementary metal-oxide-semiconductor (CMOS) technology. These findings underscore the significance of selecting the appropriate top electrode to achieve distinct device characteristics. Both device structures, when evaluated, demonstrated repeatable, low-power, and shapeless bipolar resistive transitions. However, it's worth noting that $Au/HfO_2/Si$ devices exhibited lower device-to-device reproducibility. Additionally, the $Au/HfO_2/Si$ devices exhibited N-type negative differential resistance (NDR), suggesting that the activation of oxygen vacancy migration transitions through Joule heating is responsible for the SET (Set-Reset) process in the unstable unipolar mode.

In addition, the process of synthesis and development of oxide films is also an important aspect. In this work, a general material development methodology was applied. Study by I. Zrinski *et al.* [20] is based on the investigation of composite memristors based on the anodic oxidation of Hf and then deposition on Ta thin films. The structure consisted of the sequential deposition of thin layers of Ta and Hf. During the anodization process carried out in a citrate buffer electrolyte, nanoscale columnar structuring of Ta_2O_5 within HfO_2 occurred. This phenomenon was driven by the higher electrical resistance exhibited by HfO_2. With a narrower resistive path in HfO_2, the ionic current induced localized growth of tantalum oxide (Ta oxide) toward the interface with the electrolyte. This growth process follows the principles of the Rayleigh-Taylor instability. The authors also investigated the membrane properties of the resulting composite oxide depending on the Hf/Ta thickness ratio. One distinct zone with potential for membrane applications was identified. Here, both unipolar and bipolar

memristors with high stability and retention capacity were found. This is due to the formation of conductive filaments mainly along the interfaces between the oxides. In the course of research, there is a need to understand the mechanisms of resistive switching in various dielectric materials. In the studies of A. Younis & S. Li [21] highlight the available research methods. High-resolution microscopes, including transmission electron microscopy, scanning electron microscopy, and conductive atomic force microscopy, have been instrumental in gaining insights into these mechanisms. These advanced microscopy techniques have proven to be highly effective methods for studying and understanding the underlying processes [22; 23].

Summarizing the results, it is worth emphasizing that the valence change mechanism is an important factor in ionic memristive effects in metal oxides at the nanoscale, and understanding this mechanism is important for the development of high-performance computing systems and digital and analogue circuits. Studies indicate that various methods, including modelling, simulation, in-situ characterization and device simulation, have been used to study the mechanism of valence change in memristive devices.

Conclusions

In this paper, the ionic membrane effects in nanometre-sized metal oxides and their influence on the change of metal cation valence were discussed in detail. A comprehensive analysis of the literature and experimental results has provided a deeper understanding of the nature of these effects. In particular, it was found that bipolar valence change is a major trend in modern electronic materials and devices. The movement of mobile donor ions, which are mainly represented by oxygen vacancies and cationic interstitials, has been found to be a key mechanism for these effects. Experiments have confirmed that under the influence of an external electric field, the resistance of both materials changes. TiO_2 exhibits a decrease in resistance with increasing voltage, while ZrO_2 shows an increase in resistance.

The results confirm that various mechanisms are behind the membrane effects, including ionic migration, electrochemical reactions, oxide decomposition, and defect reorganization. Additional experiments at different temperatures showed that temperature significantly affects the ionic membrane effects. Increasing the temperature led to a noticeable increase in the intensity of these effects in both materials. Using X-ray diffractometry and infrared spectroscopy, it was found that the electric field causes changes in the valence of metal cations in both materials. These results confirm that various mechanisms are behind the membrane effects, including ionic migration, electrochemical reactions, oxide decomposition, and defect reorganization.

Understanding memristive phenomena opens up new opportunities for creating highly efficient and intelligent electronic systems that can adapt to the needs of modern society. Further research into these effects is essential for the development of new types of nanoelectronic devices, such as memristors, that can store information and be used in artificial intelligence, neural networks, and other applications. Development in this area could lead to the creation of even more advanced technologies in the field of electronics and computer science.

Acknowledgements

None.

Conflict of Interest

None.

References

[1] Shovkoplyas DY, Tugay SB. Method for measuring the number of memristor overwrites. In: Proceedings of the XIII Scientific and Practical Conference “Perspective directions of modern electronics”. Kyiv: National Technical University of Ukraine “Igor Sikorsky Kyiv Polytechnic Institute”; 2019. P. 182-6.

[2] Shamaev VV, Zhitlukhina ES, Zalutska NM, Ochkan KO. Heterogeneous ordering of oxygen vacancies in yttrium-barium cuprate. *Met Adv Tech*. 2021;43(6):819–30. DOI: 10.15407/mfint.43.06.0819.

[3] Zalevskii DV. Properties of materials for resistive random access memory [dissertation]. Kryvyi Rih: Kryvyi Rih State Pedagogical University; 2023. 169 p. DOI: 10.31812/123456789/7070.

[4] Khodakovskii IM. Methods and models of building memory devices using nano- and molecular technologies [dissertation]. Kyiv: National Technical University of Ukraine “Igor Sikorsky Kyiv Polytechnic Institute”; 2019. 145 p.

[5] Kravchenko YO. Structure and properties of multi-layer and multi-element nanometer-scale coatings on the basis (TiAlSiY)N/MeN (Me=Mo, Cr, Zr) [dissertation]. Sumy: Sumy State University; 2020.

[6] Lemeshko AV, Antonenko AV, Petryk AV, Myronov SO. Neuromorphy systems as a tool for implementation of artificial intelligence. *Sci Notes Vernadsky KPI Ser Tech Sci.* 2023;34(74(3)):175–83. DOI: 10.32782/2663-5941/2023.3.1/28.

[7] Chua L. Memristor – The missing circuit element. *IEEE Trans Circ Theory*. 1971;18(5):507–19. DOI: 10.1109/TCT.1971.1083337.

[8] Yang Y, Zhang X, Qin L, Zeng Q, Qiu X, Huang R. Probing nanoscale oxygen ion motion in memristive systems. *Nat Commun*. 2017;8:15173. DOI: 10.1038/ncomms15173.
[9] Lu D, Jiang Q, Kiang Y, Li J, Zhang Q, Huang Y, Hou B. Influencing factors for the migration of zinc ions in metal oxide powders. *J Mater Res Technol.* 2023;24:1638–52. DOI: 10.1016/j.jmrt.2023.03.106.
[10] Milano G, Miranda E, Fretto M, Valov I, Ricciardi C. Experimental and modeling study of metal-insulator interfaces to control the electronic transport in single nanowire memristive devices. *ACS Appl Mater Interf*. 2022;14(47):53027–37. DOI: 10.1021/acsami.2c11022.
[11] Dittmann R, Menzel S, Waser R. Nanoionic memristive phenomena in metal oxides: The valence change mechanism. *Adv Phys*. 2021;70(2):155–349. DOI: 10.1080/00018732.2022.2084006.
[12] Jeon YJ, An H, Kim Y, Jeon YP, Kim TW. Highly reliable memristive devices with synaptic behaviour via facilitating ion transport of the zeolitic imidazolate framework-8 embedded into a polyvinylpyrrolidone polymer matrix. *Appl Surf Sci*. 2021;567:150748. DOI: 10.1016/j.apsusc.2021.150748.
[13] Kwon KC, Baek JH, Hong K, Kim SY, Jang HW. Memristive devices based on two-dimensional transition metal chalcogenides for neuromorphic computing. *Nano-Micro Lett*. 2022;14:58. DOI: 10.1007/s40820-021-00784-3.
[14] Li Z, Tang W, Zhang B, Yang R, Miao X. Emerging memristive neurons for neuromorphic computing and sensing. *Sci Technol Adv Mater*. 2023;24(1):2188878. DOI: 10.1080/14686996.2023.2188878.
[15] Singh C, Ray N. Memristors and resistive switching in metal oxides. In: Optical Properties of Metal Oxide Nanostructures. Singapore: Springer; 2023. P. 431–55. DOI: 10.1007/978-981-99-5640-1_14.
[16] Kindsmüller A, Schmitz C, Wiemann C, Skaja K, Wouters DJ, Waser R, *et al*. Valence change detection in memristive oxide based heterostructure cells by hard X-ray photoelectron emission spectroscopy. *APL Mater*. 2018;6:046106. DOI: 10.1063/1.5026063.
[17] Nagashima K, Yanagida T, Oka K, Kanai M, Klamchuen A, Rahong S, *et al*. Prominent thermodynamical interaction with surroundings on nanoscale memristive switching of metal oxides. *Nano Lett*. 2012;12(11):5684–90. DOI: 10.1021/nl302880a.
[18] Tappertzhofen S, Di Martino G, Hodmann S. Nanoparticle dynamics in oxide-based memristive devices. *Phys Status Solidi A*. 2019;217(6):1900587. DOI: 10.1002/pssa.201900587.
[19] Saylan S, Aldosari HM, Humood K, Abi Jaoude M, Ravaux F, Mohammad B. Effects of top electrode material in hafnium-oxide-based memristive systems on highly-doped Si. *Sci Rep*. 2020;10:19541. DOI: 10.1038/s41598-020-76333-6.
[20] Zrinski I, Minenkov A, Mardare CC, Hassel AW, Mardare AI. Composite memristors by nanoscale modification of Hf/Ta anodic oxides. *J Phys Chem Lett*. 2021;12(37):8917–23. DOI: 10.1021/acs.jpclett.1c02346.
[21] Younis A, Li S. Microscopic investigations of switching phenomenon in memristive systems: A mini review. *RSC Adv*. 2018;50(8):28763–4. DOI: 10.1039/C8RA05340E.
[22] Bataiev YM, Bataiev MM, Kornienko OA, Lavrynenko OM, Pavlenko OYu. EPR-spectral, magnetic, and ionic features of CeO2, Yb2O3, Yb2O3-CeO2 powders and ceramics based on REO oxides. *Sci Herald Uzhhorod Univ Ser Phys*. 2021;49:9–18.
[23] Sargsyan G, Gukasyan P, Sargsyan H, Poveda R. Diffusion flames and a semi-empirical method for estimating the distribution of hydrogen molecules in propane flames. *Sci Herald Uzhhorod Univ Ser Phys*. 2023;53:42–52. DOI: 10.54919/physics/53.2023.42.

Іонні мемристивні ефекти нанометрового масштабу в оксидах металів: розуміння процесу зміни валентності

Віктор Володимирович Заводянний

Кандидат фізико-математичних наук, доцент
Херсонський державний аграрно-економічний університет
25031, просп. Університетський, 5/2, м. Кропивницький, Україна
https://orcid.org/0000-0002-8224-8215

Анотація

Актуальність. Актуальність дослідження обумовлена великим потенціалом мемристивних ефектів, які виявляються у зміні опору матеріалу під впливом зовнішнього електричного поля та іонних потоків.

Мета. Метою є проведення аналізу та вивчення механізмів іонних мемристивних ефектів з детальним розглядом процесу зміни валентності металевих катіонів.

Методологія. В основі роботи було дослідження нанометрових оксидів металів TiO_2 та ZrO_2. Матеріали були отримані шляхом синтезу за методом хімічного відкладання, використовуючи високочисті прекурсори.

Результати. Отримані результати відкривають широкі можливості для практичного використання іонних мемристивних ефектів. У ході досліджень іонних мемристивних ефектів у плівках на основі TiO_2 та ZrO_2 встановлено, що зміна опору відбувається за рахунок різних механізмів, включаючи іонну міграцію, електрохімічні реакції та реорганізацію дефектів. Під впливом зовнішнього електричного поля спостерігається зміна опору обох матеріалів. У TiO_2 відбувається зменшення опору зі збільшенням напруги, в той час як в ZrO_2 спостерігається збільшення опору. Під час додаткових експериментів в температурному діапазоні 25-200 °C, виявлено, що температура суттєво впливає на іонні мемристивні ефекти. При її підвищенні спостерігається помітне збільшення інтенсивності цих ефектів в обох матеріалах.

Висновки. Використання рентгенівської дифрактометрії та інфрачервоної спектроскопії дозволило виявити, що під впливом електричного поля відбуваються зміни у валентності металевих катіонів у обох плівках. Аналіз змін у рентгенівських та інфрачервоних спектрах, засвідчив наявність модифікації кристалічної та молекулярної структури в реакції на електричне поле. Зокрема, зміна позицій та інтенсивності піків свідчить про перебудову зв'язків у кристалічній ґратці. У статті пропонуються нові дослідження, щоб розширити розуміння цих ефектів та розглянути можливі шляхи покращення мемристивних пристроїв. Дослідження іонних мемристивних ефектів у TiO_2 та ZrO_2 має важливе практичне значення для розвитку електроніки та створення нових поколінь мемристорів і нейроморфних систем.

Ключові слова: електронні пристрої; тонкі плівки; електропровідність; резистивне перемикання; окисно-відновний механізм

Scientific Herald of Uzhhorod University
Series "Physics"

Journal homepage: https://physics.uz.ua/en
Issue 54, 18–26
Received: 26.07.2023. Revised: 31.10.2023. Accepted: 18.12.2023

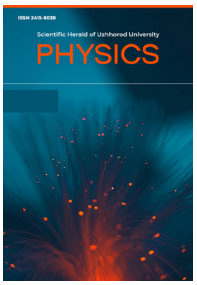

UDC 621.54
PACS 73.40. Lq, 81.05. Hd
DOI: 10.54919/physics/54.2023.18

Influence of the phthalimide on the process of electrical aging of the high-pressure polyethylene

Shucayat Aman Zeynalov
PhD in Physics, Associate Professor
Azerbaijan Technical University
AZ 1073, 25 H. Javid Ave., Baku, Azerbaijan
https://orcid.org/0000-0002-0040-6057

Farhad Shamil Kerimov
PhD in Physics, Associate Professor
Azerbaijan Technical University
AZ 1073, 25 H. Javid Ave., Baku, Azerbaijan
https://orcid.org/0009-0005-8006-5481

Sevinj Ittifaq Safarova*
PhD in Physics, Associate Professor
Azerbaijan Technical University
AZ 1073, 25 H. Javid Ave., Baku, Azerbaijan
https://orcid.org/0009-0003-5928-1177

Sayyara Heydar Sadygova
PhD in Physics, Associate Professor
Azerbaijan Technical University
AZ 1073, 25 H. Javid Ave., Baku, Azerbaijan
https://orcid.org/0009-0003-0492-4825

Tahir Pasha Musaev
PhD in Physics, Associate Professor
Azerbaijan Technical University
AZ 1073, 25 H. Javid Ave., Baku, Azerbaijan
https://orcid.org/0009-0001-6719-874X

Abstract

Relevance. The use of polyolefins without additional processing methods, namely, the increase in their electrophysical characteristics, is an actual modern requirement. For this, it is necessary to use the mechanism of ionization ageing where the role of the modifying additive must be elucidated by the method of infrared spectroscopy in high-pressure polyethylene.

Suggested Citation:
Zeynalov SA, Kerimov FS, Safarova SI, Sadygova SH, Musaev TP. Influence of the phthalimide on the process of electrical aging of the high-pressure polyethylene. *Sci Herald Uzhhorod Univ Ser Phys.* 2023;(54):18–26. DOI: 10.54919/physics/54.2023.18

*Corresponding author

Purpose. The research aims to study the effect of low molecular weight organic additives of phthalimide on molecular structural changes in polymers that occur under external action.

Methodology. The impact of electrical discharges on polymer dielectrics was carried out in a test cell of an asymmetric type. Tested polymer film before and after pre-stretching was tightly stretched onto this plate following the research procedure. To create an air gap of constant thickness between the top electrode and the polymer film, 1.5 mm thick glass spacers were placed along the edges.

Results. The electrical strength (lifetime) of high-pressure polyethene (LDPE) and its optimal modification before and after electrical ageing was investigated. Following experimental data, at the content of 0.05 wt. % LDPE its electrical strength reaches a maximum value compared to both the original LDPE and LDPE at other additive contents. The introduction of 0.05 wt.% phthalimide into high-pressure polyethene contributes to a noticeable decrease in the intensity of the formation of C = 0 groups, which is the measure of the oxidative degradation of polymer chains.

Conclusions. The optimal composition of the phthalimide was determined and their electrophysical properties were studied. It was found that composites with additions of 0.05 wt.% phthalimide significantly improve the electrophysical properties of LDPE.

Keywords: infrared spectrum; lifetime; polymer chains; electrophysical properties; electrical durability

Introduction

The most important advantages of polymeric materials, which include first of all a low specific weight, are the ability to be processed in a product of complex configurations using productive and accessible techniques, the possibility of imparting to them a complex of valuable technical properties (chemical resistance, strength, high electrical insulating characteristics, etc.), as well as the availability of a wide raw material base.

Furthermore, a good combination of physical and mechanical properties of polymeric materials makes it possible to use them more and more widely as electrical insulation and dielectrics in the cable industry, capacitor building, and in the production of electrical machines and appliances.

The use of these materials has revealed some common disadvantages of this type of material. E.M. Godzhaev *et al.* [1] noted that one of the most significant among them is the tendency of polymers to so-called “ageing”, which is expressed by the deterioration of properties during storage, processing, and operation, that occurs in strong electric fields by the deterioration of the electrical and mechanical properties of polymer insulation mainly due to ionization processes developing in air inclusions and pores inside the insulation. According to A.R. Sadigova *et al.* [2] a significant breakthrough is taking place in connection with the new possibilities of nanotechnologies, namely, the possibility of regulating the supramolecular structure of polymer composites at the nano level. Nanofilled systems are increasingly being studied to improve the physical and mechanical characteristics of polymers.

A.A. Khadıyeva *et al.* [3] aimed to develop new polymer compositions with increased electrical strength, which prevent the deterioration of the physical and mechanical properties of polymeric materials and compositions based on them and suppress destructive processes under the separate and simultaneous action of various factors, for example, a strong electric field and discharges, various irradiations of temperature, mechanical loads, etc., as well as the effect of the organic additive on the supramolecular structure of the polymer composition

Studies [4; 5] noted that it is to obtain a three-dimensional image of the surface, a scanning electron microscope is employed, which uses electrons scattered or emitted by the surface of the sample. The sample, in this case, is fixed, dried, and coated with a thin film of heavy metal, and then scanned with a narrow beam of electrons. At the same time, the number of electrons scattered when the surface is irradiated is estimated. J. Almond *et al.* [6] claimed the use of SPM for the study of objects of intensity control of the second beam, moving synchronously with the first and forming an image on the monitor screen. The resolution of the method is about 10 μm. The thickness of the samples studied by this method is determined by the penetrating power of the electrons or their energy.

Scanning probe microscopy is one of the most powerful modern methods for studying the morphology and local properties of a solid body with high spatial resolution. Scanning probe microscopy has evolved from an exotic technique, available only to a limited number of research groups, to a widespread and successfully used tool for studying surface properties. According to D. Nečas [7], almost no research in the field of surface physics and thin-film technologies is complete without the use of scanning probe

microscopy methods. The development of scanning probe microscopy also served as the basis for the development of new methods of nanotechnology – technologies for creating structures with nanometer scales. Currently, probe microscopy is a rapidly developing field of technology and applied scientific research.

The research aims to develop new polymer compositions with increased electrical strength and resistance to electrical ageing, as well as to identify the effect of additives on the supramolecular structure of the polymer composition.

Materials and Methods

High-pressure performance polyethene (LDPE) grade 10803-020 (Azerbaijan) was chosen as the object of study and the organic compound phthalimide (chemical formula $C_6H_4(CO)_2NH$ was used as an additive. The size of the additive particles was less than 50 μm. Additives in the amount of 0.01-0.1 wt.% were introduced into the LDPE by mechanical mixing. Research samples were made as films with a thickness of 50–60 μm by pressing on a hydraulic press. Technological parameters of pressing are: temperature – 150°C, pressure – 15 MPa, pre-heating time – 10 min, holding time under pressure – 5 min, cooling time – 2 min. Measurement of the electrical durability (lifetime) of the tested samples was carried out on the breaking apparatus, where a special cell was developed, consisting of two steel disk electrodes with diameters of 30 and 10 mm, respectively [6-8].

The impact of electrical discharges on polymer dielectrics was carried out in a test cell of an asymmetric type. The studied polymer film was placed between two metal electrodes. A smooth stainless-steel plate (nickel-plated on one side) with dimensions 180×130 mm was taken as the lower grounded electrode. Following the procedure, the tested polymer film before and after pre-stretching was tightly stretched onto this plate. To create an air gap of constant thickness between the top electrode and the polymer film, 1.5 mm thick glass spacers were placed along the edges. A schematic diagram of the described cell is shown in Figure 1. A high-power frequency voltage (HV) was applied to the cell electrodes from an AII-70 apparatus (Azerbaijan). Research was carried out at Azerbaijan Technical University.

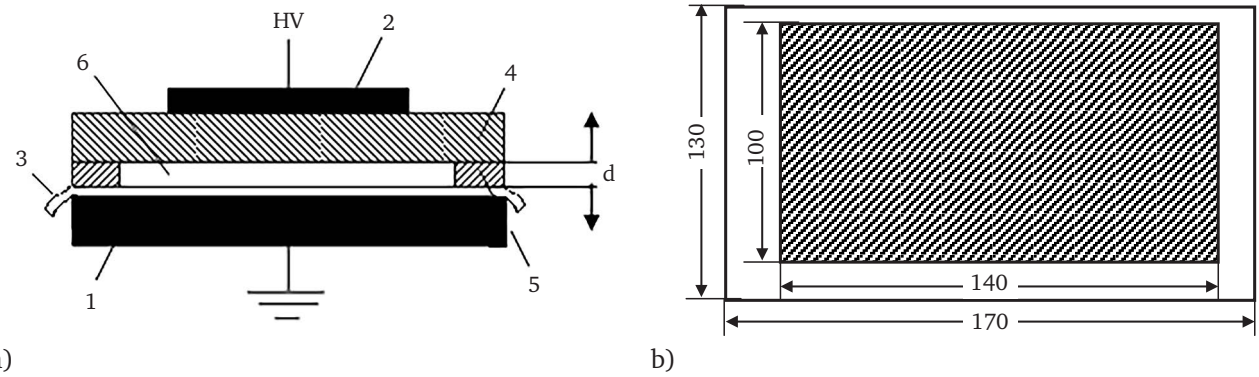

a) b)

Figure 1. Test cell with an air gap
Note: 1 – metal Ground electrode, 2 – metallized glass plate, 3 – metal coating, 4 – glass spacers (b), 5 – polymer film HV (a)
Source: compiled by the authors

The IR-spectra (IR – infrared) of the samples were recorded using UR-20 (UR – ultra red, Azerbaijan) spectrophotometer in the range of (700-3600 cm^{-1}) of both initial LDPE films and its optimal modifications before and after electrical ageing. When studying the changes in the IR spectra of the samples with the time of their ageing, a special frame was used, which was used to periodically record the spectrum of the same part of the sample during the entire test period. The UR-20 operating mode was characterized by the following parameters: scanning speed – ~400 cm^{-1}/min, fricative program – "7.5", gain – "7-8", steam speed – 4 min/100%. The spectra were compared for films of equal thickness (the IR spectrum was carried out at the Institute of Physics of the Academy of Sciences of the Republic of Azerbaijan).

Results and Discussion

Research in the field of creating materials with special and practically important electrophysical properties based on polymer structures saturated with capture centres with different values of activation energy, in which electrons are stabilized, is highly relevant. Depending on the nature of the filler, the shape, size, and nature of the distribution of particles in the matrix, as well as on the interaction between the constituent components, polymer composites with different electrophysical, spectral-luminescent and other properties are obtained.

The introduction of various fillers leads to the expansion of the possibilities of the practical application of the composite material since the nature of the aggregation of filler particles, crystallization

conditions and several other factors change the morphology of the polymer matrix, and as a result, the composite materials obtained on their basis acquire unique properties. Figure 2 shows the dependence of the short-term electric strength E_s of low-density polyethene on the amount of phthalimide. With an increased percentage by weight of phthalimide, its electrical strength increases and reaches its maximum value at 0.05 wt.% of phthalimide. With a further increase in the amount of phthalimide to 0.1 wt.%, a sharp decrease in the electrical strength of the material is observed.

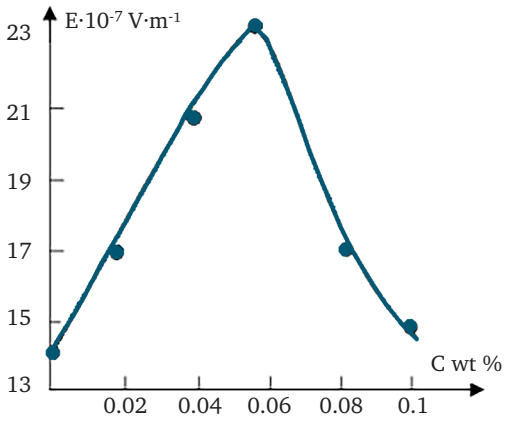

Figure 2. The electrical strength of the LDPE film depends on the amount of phthalimide
Source: compiled by the authors

The observed increase in electrical strength of polyethene films at the optimum content (0.05 wt.% FI) is associated with structural changes occurring after the introduction of additives into them [9; 10]. This is also confirmed by the study of the effect of adding a small amount of phthalimide on the time dependence of the electrical strength of the LDPE film before and after electrical ageing (Fig. 3). Figure 3 shows a plot of the logarithm of the lifetime of the initial LDPE modified by phthalimide additives (LDPE + 0.05 wt.% FI) on the electric field strength before and after electrical ageing.

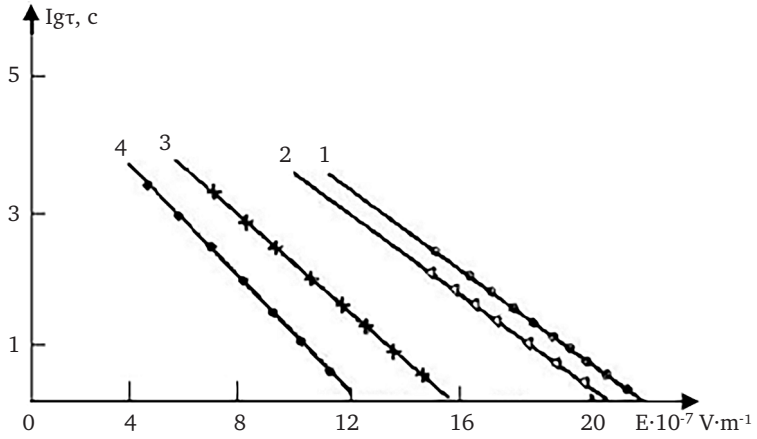

Figure 3. Dependence of the electrical durability of the initial and modified (LDPE + 0.05 wt% phthalimide) LDPE films before (1, 3 respectively) and after electrical ageing in the air at U = 7 kV, t = 5 hours (2, 4) on the electric field strength
Source: compiled by the authors

As can be seen from Figure 3, in all cases at a given temperature with an increase in the electric field strength, the logarithm of the lifetime decreases linearly, i.e., the well-known relation $\tau = B\exp(-\beta E)$ is true, where B and β are parameters depending on the composition of the test material and the temperature of the electrical durability [11-13]. Figure 3 shows the introduction of 0.05 wt% phthalimide into LDPE increasing the electrical strength from $14 \cdot 10^{-7}$ V·m^{-1} (line 3) to $22.5 \cdot 10^{-7}$ V·m^{-1} (line 1). At the same time, the lifetime of the modified LDPE film is relatively stable during electrical ageing under the action of electrical discharges. Indeed, after the electric discharge, the electric strength of

LDPE + 0.05 wt.% phthalimide film decreases slightly, i.e. from $22.5 \cdot 10^{-7}$ V·m^{-1} (line 1) to $21 \cdot 10^{-7}$ V·m^{-1} (line 2), while LDPE film without additive has a significant drop in strength from $14 \cdot 10^{-7}$ V·m^{-1} (line 3) to $8 \cdot 10^{-7}$ V·m^{-1} (line 4).

Sh. Zeynalov *et al.* [14] studied the effect of phthalimide additives in the optimal amount on the change in electrical strength under ultraviolet irradiation in air. Research results have shown that the introduction of phthalimide additives into low-density polyethene in an optimal amount leads to a significant increase in its electrical strength and, secondly, the detected increased properties of the modified LDPE remain unchanged after UV irradiation with a duration of 15 hours in air. The mechanism of growth of the electrical strength of polyethene with the introduction of micro additives of phthalimide up to 0.05 wt %, as well as an increase in the resistance of polyethene to electrical ageing can be explained based on the change in the intensity of some bands, and the appearance of background on the IR spectra. Figures 4 and 5 present the experimental results obtained from the absorption bands of the IR spectra for LDPE films and their optimal modifications.

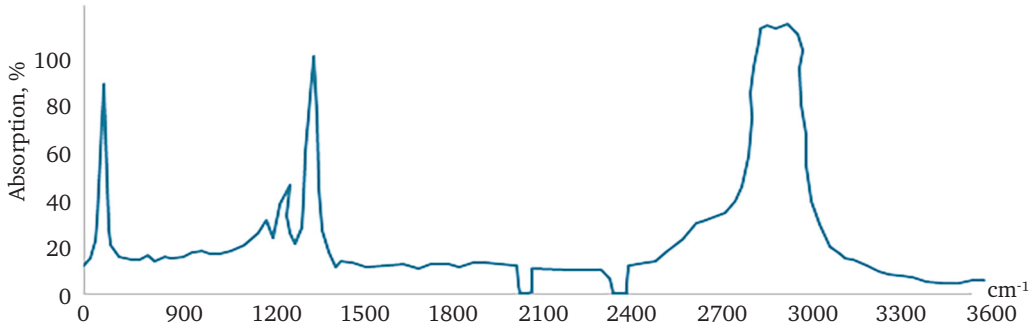

Figure 4. IR spectra of LDPE films before electrical aging
Source: compiled by the authors

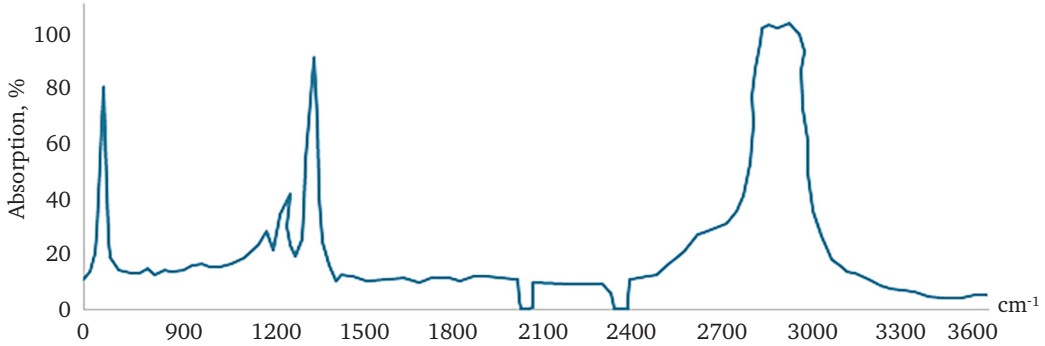

Figure 5. IR spectra of the LDPE film with the optimal amount of phthalimide before electrical ageing
Source: compiled by the authors

A comparison of these spectra shows that in all the cases considered, the introduction of the modifier used in the indicated amount into LDPE does not contribute to the appearance of new absorption bands, i.e., practically does not change the shape of their IR spectra. This suggests that these modifiers in the proposed amount are technologically compatible with LDPE. In other words, they mainly affect the physical structure of LDPE.

Indeed, the achievement of the effect of adding small amounts is mainly due to interstructural plasticization. A.A. Garibli *et al.* [15] examined the interaction between components in the composite material consisting of nanosilicon and polypropylene. This investigation utilizes Fourier Transform Infrared Spectroscopy (FTIR) and X-ray diffraction (XRD) methods to analyse and characterize the composite. XRD was used to utilize and investigate the crystalline structure and phase composition of the composite. XRD is a powerful technique for determining the arrangement of atoms within the material and identifying any crystallographic changes that may occur due to the interaction between nanosilicon and polypropylene. S.H. Kim *et al.* [16] addressed the decomposition of low-density polyethene and the energy output achieved through the utilization of dielectric barrier discharge under varying electrical circumstances. Z. Qiao *et al.* [17] and B.C. Smith [18] aimed to gain insights into the long-term performance of polyethene insulation under thermal ageing conditions, which is crucial for the reliability of track cable systems. An

established understanding of the space charge behaviour in aged polyethene insulation is essential for improving the maintenance and lifespan of track cables, ensuring the safe and efficient operation of rail transportation networks.

To establish the contribution of the phthalimide additive to the process of electrical ageing of the LDPE film, similar structural studies of the samples were carried out after their electrical ageing. These results are shown in Figures 6 and 7.

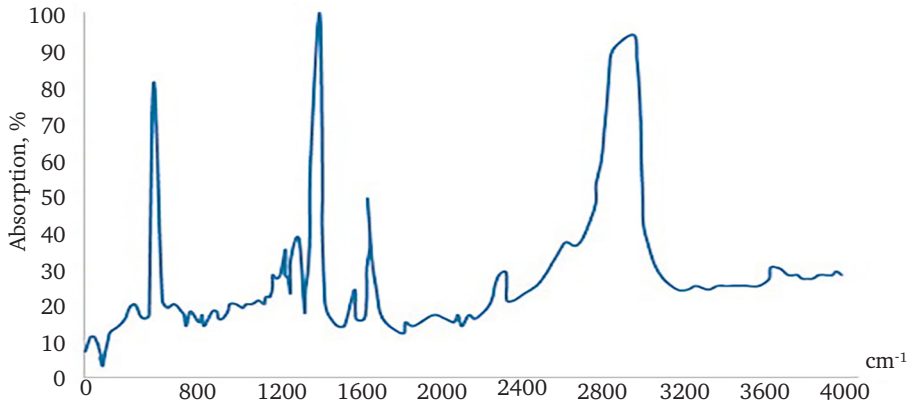

Figure 6. Change in the IR spectra of the LDPE film after electrical ageing under `the action of discharges in air

Note: U =7 kV, t=5 hours

Source: compiled by the authors

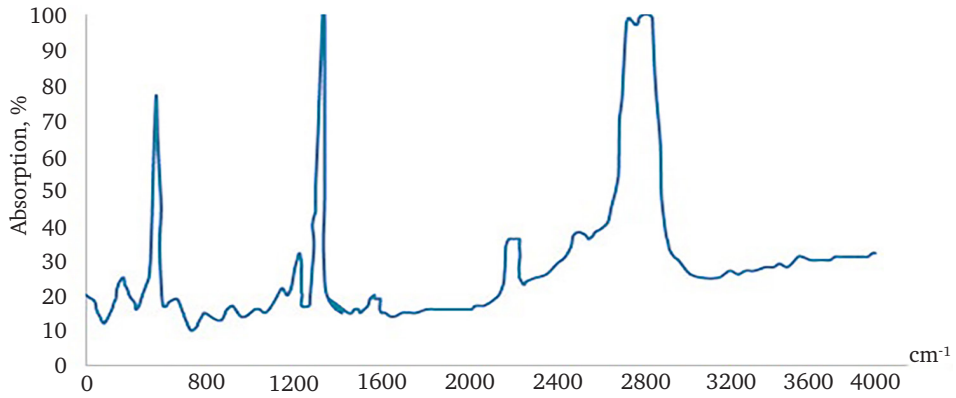

Figure 7. Change in the IR spectra of an LDPE film with a modifying additive of phthalimide at 0.05 wt% after electrical ageing under the action of discharges in air

Note: U =7kV, t =5 hours

Source: compiled by the authors

As can be seen from Figures 6 and 7 after the electrical ageing of LDPE films, a new absorption band is observed in the IR spectra and the bands 1720-1710 (C = 0 groups) are the most pronounced. However, judging by the change in the intensity of the absorption band of the C = 0 groups of LDPE films all other things being equal, the amount of phthalimide applied to LDPE, the intensity of the absorption bands of the terminal carbonyl groups decreases significantly.

Since the intensity of absorption in the IR spectrum in the first approximation is proportional to the number of corresponding groups in the sample, it can be concluded that the used modifier, due to the presence of highly dispersed particles, acts as an active structure former, homogenizing the LDPE structure, and thereby slows down the course of oxidative processes. H. Boughrara *et al*. [19] explored an easy and effective method to enhance the compatibility of blends containing low-density polyethene (LDPE) and poly(ε-caprolactone) (PCL). The research investigated the use of specific compatibilizers or additives to promote better mixing and interaction between LDPE and PCL, ultimately improving the overall performance of the blend. Enhanced compatibilization of LDPE/PCL blends can form materials with tailored properties, making them suitable for various applications, including packaging, biomedical materials, and sustainable polymer composites. R.P. D'Amelia *et al.* [20], using

Fourier Transform Infrared Spectroscopy (FTIR), studied the chemical interactions and structural characteristics of these polymer copolymers and blends. FTIR allows for the detection and analysis of functional groups present in the samples, as well as the determination of the degree of polymerization. Alongside FTIR, elemental analysis is employed to accurately determine the composition of the samples, including the content of hydrogen, carbon, and other elements in the polymer materials [21]. This is crucial for the quantitative assessment of copolymers and blends. This research has significant industrial applications, where the precise composition and structural characteristics of polymer materials impact their properties and quality [22].

Thus, in this case, the rate of decrease in the electrical strength of the LDPE film during its ageing with the introduction of a small number of additives also indicates the formation of densely packed structures due to fine spherulite organization, which prevents oxygen diffusion and the development of ionization processes during electrical destruction, which is in good agreement with the change in IR spectra.

Conclusions

The composition and amount of a low molecular weight organic additive modifying the electrophysical properties of LDPE 10803-020 have been determined. The developed modification of LDPE is distinguished by a significantly small number of additives used and their technological compatibility. A systematic study of the electrophysical properties of the LDPE film and its developed modifications has been carried out. Composites with the addition of 0.05 wt% phthalimide significantly increase the electrical strength, and volumetric electrical resistance and reduce the dielectric loss tangent, i.e., there is a noticeable correlation between these characteristics.

The structural changes in LDPE and its modifications were studied by IR spectroscopy, which was used to establish the contribution of the modifying organic additive phthalimide to the stability of the electrophysical properties of LDPE during its ionization ageing under the action of electric discharges. It is shown that the introduction of the modifiers used in the indicated amount into LDPE contributes to a noticeable decrease in the intensity of the formation of c = 0 groups (1720 sm^{-1}), which is a measure of the oxidative degradation of polymer targets. The experimental facts confirm the assumption that the proposed phthalimide modifiers in a small amount (0.05 wt%) are artificial nuclei of structure formation for LDPE. Consequently, a more ordered structure of LDPE, containing the optimal amount of modifier, will hinder the diffusion of atmospheric oxygen polymers even during their ionization ageing.

A qualitative assessment of the change in the LDPE film with the introduction of small additives is the determination of the morphology of supramolecular formations using electron scanning microscopy and X-ray diffraction. The data obtained allow us to approach the explanation of experimental results from a scientific point of view, establish the relationship between the structure and properties of polymer products, and conduct a targeted search for the most optimal alloying additives that can improve the physical, mechanical, and technological properties of the polymer. In addition, the dielectric and mechanical antistatic characteristics of the specified polymer composition were studied before and after electrical, UV and gamma irradiation.

Further investigations could delve deeper into the underlying mechanisms of how phthalimide interacts with high-pressure polyethene during electrical ageing. This might involve advanced analytical techniques and computational modelling to provide a more comprehensive understanding of the processes involved. Research could focus on optimizing the concentration of phthalimide to achieve the most effective mitigation of electrical ageing. This could involve a systematic exploration of various concentrations to find the optimal balance between performance improvement and material cost. Extending the duration of electrical ageing experiments could help assess the long-term stability and effectiveness of phthalimide as an ageing inhibitor. This would be valuable for applications where extended lifetimes are crucial, such as high-voltage insulation materials.

Acknowledgements

None.

Conflict of Interest

None.

References

[1] Godzhaev EM, Kerimov FSh, Alekperov AM. Inluence of unirradiation on the electrical properties of a high-density polyethylene film modified with phthalimide additive. *Azerb J. Phys*. 2022;2022:38–40.

[2] Sadygova AR, Abbasov II, Safiev ES, Asilbeyli PB, Alekperov VA. Influence of nanoclay microadditives on the molecular processes and kinetics of electrical and mechanical destruction of polyethylene. *Nanosyst Nanomater Nanotechnol Nanosyst*. 2019;17(1):155–65. DOI: 10.15407/nnn.17.01.155.

[3] Khadıyeva AA, Asılbeylı PB, Sadygova AR, Ismaılov IM. Molecular processes in electric destruction of nanocomposites on the basis of PE and nanoclay after external factors. 2022. Baku: Institute of Physics; P. 84–8.

[4] Chiong H, Daliparthi SPR, Deshpande HS, Guggenheim TL, Khouri FF, Kumar MS, Navarro De Castro MA, Odle RR, Sivakumar P, Dhumal SS, Sreeramagiri SK, Smith BA. Manufacturing processes of bis (phthalimide) s and polyetherimides, and bis (phthalimide) s and polyetherimides formed therefrom. Publication of ES2672580T3. June 15, 2018. Available from: https://patents.google.com/patent/ES2672580T3/en.
[5] Cubric IS, Cubric G, Križman IK Kovacevi M. Evaluation of changes in polymer material properties due to aging in different environments. *Polymers*. 2022;14:1682. DOI: 10.3390/polym14091682.
[6] Almond J, Sugumaar P, Wenzel MN, Hill G, Wallis C. Determination of the carbonyl index of polyethylene and polypropylene using specified area under band methodology with ATR-FTIR spectroscopy. *e-Polym*. 2020;20:369-381. DOI: 10.1515/epoly-2020-0041.
[7] Nečas D, Klapetek P. Synthetic data in quantitative scanning probe microscopy. *Nanomater*. 2021;11(7):1746. DOI: 10.3390/nano11071746.
[8] Greene JP. 12-Polymer composites. *Automot Plast Compos*. Materials and Processing. *Plastics Design Library*. 2021;2021:191–222. DOI: 10.1016/B978-0-12-818008-2.00007-6.
[9] Cundiff KN, Madi Y, Benzerga AA. Photo-oxidation of semicrystalline polymers: Damage nucleation versus growth. *Polym*. 2020;188:122090. DOI: 10.1016/j.polymer.2019.122090.
[10] Rodriguez AK, Mansoor B, Ayoub G, Colin X, Benzerga AA. Effect of UV-aging on the mechanical and fracture behavior of low density polyethylene. *Polym Degrad Stab*. 2020;180:109185. DOI: 10.1016/j.polymdegradstab.2020.109185.
[11] Uflyand IE, Drogan EG, Burlakova VE, Kydralieva KA, Shershneva IN, Dzhardimalieva GI. Testing the mechanical and tribological properties of new metal-polymer nanocomposite mate–rials based on linear low-density polyethylene and Al65Cu22Fe13 quasicrystals. *Polym Test*. 2019;74:178–86. DOI: 10.1016/j.polymertesting.2019.01.004.
[12] Nuriev MA, Magerramov AM, Shukyurova AA. Electrical conductivity of nanocomposites based on low-density polyethylene and Cu2S nanoparticles. *Surf Eng Appl Electrochem*. 2018;54(1):32–7. DOI: 10.3103/S1068375518010118.
[13] Kumar V, Gulati K, Lal S, Arora S. Effect of gamma irradiation on tensile and thermal properties of poplar wood flour-linear low-density polyethylene composites. *Radiat Phys Chem*. 2020;174:108922. DOI: 10.1016/j.radphyschem.2020.108922.
[14] Zeynalov Sh, Garacayev B, Khalilov S, Kerimov F, Alekperov A. Study of the mechanical durability of a high-pressure polyethylene film and its composition at various temperatures. *Norw J Dev Int Sci*. 2022;(86):53-56.
[15] Garibli AA, Melikova SZ, Ramazanov MA, Garibov AA. The study of the interaction of components in the composite nanosilicon + polypropylene Fourier Transform Infrared Spectroscopy and X-Ray diffraction methods. *Azerb J Phys*. 2018;24(4):38-47.
[16] Kim SH, Yun UH, Kim JG. Low-density polyethylene degradation and energy yield using dielectric barrier discharge under various electrical conditions. *Energ*. 2023;16(5):2403. DOI: 10.3390/en16052403.
[17] Qiao Z, Wu W, Wang Z, Zhang L, Zhou Y. Space charge behavior of thermally aged polyethylene insulation of track cables. *Polym*. 2022;14(11):2162. DOI: 10.3390/polym14112162.
[18] Smith BC. The ınfrared spectra of Polymers II: Polyethylene. *Spectrosc*. 2021;36(9):24–9. DOI: 10.56530/spectroscopy.xp7081p7.
[19] Boughrara H, Djellali S, Haddaoui N, Staelens JN, Supiot P, Maschke U. A facile route to improve compatibilization of low-density polyethylene/poly(ε-caprolactone) blends. *Polym Degrad Stab*. 2022;204:110111. DOI: 10.1016/j.polymdegradstab.2022.110111.
[20] D'Amelia RP, Huang L, Mancuso J. Quantitative Analysis of polyvinyl alcohol-polyethylene (PVOH-PE) copolymers and polyvinyl pyrrolidone-polyvinyl acetate (PVP-PVAc) copolymers and blends using Fourier Transform ınfrared spectroscopy and elemental analysis. *World J Chem Educ*. 2019;7(1):1–11.
[21] Panov V. The scientific process of two interferometers (optical) development and the mitigation of external influence. *Sci Herald Uzhhorod Univ Ser Phys*. 2023;(53):19–30. DOI: 10.54919/physics/53.2023.19.
[22] Pylypchynets I. Optimal scheme for stimulating photofission of shielded nuclear materials on the Microtron M-30: A combination of theoretical and experimental studies. *Sci Herald Uzhhorod Univ Ser Phys*. 2022;52:16–26. DOI: 10.54919/2415-8038.2022.52.16-26.

Вплив фталіміду на процес електричного старіння поліетилену високого тиску

Шукаят Аман Зейналов

Кандидат фізико-математичних наук, доцент
Азербайджанський технічний університет
AZ 1073, проспект Г. Джавіда, 25, м. Баку, Азербайджан
https://orcid.org/0000-0002-0040-6057

Фархад Шаміль Керімов

Кандидат фізико-математичних наук, доцент
Азербайджанський технічний університет
AZ 1073, проспект Г. Джавіда, 25, м. Баку, Азербайджан
https://orcid.org/0009-0005-8006-5481

Севінь Іттіфак Сафарова

Кандидат фізико-математичних наук, доцент
Азербайджанський технічний університет
AZ 1073, проспект Г. Джавіда, 25, м. Баку, Азербайджан
https://orcid.org/0009-0003-5928-1177

Саяра Гейдар Садигова

Кандидат фізико-математичних наук, доцент
Азербайджанський технічний університет
AZ 1073, проспект Г. Джавіда, 25, м. Баку, Азербайджан
https://orcid.org/0009-0003-0492-4825

Тахір Паша Мусаєв

Кандидат фізико-математичних наук, доцент
Азербайджанський технічний університет
AZ 1073, проспект Г. Джавіда, 25, м. Баку, Азербайджан
https://orcid.org/0009-0001-6719-874X

Анотація

Актуальність. Використання поліолеодинів без додаткових методів обробки, а саме підвищення їх електрофізичних характеристик, є актуальною сучасною вимогою експлуатації. Для цього необхідно використовувати механізм іонізаційного старіння, де роль модифікуючої добавки в цьому повинна бути з'ясована методом інфрачервоної спектроскопії в поліетилені високого тиску.

Мета. Метою роботи було вивчення впливу низькомолекулярних органічних добавок фталіміду на молекулярно-структурні зміни полімерів, що відбуваються під дією зовнішнього середовища.

Методологія. Вплив електричних розрядів на полімерні діелектрики проводили в дослідній комірці несиметричного типу. Відповідно до процедури на цю пластину щільно натягували досліджувану полімерну плівку до і після попереднього розтягування. Для створення повітряного зазору постійної товщини між верхнім електродом і полімерною плівкою по краях розташовували скляні прокладки товщиною 1,5 мм.

Результати. Досліджено електричну міцність (термін служби) поліетилену високого тиску (LDPE) та його оптимальну модифікацію до та після електричного старіння. На підставі експериментальних даних встановлено, що вміст 0,05 мас. % LDPE, його електрична міцність досягає максимального значення в порівнянні як з вихідним LDPE, так і з LDPE при інших вмістах добавок. Показано, що введення 0,05 мас. % фталіміду в поліетилен високого тиску сприяє помітному зниженню інтенсивності утворення C = 0 груп, що є мірою окиснювальної деструкції полімерних ланцюгів.

Висновки. Визначено оптимальний склад фталімідів та вивчено їх електрофізичні властивості. Встановлено, що композити з добавками 0,05 мас.% фталіміду значно покращують електрофізичні властивості LDPE.

Ключові слова: інфрачервоний спектр; час життя; полімерні ланцюги; електрофізичні властивості; електрична довговічність

Scientific Herald of Uzhhorod University
Series "Physics"

Journal homepage: https://physics.uz.ua/en
Issue 54, 27–35
Received: 04.09.2023. Revised: 05.12.2023. Accepted: 18.12.2023

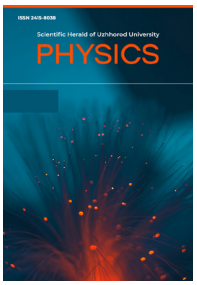

UDC 621.52
PACS 73.40. Lq, 78.20.-e, 81.05. Hd
DOI: 10.54919/physics/54.2023.27

The influence of implantation of Mg^+ ions and subsequent annealing on the composition, electronic structures, emission and optical properties of CdF_2

Akbarjon Abduvayitov
PhD in Physical and Mathematical Sciences
Tashkent State Technical University named after Islam Karimov
100095, 2 University Str., Tashkent, Uzbekistan
https://orcid.org/0000-0001-6453-6523

Gunel Imanova*
PhD in Physics, Associate Professor
Institute of Radiation Problems, Ministry of Science and Education Republic of Azerbaijan
AZ1143, 9 B. Vahabzadeh Str., Baku, Azerbaijan
UNEC Research Center for Sustainable Development and Creen Economy named after Nizami Ganjavi
AZ1007, 45A Abbas Sahhat Str., Baku, Azerbaijan
https://orcid.org/0000-0003-3275-300X

Dilnoza Tashmukhamedova
Doctor of Physical and Mathematical Sciences, Professor
Tashkent State Technical University named after Islam Karimov
100095, 2 University Str., Tashkent, Uzbekistan
https://orcid.org/0000-0001-5813-7518

Khurshid Boltaev
PhD in Physical and Mathematical Sciences
Tashkent State Technical University named after Islam Karimov
100095, 2 University Str., Tashkent, Uzbekistan
https://orcid.org/0000-0001-6453-6523

Boltakhodja Umirzakov
Doctor of Physical and Mathematical Sciences, Professor
Tashkent State Technical University named after Islam Karimov
100095, 2 University Str., Tashkent, Uzbekistan
https://orcid.org/0000-0002-9815-2111

Abstract

Relevance. In the case of bombardment with Mg metal ions, the changes are accompanied by the introduction of metal atoms and the formation of various types of compounds. Thus, CdF_2 is intensively decomposed into components in the near-surface layer in the process of ion implantation. A small part of these components

Suggested Citation:
Abduvayitov A, Imanova G, Tashmukhamedova D, Boltaev K, Umirzakov B. The influence of implantation of Mg^+ ions and subsequent annealing on the composition, electronic structures, emission and optical properties of CdF_2. *Sci Herald Uzhhorod Univ Ser Phys.* 2023;(54):27–35. DOI: 10.54919/physics/54.2023.27

*Corresponding author

can be sprayed from the surface. Due to the high chemical activity, almost all of the liberated fluorine atoms again enter into a chemical bond with both the atoms of the alloying element and the atoms of cadmium. Consequently, three-component compounds are formed in the near-surface layer. Therefore, it is necessary to define the electronic states, band energy, and optical parameters of CdF_2 and $Cd_0.6Mg_0.4F_2$ films.

Purpose. The composition, structure, and properties of CdF_2 implanted with Mg+ ions in combination with thermal and laser annealing for the first time were the research aims.

Methodology. The experimental studies were carried out at a vacuum of at least 10^{-7} Pa using the methods of Auger electron spectroscopy (AES) and ultraviolet photoelectron spectroscopy (UVES). The depth distribution profiles of atoms were determined by the AES method in combination with layer-by-layer etching of the surface with Ar^+ ions with $E_0 = 2-3$ keV.

Results. CdF_2 is intensively decomposed into components in the near-surface layer in the process of ion implantation. Consequently, three-component compounds are formed in the near-surface layer. Band-energy parameters and densities of the state of electrons in the valence band of this film are determined.

Conclusions. The effect of the implantation of Mg+ ions on the composition and electronic structure of single-crystal CdF_2/Si(III) films was studied for the first time. The densities of electronic states, band-energy and optical parameters of CdF_2 and $Cd_0.6Mg_0.4F_2$ films have been determined.

Keywords: atomic distribution profiles; ultrathin layers; band gap; heat treatment; surface layer

Introduction

Among the approaches available to solve problems of increasing the reliability and durability of machine and mechanism parts, cutting tools, and technological equipment, technological methods of surface hardening of structural materials play a key role. Photoelectrocatalytic water part offers a promising approach to change over daylight into economical hydrogen vitality. A careful understanding of the connections between the properties and capacities of photoelectrocatalytic materials plays a pivotal part in the plan and creation of productive photoelectrochemical frameworks for the water part. A study [1] presented the propels within the improvement of efficient photoelectrocatalytic materials. To begin with, the basics included within the photoelectrocatalytic water part are expounded. An important factor in the coating process is surface preparation, which includes, in addition to mechanical cleaning, the bombardment of the substrate surface with an intense stream of low-energy ions. According to studies [2; 3], these films are used for a controlled change in the E_g of dielectrics in certain cases, as well as for obtaining consistent layers at the interface of SIS (semiconductor-insulator-semiconductor) structures in three-dimensional integrated circuits. CdF_2/Si (111) hetero-structures with a CaF_2 buffer layer are of particular interest. The minimum thickness of the CaF_2 buffer layer is 0.9 nm. In this case, Z.A. Tursunmetova *et al.* proved that CaF_2 plays the role of a barrier layer for the chemical reaction between CdF_2 and Si substrates [4].

The study [5] confirmed that single-crystal cadmium fluoride is a solid dielectric that can be converted into a semiconductor by doping with donor impurities and subsequent heating in a reducing atmosphere. CdF_2 and CaF_2 share a common fluorite-type cubic crystal structure with similar lattice parameters, making them suitable for use in superlattices. However, their electronic and optical characteristics exhibit notable distinctions. Despite having a sizable band gap of approximately 8 eV, CdF_2, when appropriately doped and annealed, can exhibit n-type semiconductor properties. Additionally, research by R.C. Palomera *et al.* has shown that CdF_2 can exhibit efficient electroluminescence and, owing to its high density (6.38 g/cm^3) and relatively rapid luminescence decay time, can be employed as a scintillator [6].

In contrast, CaF_2 is an insulator with an exceptionally wide band gap, estimated to be between 11.8 and 12.1 eV, and it finds widespread use in various optical applications, such as resonant tunnelling diodes and quantum cascade lasers. R.B. Hughes-Currie *et al.* suggested that this behaviour can be attributed to the substantial (2.9 eV) discontinuity in the conduction band at the CdF_2-CaF_2 interface, as detected by X-ray photoelectron spectroscopy [7]. This study also delves into laser spectroscopy of Eu_2+ and Eu_3+ ions doped in CaF_2 within the CdF2-CaF_2 matrix and investigates the distribution of defect positions for dopant ions.

The electron beam method occupies a special place among the existing vacuum-plasma deposition methods. The studies [8; 9] noted that the essence of the method is in the kinetic energy of the electron beam being used to evaporate the substance and it converts into thermal energy in the treatment zone.

R. Shendrik & E. Radzhabov noted that it is also important to use these methods in modern micro- and nano-electronics to apply conductive and dielectric layers of different thicknesses [10].

The ion implantation method has been effectively used to obtain nanosized multicomponent structures and layers on the surface and subsurface region of semiconductors and dielectric films [11; 12]. The composition of CdF_2 implanted with Mg+ ions in combination with thermal and laser annealing for the first time was analysed in this study.

Materials and Methods

Well-polished and etched n-type CdF_2 (111) single crystals were used as research objects. The tests were introduced in an ultrahigh vacuum gadget – "EPOS-PVD-DESK-PRO" (Russia), which comprises two compartments. Strengthening, warm oxidation, and particle assault were carried out within the, to begin with compartment. The composition, thickness of state of valence electrons, band-energy parameters, outflow, and optical properties were considered within the moment one. The value of n determined by the ERES method already at small film thicknesses (d ~ 100 Å) differs sharply from n for Si and becomes characteristic of dielectrics. ERES method was applied to determine the inelastic mean free path (IMFP) of electrons, which is of crucial importance for quantitative electron spectroscopy. For this reason, it is highly desirable to verify the reliability of the ERES method for a variety of elements and different experimental geometries. The composition of CdF_2 implanted with Mg^+ ions in combination with thermal and laser annealing, was studied for the first time. Therefore, even at a film thickness of d ~ 600 Å, the refractive index of light almost does not differ from the value of n for a thick film. Based on this, it can be assumed that the penetration depth of photons with hν > 10 eV for CdF_2 lies in the range of 600-800 Å.

Most things were carried out in a vacuum of at the slightest 10-7 Dad utilizing the strategies of Wood screw electron spectroscopy (AES) and bright photoelectron spectroscopy (UVES). The profundity dissemination profiles of particles are decided by the AES strategy in combination with layer-by-layer carving of the surface with Ar^+ particles with E_0 = 2-3 keV. Before ion implantation, CdF_2 is degassed by heating to T = 900 K for 3 hours in combination with soft etching of the surface with Ar^+ ions at a vacuum of 10^{-7} Pa. Implantation of Mg+ ions are carried out with E_0 = 1 keV doses D = $8 \cdot 10^{16}$ cm^{-2}. For comparison with the beginning of implantation, the conduction of Ar^+ ions with different energies at D = Dn. The optical method, SERE method and the Auger electron spectroscopy method were used to determine the values of n for Si with a CdF_2 surface film of different thicknesses.

Results and Discussion

The crystal lattice of CdF_2 has a cubic fluorite-type structure and a lattice constant close to that of silicon. H.M. Mahmudov *et al.* noted it has been established that the MBE growth of the CdF_2/Si (111) film at the initial stage proceeds according to the Stranski-Krastanov mechanism, and then the growth occurs according to the Frank-Van der Merve mechanism [13]. The (1×1) CdF_2(111) surface is formed after high-temperature (T = 1120 K) heating of films with d ≥ 150 ÷ 200 Å [14].

As follows from Table 1, in the case of thin CdF_2 films, n is strongly affected by the silicon substrate. The role of the substrate is especially noticeable in the visible and infrared regions of light, i.e., in the region where the energy of electromagnetic radiation (ħν < 2 eV) is much less than the band gap of the CdF_2 film (E_g ~ 7.5-8 eV). In the indicated energy range of radiation, the dielectric film turns out to be almost transparent. Therefore, light, penetrating deep into the sample, mainly interacts with silicon atoms. Some decrease in n in the case of thick films is apparently due to the presence of impurity atoms in the bulk of the CdF_2 film. In the region of ultraviolet radiation, especially at hν > 10.2 eV (<1200 Å), a strong absorption of light by the film occurs. Therefore, even at a film thickness of d ~ 600 Å, the refractive index of light almost does not differ from the value of n for a thick film. Based on this, it can be assumed that the penetration depth of photons with hν > 10 eV for CdF_2 lies in the range of 600-800 Å.

Table 1. The values of the refractive index n for CdF_2 films

Method	Film thickness d, Å							
	0 (Si)	100	200	400	600	800	1200	2000
Optic: =1050 Å (UF)	3.5	3.0	2.2	1.8	1.6	1.6	1.55	1.55
=6700 Å (R)	3.4	3.2	3.2	-	3.2	3.0	3.0	3.0
=10640 Å (IR)	3.1	3.1	3.0	-	-	-	3.0	2.9
SERE	3.35	1.7	1.48	1.52	-	1.43	-	1.45

Source: compiled by the authors

A slight difference between n of a film with a thickness of d ~ 100 Å and n for a thick film is probably caused not only by the contribution of the matrix to the excitation of interband transitions and plasma oscillations but also by the imperfection of the stoichiometric composition and crystal structure of

the film due to the influence of the substrate. In the case of thick films, the values of n obtained by the elastically reflected electron spectroscopy (ERES) method and by the optical method in the ultraviolet region are close.

During the bombardment of CdF_2 with ions of inert gases Ar+, CdF_2 is decomposed into components, the surface layers are disordered, the diffusion of atoms, the evaporation of atoms from the surface, etc. In the case of bombardment with Mg metal ions, these changes are accompanied by the introduction of metal atoms and the formation of various types of compounds. To clarify this, the dependence of I_F – (fluorine intensity) on the depth h of a CdF_2 film bombarded with Ar^+ ions with different energies at $D = D_s$ (Fig. 1), where D_s is the ion saturation dose, was analysed. Figure 1 shows that at $E_0 = 0.5$ keV, the intensity of the IF peak sharply (by a factor of ~ 4) decreases and it practically does not change up to a depth of h = 20-25 Å, which corresponds to the projected range of Ar^+ ions. It is also confirmed by the data presented in the work [15].

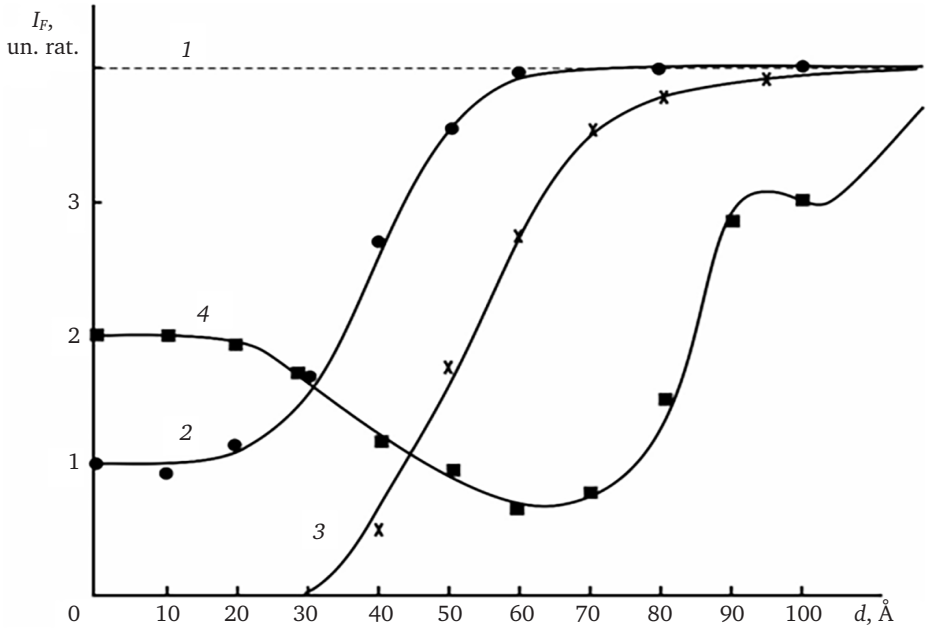

Figure 1. Depth distribution profiles of F atoms of CdF_2 bombarded with Ar^+ ions at $D = D_H$ with different energies E_0, keV
Note: 1 – undoped CdF_2, 2 – 0.5; 3 – 1; 4 – 5, D_H - saturation dose
Source: compiled by the authors

All F atoms in the form of F_2 molecules evaporate from these layers. In the range d ≈ 25 – 50 Å, the IF concentration increases and, starting from h ≈ 50 Å, the stoichiometric composition of CdF_2 is completely established. However, further studies showed that these CdF_2 layers down to a depth of h ≈ 130 – 150 Å were strongly disordered. In the case of $E_0 = 1$ keV, the surface layers of CdF_2 up to a depth of h = 30 – 40 Å are completely decomposed into components and almost all F atoms evaporate from these layers; an amorphous Cd film with a thickness of d = 30 – 40 Å is formed on the surface (curve 3, Fig. 1). When CdF_2 is bombarded with $E_0 = 5$ keV, the highest rate of decomposition occurs at the depth of the projected range of Ar^+ ions (h ≈ 60 – 70 Å). Most of the fluorine atoms escape into the vacuum, while the other part diffuses deep into the target; therefore, the concentration of F at a depth h = 80 – 100 Å increases significantly. A different picture is observed during the implantation of Mg^+ ions in CdF_2.

Figure 2 shows the Auger spectra of a well-cleaned CdF_2 surface before and after implantation of Mg^+ ions with $E_0 = 1$ keV at $D = D_n = 8 \cdot 10^{16}$ cm^{-2}. It can be seen that after implantation of ions, the intensity of Cd and F ions decreases up to 2-3 times and peaks characteristic of Mg appear. With this ion-doped layer, compounds of the Mg-F and Mg-Cd-F types are predominantly formed. Most of the Mg atoms do not enter into a chemical bond and accumulate on the surface. Auger analysis shows that the surface concentration of Mg atoms is ~ 40-45 at.%. Cd-35 40 at.%, and F – 15-20 at.%.

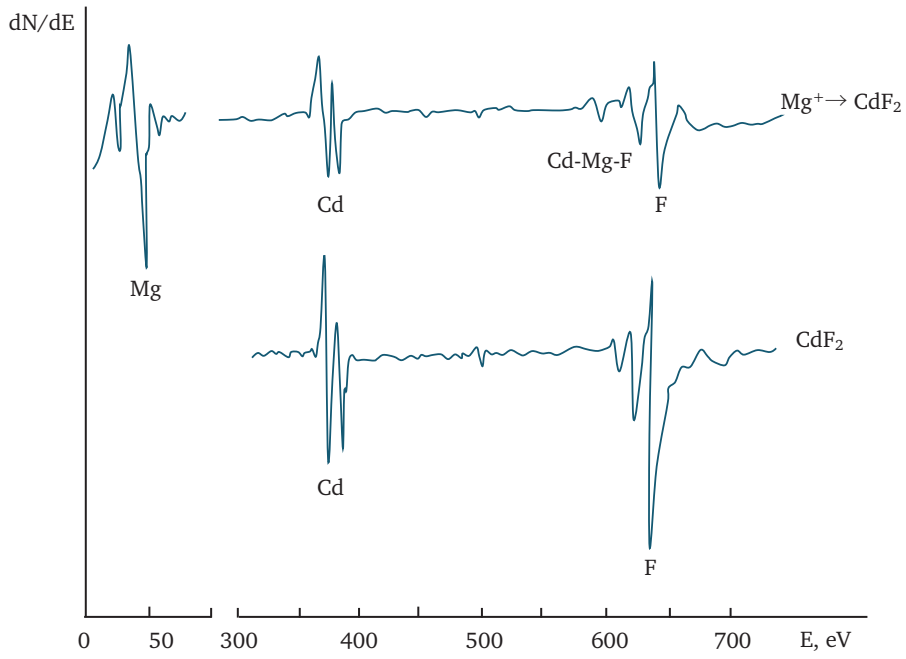

Figure 2. Auger spectra
Note: 1 – well-cleaned CdF_2 surface; 2 – CdF_2 implanted with Mg^+ ions with $E_0 = 1$ keV at $D = 8 \cdot 10^{16}$ cm^{-2}
Source: compiled by the authors

In this way, CdF_2 is goal decayed into components within the near-surface layer within the particle implantation. The study [16] noted that a small portion of these components can be splashed from the surface. Due to the prolonged chemical reaction, nearly all of the freed fluorine iotas join both the molecules of the alloying component and the atoms of cadmium. Subsequently, three-component compounds are shaped within the near-surface layer. As follows from the experimental data, at $E_0 \leq 3$ keV, along with the formation of various compounds, "excess" atoms of the alloying element appear, the concentration of which increases with increasing dose (Fig. 3a). At high ion energies ($E_0 \geq 3$ keV) a noticeable desorption of fluorine from the surface occurs, which leads to the accumulation of Cd atoms near the surface (Fig. 3b). The highest concentration of the latter is 40-45 at.%. The stoichiometric composition characteristic of CdF at E = 3 keV is restored only at d = 120 Å.

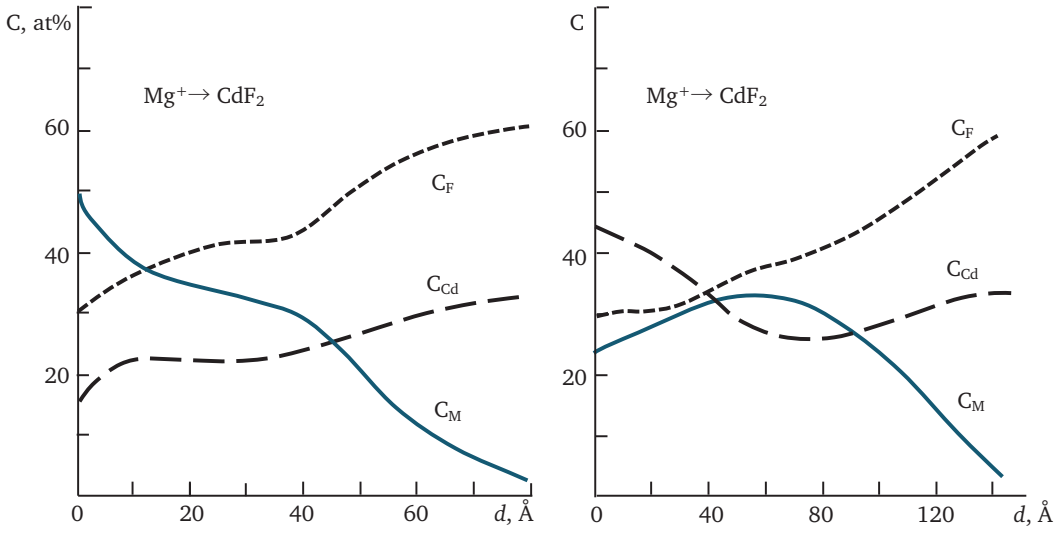

Figure 3. Dependences of C_{Mg}, C_{Ca}, C_F on d for CdF_2, doped ionic Mg^+ with $E_0 = 0.5$ keV and 3 keV. $D = 8 \cdot 10^{16}$ cm^{-2}

Source: compiled by the authors

The influence of post-implantation thermal and laser annealing on the composition, structure, and properties of the ionic implanted CdF_2 film was also studied. The experimental results showed that the optimal heating temperature for CdF_2 implanted with Mg^+ ions is 900 K. In this case, the near-surface layers are completely crystallized and films of the $Cd_{0,7}Mg_{0,3}F_2$ type with a thickness of ~ 25-30 Å are formed on the CdF_2 surface [17; 18]. In the case of laser annealing at an energy density of ~ 1.7 J·cm^{-2}, a $Cd_{0,6}Mg_{0,4}F_2$ film with good stoichiometric composition is formed with a thickness of ~ 40 – 45 Å (Fig. 4).

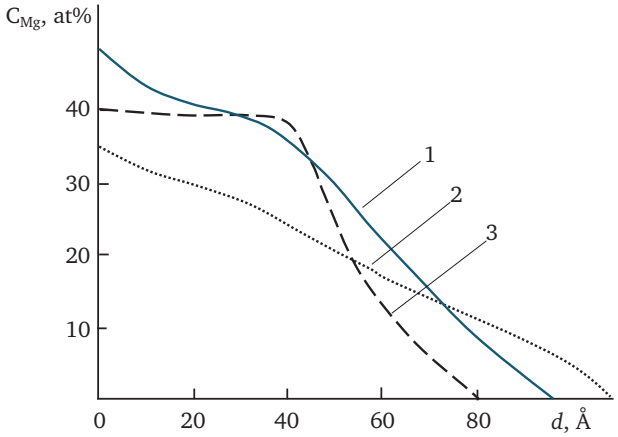

Figure 4. Dependences C_{Mg} (h) for CdF_2 implanted with Mg^+ ions with E_0 = 1 keV at D = 8 · 10^{16} cm^{-2} after heating at T = 900 K (curve 1), after laser annealing with W = 1.7 J·cm^{-2} (curve 2) and spectrum in the initial case (curve 3)
Source: compiled by the authors

Figure 4 shows the UVE spectra of the CdF_2 and $Cd_{0,6}Mg_{0,4}F_2$ films. It can be seen that the density of states of the electrons in the valence band differs significantly from the current density for CdF_2 [19; 20]. Possible mechanisms for the formation of maxima are given in the CED of photoelectrons. The parameters of energy bands $Cd_{0,6}Mg_{0,4}F_2$ are estimated in Figure 5 based on Table 2.

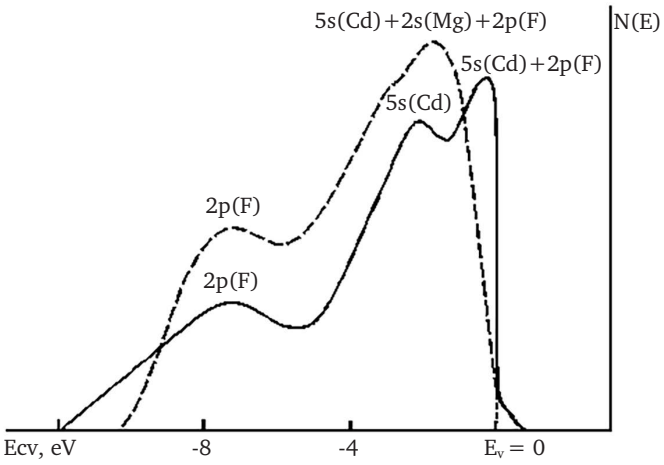

Figure 5. Ultraviolet photoelectron spectra of CdF_2 and $Cd_{0,6}Mg_{0,4}F_2$ films
Source: compiled by the authors

Table 2. Parameters of energy bands CdF_2 and $Cd_{1-x}Mg_xF_2$

Parameters, eV	CdF_2	$Cd_{0,6}Mg_{0,4}F_2$
E_V	9.8	10.6
E_F	2.3	-
E_g	7.6	8.5
χ	2.2	2.1

Source: compiled by the authors

Table 3 lists the optical parameters (n and r) measured at a light wavelength of 1050 Å (UVE) for CdF_2 and $Cd_{0.6}Mg_{0.4}F_2$.

Table 3. Optical parameters of CdF_2 film and CdF_2 film $Cd_{0.6}Mg_{0.4}F_2$ measured at $\lambda = 1050$ Å

Optical parameters	CdF_2 d = 800 Å	$Cd_{0.6}Mg_{0.4}F_2$ d = 40-45 Å
n	1.6	1.5
r, %	9	11

Source: compiled by the authors

The E_g value of the three-component film is noticeably larger in comparison to the E_g of the CdF_2 film. Based on the data, the change in the Mg concentration correlates with the change in the band gap of the dielectric CdF_2 film [21; 22]. However, the x value could be varied in the range from 0.2 to 0.5 by implantation of Mg^+ ions followed by annealing. It can be seen from Table 3 that $Cd_{0.6}Mg_{0.4}F_2$ nanofilms do not significantly change the values of n and r for light with a wavelength of 1050 Å.

Similar studies have been conducted by other researchers. The paper [6] presents a systematic study on Cd1−xMgxTe thin film development via co-evaporation of CdTe and Mg. Deposition rates were adjusted to create films with varying stoichiometry and a wide range of band gaps (1.47 to 2.41 eV). Structural parameters varied systematically with Mg content, but XRD reflections remained similar to pure CdTe at lower Mg concentrations. XPS analysis shed light on Mg incorporation, supporting band gap variations seen in UVE–Vis spectroscopy. Mg consideration affected film photoresponse. A.M. Bothwell *et al.* [1] analysed photoluminescence, carrier lifetime, and quantum effectiveness, which showed enhancements when a shorter preheat time was utilized. Auxiliary particle mass spectrometry profiles showed that $CdCl_2$ passivation was protected when CdMgTe was briefly preheated. Moreover, extra gadgets were subjected to an HCl corrosive carve treatment and a CdTe cap layer, autonomously, after applying the CdMgTe layer. This was done to play down magnesium oxidation [23]. The CdTe cap gadget illustrated a beginning guarantee, accomplishing a gadget proficiency of 13.1%. The study conclusions [2] are comparative to those achieved in this research. There was a survey of the exploratory comes about on the consideration of the Si, GaAs, and CaF_2 surface layers that are made utilizing the low-energy particle implantation displayed. Optical and electron spectroscopy and microscopy are utilized within the tests.

Conclusions

The effect of the implantation of Mg^+ ions on the composition and electronic structure of single-crystal CdF_2/Si (III) films was studied for the first time. After heating at T = 900 K CdF_2 implanted with Mg^+ ions at $D = 8 \cdot 10\text{-}16$ cm^{-2}, a $Cd_{0.6}Mg_{0.4}F_2$ film with a thickness of 40-45 Å is formed. For this film, the value of E_g was ~ 8.5 eV. During the bombardment of CdF_2 with ions of inert gases Ar^+, CdF_2 is decomposed into components, the surface layers are disordered, the diffusion of atoms, the evaporation of atoms from the surface, etc. In the case of bombardment with Mg metal ions, these changes are accompanied by the introduction of metal atoms and the formation of various types of compounds. Most of the fluorine atoms escape into the vacuum, while the other part diffuses deep into the target; therefore, the concentration of F at a depth h = 80 – 100 Å increases significantly. A different picture is observed during the implantation of Mg^+ ions in CdF_2. Thus, CdF_2 is intensively decomposed into components in the near-surface layer in the process of ion implantation. A small portion of these components can be showered from the surface. Due to the prolonged chemical action, nearly all of the freed fluorine particles once more enter into a chemical bond with both the molecules of the alloying component and the molecules of cadmium. Thus, three-component compounds are shaped within the near-surface layer. The densities of electronic states, band energy, and optical parameters of CdF_2 and $Cd_{0.6}Mg_{0.4}F_2$ films have been determined. This effect can be interesting for application in optical memory cells. Further research may involve delving deeper into the mechanisms driving these changes, investigating the stability of the modified material under different conditions, and potentially optimizing the process for specific applications. Additionally, exploring the potential applications of the modified CdF_2 material in fields such as optoelectronics, photonics, or materials science could be a valuable avenue for future research. Photonics and optoelectronics have emerged as key disciplines in the advancement of technology, with vast potential for various applications. In recent years, there has been a growing interest in exploring the unique properties of two-dimensional materials and their integration into photonic and optoelectronic devices. This field holds great promise for revolutionizing several industries, including telecommunications, energy, sensing, and computing.

Acknowledgements

None.

Conflict of Interest

None.

References

[1] Bothwell AM, Drayton JA, Jundt P, Sites JR. CdMgTe as an electron reflector for MgZnO/CdSeTe/CdTe Solar Cells. IEEE 46th Photovoltaic Specialists Conference (PVSC). Chicago: IEEE; 2019. P. 149–154. DOI: 10.1109/PVSC40753.2019.8980651.

[2] Yao T, An X, Han H, Chen JQ, Li C. Photoelectrocatalytic materials for solar water splitting. *Adv Energy Mater*. 2018;8:1800210. DOI: 10.1002/aenm.201800210.

[3] Bekpulatov IR, Imanova GT, Kamilov TS, Igamov BD, Turapov IKh. Formation of n-type CoSi monosilicide film which can be used in instrumentation. *Int J Mod Phys B*. 2023;37(17):22350164. DOI: 10.1142/S0217979223501643.

[4] Tursunmetova ZA, Imanova GT, Bekpulatov IR. Method for low-temperature vacuum-thermal cleaning of surface single crystals Si and GaAs. *Journal of Polytechnic*, 2022;25(2):921–927. DOI: 10.2339/politeknik.1119884.

[5] Mahmudov H, Mahmudov HM, Suleymanov TY, Aliyev SM. Kinetics and mechanism of formation of gaseous products obtained by radiation-catalytic conversion of n-hexane on the surface of nano-ZrO_2. *J Radiat Res*. 2018;5(2):119–125.

[6] Palomera RC, Martínez OS, Pantoja-Enriquez J, Mathews NR, Reyes-Banda MG, Krishnan B, et al. Development and studies of $Cd_{1-x}Mg_xTe$ thin films with varying band gaps to understand the Mg incorporation and the related material properties. *Appl. Eng*. 2017;114:1169–1175. DOI: 10.1016/j.applthermaleng.2016.10.163.

[7] Hughes-Currie RB, Salkeld AJ, Ivanovskikh KV, Reid MF, Wells J-PR., Reeves RJ. Excitons and interconfigurational transitions in $CaF_2:Yb^{2+}$ crystals. *J Lumin*. 2015;158:197–202. DOI: 10.1016/j.jlumin.2014.09.050.

[8] Abduvaiitov AA, Boltaev KhKh. Composition of uncontrolled impurities and their chemical states and depth profiles at the Al-Si interface. *Tech Phys.* 2015;60(4):621. DOI: 10.1134/S1063784215040027.

[9] Dotan H, Mathews N, Hisatomi T, Gratzel M, Rothschild A. On the solar to hydrogen conversion efficiency of photoelectrodes for water splitting. *J Phys Chem Lett*. 2014;5(19):3330–3334. DOI: 10.1021/jz501716g.

[10] Shendrik R, Radzhabov E. Absolute light yield measurements on SrF_2 and BaF_2 doped with rare earth ions. *IEEE Trans Nucl Sci*. 2014;61(1):402–410.

[11] Izumi A, Kawabata K, Tsutsui K, Sokolov NS, Novikov SV, Khilko AYu. Growth of $CdF_2CaF_2Si(111)$ heterostructure with abrupt interfaces by using thin CaF2 buffer layer. *Appl Surf Sci.* 1996;104–105:417–421. DOI: 10.1016/S0169-4332(96)00180-8.

[12] Umirzakov BE, Tashmukhamedova DA, Muradkabilov DM, Boltaev KhKh. Electron spectroscopy of the nanostructures created in Si, GaAs, and CaF_2 surface layers using low-energy ion implantation. *Techn. Phys*. 2013;58(6):841–844. DOI: 10.1134/S1063784213060261.

[13] Mustafayev II, Mahmudov HM. Radiation-thermal desulphurization of organic fuels. *J Radiat Res.* 2015;2(2):65–70.

[14] Shchenlin AS, Kupchikov AK, Angervaks AE, Onopko DE, Ryskin AI, Ritus AI, et al. Radio-frequency response of semiconducting CdF_2: In crystals with Schottky barriers *Phys Rev B*. 2001;63:205207. DOI: 10.1103/PhysRevB.63.205207.

[15] Ryskin AI, Shcheulin AS, Angervaks AE. Semiconductor CdF_2:Ga and CdF_2:In crystals as media for real-time holography. *Materials,* 2012;5(5):784–817. DOI: 10.3390/ma5050784.

[16] Sokolov NS, Suturin SM. MBE growth of calcium and cadmium fluoride nanostructures on silicon. *Appl Surf Sci*. 2001;175–176:619–628. DOI: 10.1016/S0169-4332(01)00075-7.

[17] Hedin L. On correlation effects in electron spectroscopies and the GW approximation. *J Phys: Condens Matter Rev B*. 1999;11:R489. DOI: 10.1088/0953-8984/11/42/201.

[18] Denda J, Uryu K, Watanabe M. Resistance switching memory characteristics of $Si/CaF_2/CdF_2$ quantum-well structures grown on metal ($CoSi_2$) layer. *Jpn J Appl Phys.* 2013;52:04CJ07. DOI: 10.7567/JJAP.52.04CJ07.

[19] Jinen K, Kikuchi T, Watanabe M, Asada M. Room-temperature electroluminescence from single-period (CdF2/CaF2) inter-subband quantum cascade structure on si substrate. *J Appl Phys.* 2006;45:3656. DOI: 10.1143/JJAP.45.3656.

[20] Izumi A, Hirai Y, Tsutsui K, Sokolov NS. Study of band offsets in $CdF_2/CaF_2/Si(111)$ heterostructures using x-ray photoelectron spectroscopy. *Appl Phys Lett*. 1995;67:2792. DOI: 10.1063/1.114595.

[21] Valkovskiy GA, Durnev MV, Zamoryanskaya MV, Konnikov SG, Krupin AV, Moroz AV, et al. Investigation of the structure and luminescence properties of CdF_2-CaF_2: Eu superlattices on Si(111). *Phys Solid State*. 2013;55:1498–1504. DOI: 10.1134/S1063783413070330.

[22] Panov V. The scientific process of two interferometers (optical) development and the mitigation of external influence. *Sci Herald Uzhhorod Univ Ser Phys*. 2023;(53):19–30. DOI: 10.54919/physics/53.2023.19.

[23] Tsysar MO, Zakora AP, Babak AM, Ivakhnenko SO, Zanevsky OO. Dependence of the Static strength of type Ib single crystal diamonds with octahedral habit on their size. *Sci Herald Uzhhorod Univ Ser Phys*. 2021;50:25–30.

Вплив імплантації іонів Mg^+ та подальшого відпалу на склад, електронну структуру, емісійні та оптичні властивості CdF_2

Акбаржон Абдумаджидович Абдувайтов

Кандидат фізико-математичних наук
Ташкентський державний технічний університет імені Іслама Карімова
100095, вул. Університетська, 2, м. Ташкент, Узбекистан
https://orcid.org/0000-0001-6453-6523

Гунель Іманова

Кандидат фізичних наук, доцент
Інститут радіаційних проблем Міністерства науки і освіти Азербайджанської Республіки
AZ1143, вул. Б. Вагабзаде, 9, м. Баку, Азербайджан
Дослідницький центр сталого розвитку та зеленої економіки UNEC імені Нізамі Гянджеві
AZ1007, вул. Аббаса Саххата, 45A, м. Баку, Азербайджан
https://orcid.org/0000-0003-3275-300X

Дільноза Артикбаевна Ташмухамедова

Доктор фізико-математичних наук, професор
Ташкентський державний технічний університет імені Іслама Карімова
100095, вул. Університетська, 2, м. Ташкент, Узбекистан
https://orcid.org/0000-0001-5813-7518

Хуршид Хамідович Болтаєв

Кандидат фізико-математичних наук
Ташкентський державний технічний університет імені Іслама Карімова
100095, вул. Університетська, 2, м. Ташкент, Узбекистан
https://orcid.org/0000-0001-6453-6523

Болтаходжа Ерматович Умірзаков

Доктор фізико-математичних наук, професор
Ташкентський державний технічний університет імені Іслама Карімова
100095, вул. Університетська, 2, м. Ташкент, Узбекистан
https://orcid.org/0000-0002-9815-2111

Анотація

Актуальність. При бомбардування іонами металу Mg зміни супроводжуються впровадженням атомів металу та утворенням різного типу сполук. Таким чином, CdF_2 інтенсивно розкладається на компоненти в приповерхневому шарі в процесі іонної імплантації. Невелику частину цих компонентів можна розпорошувати з поверхні. Завдяки високій хімічній активності майже всі звільнені атоми фтору знову вступають у хімічний зв'язок як з атомами легуючого елемента, так і з атомами кадмію. Внаслідок цього в приповерхневому шарі утворюються трикомпонентні сполуки. Тому необхідно визначити електронні стани, визначено зонно-енергетичні та оптичні параметри плівок CdF_2 та Cd_0, $6Mg_0$, $4F_2$.

Мета. У цій роботі вперше досліджено склад, структуру та властивості CdF_2, імплантованого іонами Mg^+, у поєднанні з термічним та лазерним відпалом.

Методологія. Експериментальні дослідження проводили в умовах вакууму не менше 10-7 Па методами електронної спектроскопії (AES) та ультрафіолетової фотоелектронної спектроскопії (UVES). Профілі розподілу атомів по глибині визначали методом AES у поєднанні з пошаровим травленням поверхні іонами Ar+ з E_0 = 2-3 кеВ.

Результати. CdF_2 інтенсивно розкладається на компоненти в приповерхневому шарі в процесі іонної імплантації. Внаслідок цього в приповерхневому шарі утворюються трикомпонентні сполуки. Визначено зонно-енергетичні параметри та густини станів електронів у валентній зоні цієї плівки.

Висновки. Вперше досліджено вплив імплантації іонів Mg^+ на склад та електронну структуру монокристалічних плівок CdF_2/Si(III). Визначено густини електронних станів, зонно-енергетичні та оптичні параметри плівок CdF_2 та Cd_0, $6Mg_0$, $4F_2$.

Ключові слова: профілі розподілу атомів; надтонкі шари; заборонена зона; термообробка; поверхневий шар

Scientific Herald of Uzhhorod University
Series "Physics"

Journal homepage: https://physics.uz.ua/en
Issue 54, 36–46
Received: 16.08.2023. Revised: 20.11.2023. Accepted: 18.12.2023

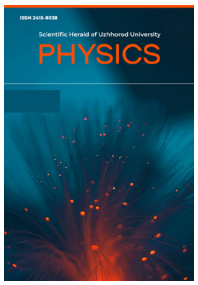

UDC 547
PACS 68.49.Uv
DOI: 10.54919/physics/54.2023.36

The appearance of standing wave structures in the reaction medium during the diffusion development of the chain reaction process

Garnik Sargsyan*
PhD in Physical and Mathematical Sciences, Senior Researcher
A.B. Nalbandyan Institute of Chemical Physics
of the National Academy of Sciences of the Republic of Armenia
0014, 5/2 Paruyr Sevak Str., Yerevan, Republic of Armenia
https://orcid.org/0000-0002-4832-0623

Anatolii Silveistr
Doctor of Pedagogical Sciences, Professor
Vinnytsia Mykhailo Kotsiubynskyi State Pedagogical University
21001, 32 Ostrozhsky Str., Vinnytsia, Ukraine
https://orcid.org/0000-0002-3633-3910

Mykhailo Lysyi
PhD in Physical and Mathematical Sciences, Associate Professor
Vinnytsia National Technical University
21021, 95 Khmelnytske Highway, Vinnytsia, Ukraine
https://orcid.org/0000-0002-5155-966X

Mykola Mokliuk
PhD in Pedagogical Sciences, Associate Professor
Vinnytsia Mykhailo Kotsiubynskyi State Pedagogical University
21001, 32 Ostrozhsky Str., Vinnytsia, Ukraine
https://orcid.org/0000-0002-8717-5940

Hrachya Sargsyan
PhD in Physical and Mathematical Sciences, Senior Researcher
A.B. Nalbandyan Institute of Chemical Physics
of the National Academy of Sciences of the Republic of Armenia
0014, 5/2 Paruyr Sevak Str., Yerevan, Republic of Armenia
https://orcid.org/0009-0006-4188-158X

Abstract

Relevance. Understanding the dynamic behavior of radicals in reactors undergoing gas-phase oxidation of organic substances is crucial for optimizing reactor design and safety across industries.

Suggested Citation:
Sargsyan G, Silveistr A, Lysyi M, Mokliuk M, Sargsyan H. The appearance of standing wave structures in the reaction medium during the diffusion development of the chain reaction process. *Sci Herald Uzhhorod Univ Ser Phys.* 2023;(54):36–46. DOI: 10.54919/physics/54.2023.36

*Corresponding author

Purpose. This study aims to elucidate the emergence of standing wave structures influenced by feedback mechanisms in reactors with cylindrical and spherical symmetry, using mathematical principles governing the propagation of oscillations and shock waves in diffusion-driven chain reactions.

Methodology. Materials and methods for the research included a computer simulation using MATHCAD 2001i, and comparative analysis of experimental data obtained from reactor experiments. The computational modeling revealed vivid formations of standing wave structures in reactors influenced by feedback mechanisms.

Results. The impact of reverse connections in reactors with cylindrical and spherical symmetry significantly contributed to the formation of various standing wave structures of radical concentrations within the reaction zone. It was found that these structures were largely imperceptible visually and could only be observed when the reaction was accompanied by intense light emission. These visual representations served as compelling evidence of the intricate interplay between reaction kinetics and feedback effects. The study emphasized the importance of understanding and predicting the root causes of instabilities, ultimately enhancing the reliability and safety of reactors across various industries. The results demonstrated a correlation between specific feedback mechanisms and the spatial distribution of standing wave structures.

Conclusions. The derived computational patterns, as presented in this paper, provide compelling evidence supporting the feasibility of standing wave structure formation within reactors when influenced by feedback mechanisms. The study unveiled the potential for fine-tuning reactor parameters to influence the formation and stability of these structures. The findings represented a significant stride towards a more comprehensive understanding of dynamic regimes in reactors, with implications for reactor design, operation, and safety protocols. The insights garnered from uncovering standing wave structures influenced by feedback mechanisms offered valuable opportunities to optimize reactor design and operational safety, leading to more efficient and sustainable processes.

Keywords: oxidation; back bonding; modeling of dynamic modes; radicals; oscillatory phenomena; stationary process

Introduction

The study of standing wave structures within reaction mediums is of paramount relevance in chemical engineering and reactor dynamics, holding substantial implications for reactor design and safety. The inhibitory effect of formaldehyde on oxidation reactions introduces complexity, prompting an inquiry into whether inhibition alone leads to the emergence of feedback mechanisms capable of establishing oscillatory modes within the system.

Combined with recent advances in understanding the complexity of low-temperature oxidation processes in confined spaces, it has become increasingly important to combat the emergence of nonlinear relationships. Research by C. Lin *et al.* demonstrated the effects of nonlinear reaction kinetics and large inelastic strain on the oxidation process, further emphasizing the importance of understanding nonlinear relationships in oxidation reactions [1]. Moreover, recent studies of these authors shed light on how pulsation phenomena can occur as a result of the interaction of the intermediates with concentrated ionic complexes near the surface, resulting in the generation of subtle shock waves [2]. Such discoveries as T. Abrahamyan *et al.*, have profound implications not only for the operational integrity and efficiency of reactors using chain processes, but also for basic scientific research aimed at mastering these complex processes [3]. Oscillatory phenomena, including concentration and temperature fluctuations, are key issues in the field of industrial chain processes. In the context of standing wave structures, it is notable that it can lead to the development of functional gradients in which the concentration or activity of a particular component exhibits spatial variations.

This phenomenon is of particular importance in applications such as synthetic biology, where precise spatial organization is critical to the functionality of the system as wrote S. Kretschmer *et al.* [4]. Accordingly, researchers as E. Villar-Sepúlveda & A.R. Champneys are devoting themselves to studying the spatial arrangement and dynamic behavior of radicals in standing wave structures with the main goal of improving reactor design and increasing its operational safety [5]. The focus is on understanding the specific conditions and underlying mechanisms that lead to the formation of these distinctive structures. The implications of this research extend to improving reactor design and operational safety of processes involving gas-phase oxidation reactions. By revealing the spatial arrangement of radicals and the dynamic interactions, valuable information can be obtained to optimize reaction parameters, improve efficiency,

and ensure safe operations. Obtaining comprehensive information and the ability to predict these phenomena is of paramount importance for reactor protection, especially in critical areas such as chemistry. In this regard, there is an urgent need for model studies focused on processes characterized by chain development as D. Gaskins *et al*. mentioned [6]. This endeavor serves a dual purpose: to anticipate and proactively develop complex processes in key sectors such as chemical engineering, energy, biology and various fields of human activity.

In light of these considerations, this study harnesses the mathematical framework governing the birth and propagation of oscillations and shock waves within diffusion-driven chain reactions. The primary aim is to delve into the establishment of standing wave structures of radicals within reactors immersed in the gas-phase oxidation of organic substances. Through this comprehensive inquiry, an effort is being made to enhance the comprehension of the dynamic behavior of radicals and spatial organization, ultimately contributing to the advancement of reactor design and operational safety.

Materials and Methods

Prior to commencing the experimental phase, an extensive review of existing literature was conducted. This involved a thorough examination of scientific publications, articles, monographs, and reports, providing a comprehensive overview of the current state of the issue surrounding the formation of structures of standing waves of radicals in reactors engaged in gas-phase oxidation of organic substances. Notably, key theoretical and experimental studies in this domain, along with the respective findings, were underscored [2; 7].

The computer modeling was executed utilizing the MATHCAD 2001i software package to validate theoretical concepts and scrutinize the behavior of the reaction medium. Within this endeavor, a mathematical model was crafted, encompassing equations elucidating the diffusion propagation of the chain reaction and the emergence of structures of standing waves of radicals. By employing MATHCAD 2001i, the numerical solution of a system of differential equations was achieved, alongside the capacity to visualize outcomes through graphs and diagrams. Following the computer modeling phase, the results thus obtained underwent a meticulous comparative analysis. This step involved a rigorous examination to ascertain the congruence or disparities between the modeled data and existing empirical evidence or theoretical predictions, thereby ensuring the robustness and accuracy of the model.

The study used mathematical modelling. The model consideration is carried out within the framework of the theory of diffusion propagation of particles with reproduction in limited volumes. The solution to the problem is reduced to solving the equation:

$$u_t = a^2\Delta u + \beta u - \text{inside the T area}, \qquad (1)$$

where: u – concentration of active particles;$a^2 = D/c$; D – diffusion coefficient of active particles; c – porosity of the medium (in case of gas medium $c = 1$); β – reproduction rate; Δ Laplace operator.

With initial and boundary conditions:

$$u(M, 0) = \varphi(M), u_\epsilon = 0. \qquad (2)$$

As a result, a function was obtained [8]:

$$u(M, T) = \sum_{n=1}^{\infty} C_n e^{(\beta - a^2\lambda_n)t} v_n(M), \qquad (3)$$

where: C_n – number describing a curve, the contour of an arc, but in this work the behavior of the concentration of active particles depending on time and space due to periodic changes in the properties of the reaction medium is also important; λ_n – characteristic parameter which, in the case of a reactor with spherical symmetry, has the form:

$$\lambda_1 = \left(\frac{\pi}{R}\right)^2. \qquad (4)$$

The use of this formula to solve the problem is more convenient, since it allows to present the complex problem of the relationship of chain oxidation processes in the most convenient way to find a qualitative picture of the influence of unnecessary connections on the type of dynamic regime in the system. Namely, the appearance of an inhibitor that destroys the leading chain radical leads to the formation of a periodic decrease and restoration of the rate of reproduction during the diffusion of active particles, by representing the coefficient β as a value periodically varying with time, namely $\beta^*|\sin(t)|$. In this approximation, equation (1) can be represented as:

$$u(M, T) = \sum_{n=1}^{\infty} C_n e^{(\beta|\sin(t)| - a^2\lambda_n)t} v_n(M). \qquad (5)$$

For simplicity, it is being considered the case of $n = 1$ and a spherically symmetric reactor. In this case, equation (2) is represented as:

$$u(M,T) = const * e^{(\beta|\sin(t)| - D*\left(\frac{\pi}{R}\right)^2)t} * \frac{\sin\left(\frac{r}{R}\right)}{\frac{r}{R}}. \qquad (6)$$

In this work, interest is focused not so much on obtaining exact numerical values characterizing the reaction, but rather on finding the range of values of these parameters leading to the establishment of standing wave structures in reactors during technological processes based on chain reactions.

Results

The investigation into the emergence of standing wave structures within the reaction medium during the progression of the diffusion-driven chain reaction process yielded compelling findings. These results provide valuable insights into the dynamic interplay of radicals and spatial organization within the reactor. To begin, it is essential to highlight the distinctive patterns and characteristics observed in the standing wave formations, shedding light on the underlying mechanisms. A quantitative analysis of key parameters, such as wave amplitude and frequency, serves to elucidate influence on the overall reaction kinetics.

The results are summarized below provide a comprehensive visual representation of the dynamic oxidation reaction of organic compounds within reactors possessing both spherical and cylindrical symmetry. This dynamic process is influenced by the presence of an inhibitory factor, either in the form of an intermediate product or through the occurrence of periodic shifts in concentration along the radical chain within the reactor wall layer.

The calculations are based on formula (2), which accommodates the introduction of an inhibitor – either an intermediate or final product of the reaction. This inhibitor exerts a significant influence on the leading chain radical, resulting in a temporary reduction in reaction rate. In cases where feedback occurs, periodic variations may manifest. This behavior is quantified by modifying the parameter β with the function $|\sin(t)|$, signifying its prevalence throughout the entire volume. Alternatively, in scenarios characterized by concentrated feedback near the reactor periphery, a factor denoted $\alpha \cdot |\sin(t)|$as is subtracted from the reactor's diameter (in the case of spherical symmetry) or radius (in the case of cylindrical symmetry). This signifies a periodic contraction of the reactor's dimensions, reflecting the feedback's spatial extent. This nuanced consideration expands the understanding of the intricate interplay between reaction kinetics and inhibitor-induced dynamics.

Periodic inhibition of a process by a reaction intermediate

In the existing literature, instances have been reported where the presence of excited formaldehyde molecules, an intermediate product of the acetaldehyde oxidation reaction, disrupts the leading radical chain, resulting in the onset of an oscillatory regime in the system [7]. This phenomenon is attributed to quantum resonance, wherein the excitation energy of formaldehyde is transferred from the leading chain to the CH_3CO_3 radical, a phenomenon detailed in theoretical studies. Empirical data affirms that the introduction of formaldehyde molecules from an external source exerts an inhibitory influence on the oxidation reaction. This effect is ascribed to the conversion of highly active radicals into less reactive species. Nevertheless, it's important to note that mere inhibition does not automatically result in the development of feedback mechanisms that can induce oscillatory dynamic modes within the system. Previous works primarily addressed scenarios involving the appearance of excited formaldehyde molecules, which were more likely to induce the formation of cold flames [2; 7]. Through simulations focusing on the generation of highly vibrationally excited formaldehyde molecules via heterogeneous recombination, a diverse range of feedback modes and intriguing phenomena were observed.

Particularly noteworthy is the proposition that feedback is concentrated near the surface, prompting inquiries into its broader impact on the overall volumetric process. This innovative perspective promises to deepen understanding of the intricate interplay between inhibition, feedback, and overall reactor dynamics. The calculation results using the MATHCAD 2001i program are shown in the Figure 1.

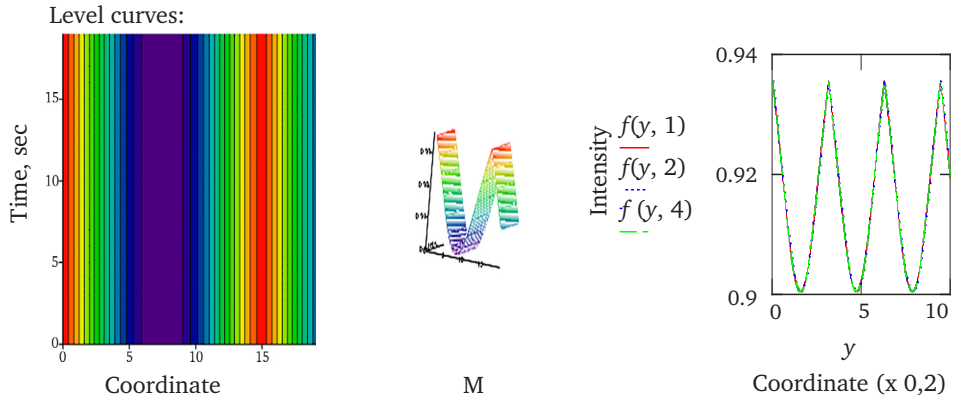

Figure 1. Establishment of the structure of standing waves in a spherical reactor due to feedback at the reactor walls calculated using the MATHCAD 2001i program
Note: according to the formula: $u(r, t) = j_s(0, \pi/(5\text{-}|\sin(t)|))$; r – coordinate; t – time
Source: developed by the authors

In the context of the stationary reaction mode, characterized by the condition $\beta - a^2\lambda_n = 0$ in equation (1), and with the radius subject to periodic variations described by $R - |\sin(t)|$, a discernible phenomenon emerges. The visual representation vividly illustrates the establishment of a standing wave structure within a reactor exhibiting spherical symmetry. This dynamic portrayal underscores the critical interplay between parameters β, α, and λ_n, demonstrating pivotal roles in shaping the distinctive patterns observed. As the reactor's radius oscillates in a periodic manner, the resulting spatial variations give rise to the formation of these intriguing standing waves [8].

While this structural phenomenon may not be readily discernible to the naked eye, it becomes detectable through sensitive sensors if the reaction is accompanied by light emission, particularly in the IR, UV, or visible spectrums. This visual insight provides a valuable perspective on the system's behavior in response to the interplay of reaction kinetics and feedback mechanisms [9]. This observation underscores the significance of specialized detection methods in revealing hidden structural intricacies within reactors. Valuable insights into the dynamic behavior of radicals and spatial organization, which are otherwise imperceptible through visual inspection alone, can be gleaned by harnessing sensitive sensors. This deeper understanding holds substantial implications for enhancing the monitoring and optimization of reactions in spherical reactors.

Periodic development of the inhibitor in the reaction medium of a spherical reactor

Figure 2 and 3 depict the outcomes of computations elucidating the impact of feedback mechanisms within the system on the reaction medium. This phenomenon leads to the emergence of a distinct standing wave structure within a reactor characterized by spherical symmetry. Notably, these visual representations showcase varying sets of characterizing parameters, providing a comprehensive view of the system's response to different conditions.

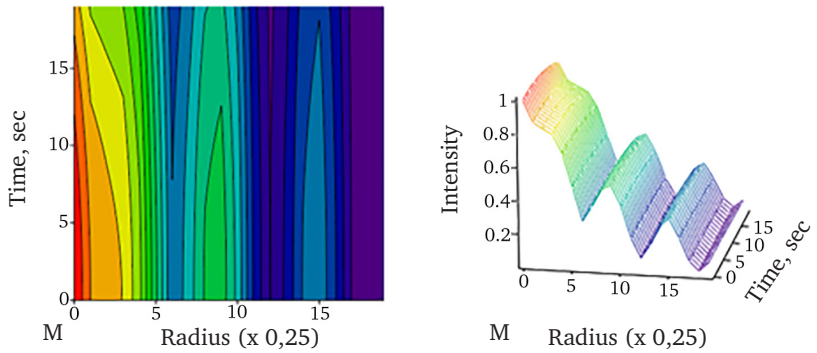

Figure 2. The structure of standing waves in the medium of a reactor with spherical symmetry in the case of the presence of nonlinear coupling in the reactor at the value of the characteristic parameters calculated using the MATHCAD 2001i program

Note: according to the formula: $u(r,t) = e^{\left(0.5*|\sin(2t)|-\frac{\pi^2}{25}\right)*t} * j_s(0,\frac{r}{5})$
Source: developed by the authors

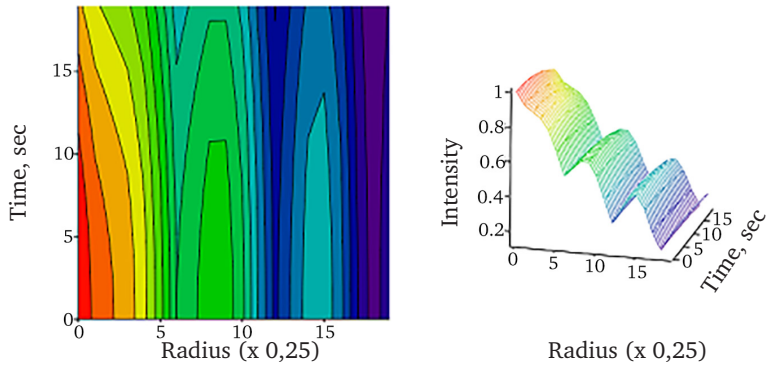

Figure 3. The structure of standing waves in the medium of a reactor with spherical symmetry in the case of the presence of nonlinear coupling in the reactor at the value of the characteristic parameters calculated using the MATHCAD 2001i program

Note: according to the formula: $u(r,t) = e^{\left(0.2*|\sin(2t)|-\frac{\pi^2}{25}\right)*t} * j_s(0,\frac{r}{5})$
Source: developed by the authors

Figures depict the formations of standing wave structures within a reactor exhibiting spherical symmetry. These structures arise in scenarios where nonlinear coupling is present, and are calculated based on the specified characteristic parameters detailed in the accompanying calculation formulas.

In these specific cases, the simulation accounts for the influence of feedback extending uniformly throughout the entire reactor volume. This dynamic process involves the periodic oscillation of the concentration of active leading radicals, with due c onsideration to the diffusion [10]. Consequently, this intricate interplay culminates in the establishment of a structured pattern of active radicals within the spherical reactor. These figures serve as a crucial visual testament to the sensitivity of the reaction dynamics to changes in the governing parameters. The nuanced variations in these parameters yield unique patterns and shapes in the standing wave structures, underscoring the intricate interplay between reaction kinetics and feedback effects. This comprehensive understanding further advances grasp of the system's behavior under diverse operational scenarios.

Periodic mode, concentrated near the surface of a cylindrical reactor

In the illustration below, it can be observed the distinctive structural patterns within a cylindrical reactor, specifically in the scenario where feedback manifests along the surface layer (Fig. 4). These results were obtained through computations using the MATHCAD 2001i program, utilizing specified values for the characteristic parameters. The formulation used for these calculations provides further context regarding the parameters that govern this intricate process.

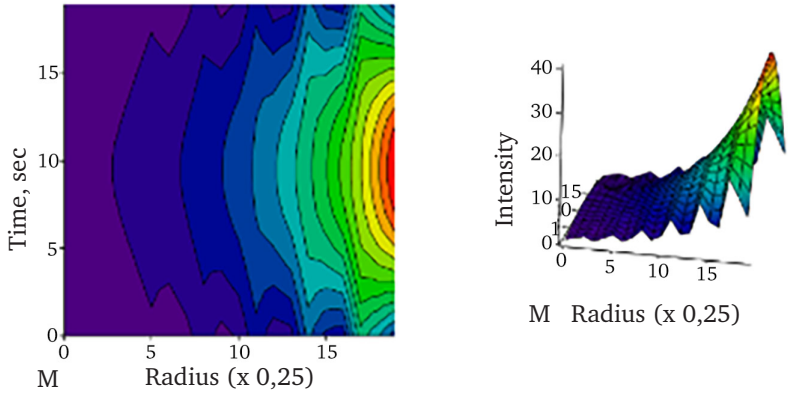

Figure 4. Formation of a structure of standing waves of concentration radicals in the case of a reactor with cylindrical symmetry at the value of the characteristic parameters calculated using the MATHCAD 2001i program

Note: according to the formula: $u(y,t) = e^{0.15*t} * 2 * J_0\left(\frac{2.4045*r}{10-4|cos(8t)|}\right)$

Source: developed by the authors

From the depicted image, it is evident that in a reactor with cylindrical symmetry, the presence of feedback leads to the establishment of a standing wave structure within the reactor volume. This observation underscores the profound impact of feedback mechanisms on the dynamic behavior of the system. Understanding the emergence of standing wave structures in reactors with cylindrical symmetry is crucial for gaining insights into the complex interplay between reaction kinetics and feedback effects. This phenomenon has significant implications for the optimization and control of processes in such reactors.

When dynamic modes are studied and the effectiveness and safety are assessed, a significant contribution can be made by recording the wave structures of radicals in the reactor if feedback occurs in the system due to the inhibition of the reaction by intermediate or final excited reaction products. In areas where the concentration of radicals is at its maximum, there is a high likelihood that the reaction radiation will be more intense. Consequently, a striped pattern can be obtained during registration allowing for the extraction of information about the nature of feedback in the reactor.

This study demonstrates the profound influence of feedback mechanisms on the spatial organization of radicals within reactors of varying symmetries. Through rigorous computational modeling and analysis, standing wave structures were observed to emerge in reactors with both spherical and cylindrical symmetry. These patterns were shown to be highly sensitive to changes in characteristic parameters, showcasing the intricate interplay between reaction kinetics and feedback effects. Additionally, the presence of nonlinear coupling in reactors with spherical symmetry further enriched the complexity of standing wave formations [11]. These findings provide valuable insights for optimizing and controlling reactions in diverse reactor configurations.

Discussion

This work introduces a novel approach, leveraging a mathematical method from existing literature to describe the propagation of chain reactions in confined volumes during the diffusion of an unstable gas. This approach provides insights into the establishment of dynamic regimes featuring standing wave structures in the system. Throughout the research, particularly noteworthy results have been obtained for the first time, shedding light on the influence of external conditions (such as heat removal, presence of excited particles, and alterations in surface properties of reaction vessels), often manifesting as feedback on systems with a chain development mechanism.

An additional point of interest lies in understanding the state of the reaction medium based on the specific structure of standing waves. By delving into this aspect, it becomes possible to anticipate the type and location of feedback within the reactor. The work of G. Sargsyan *et al*. cited elucidate the phenomenon of feedback formation near the reactor wall layer [7]. This study reveals that the presence of active centers at the vessel walls leads to the generation of excited formaldehyde molecules, which act as destructive agents for active radicals, particularly the leading chains of CH_3CO_3. This, in turn, gives rise to concentration fluctuations of these radicals in the near-surface layer of the reactor. This work, in particular, scrutinizes the impact of oscillations within the near-surface layer on the overall reactor process. The challenge is addressed by resolving the considerations of a stationary process within a reactor featuring a dynamically changing radius, specifically in cases of reactors with spherical symmetry. When the concentration of CH_3CO_3 radicals diminishes due to interactions with excited formaldehyde molecules, it is postulated that the reactor's radius contracts in proportion to the penetration depth of excited formaldehyde molecules facilitated by diffusion.

The studies outlined above provide valuable parallels and insights that complement this investigation into standing wave structures in reaction media during the diffusion-driven chain reaction process. Several key considerations for future research endeavors can be gleaned from these findings. This work aligns with the study of C.T. Hamik & O. Steinbock that explores excitation waves in reaction-diffusion media with non-monotonic dispersion relations [12]. The observations revealed the presence of rotating spiral waves and target patterns in two-dimensional excitable systems. Comparisons between results could shed light on potential commonalities and offer a basis for refining mathematical models. Another work by S. Hata *et al*. established essential conditions for wave instability in general three-component reaction-diffusion systems [13]. These conditions, expressed in terms of the Jacobian matrix of the system's uniform steady state, provide a means to determine the potential observability of wave instability with the gradual increase of species mobility. This insight can be instrumental in refining understanding of the stability and dynamics of standing wave structures, providing criteria for the emergence. In a different approach K. Regenauer-Lieb *et al*. proposed the universality of dissipative wave phenomena in Thermo-Hydro-Mechanical-Chemical (THMC) reaction-diffusion systems that operate far from equilibrium [14]. It introduced an updated formulation for chemical systems, contending that the wave operator must incorporate non-local reaction-diffusion equations. Further research could explore the applicability of this universal concept to specific context, potentially uncovering additional insights into the underlying mechanisms.

The study of D. Cuiñas *et al*. investigated the transition from traveling to standing waves in a reaction-diffusion system as a function of frequency [15]. The researchers noted that a further increase in frequency led to yet another transition, this time resulting in bulk oscillations. Future studies based on this may delve deeper into the underlying factors influencing such transitions, potentially shedding light on the nuanced interplay of feedback mechanisms in this specific system. The work of C. Hamster & P. van Heijster elucidated how stochastic patterns arising from the stochastic cell motility model equation can be harnessed to comprehend experimentally observed dynamics, particularly those pertaining to waves [16]. Understanding how stochasticity influences wave dynamics may provide valuable insights into the robustness and adaptability of standing wave structures in response to environmental perturbations. Incorporating these comparative considerations into future research endeavors holds promise for refining understanding of standing wave structures in reaction media. Additionally, it is worth noting that while the study primarily focuses on reactors with gas-phase oxidation of organic substances, the insights gained have broader implications [17]. The emergence of standing wave structures, influenced by feedback mechanisms, extends to various reaction-diffusion systems [18]. Exploring the universality of these phenomena across different contexts could open avenues for interdisciplinary research and applications in fields beyond chemical engineering.

This study highlights the importance of considering external conditions and feedback effects when designing and operating reactors. The ability to predict and control standing wave structures provides a valuable tool for optimizing process efficiency and ensuring safety [19]. This has direct relevance to industries where precise control of chemical reactions is paramount, such as in pharmaceuticals, petrochemicals, and environmental engineering. In terms of future research directions, a deeper investigation into

the role of specific feedback mechanisms and interactions with different reaction pathways could yield further insights. Additionally, exploring the potential for dynamic control of standing wave structures, for example, through modulation of external conditions, presents an intriguing avenue for enhancing process flexibility and performance.

The experimental validation of the computational models and theoretical frameworks proposed in this study would be a crucial step towards real-world application. Conducting experiments to observe and quantify standing wave structures in practical reactor setups would provide empirical support for the theoretical findings. The study not only advances understanding of standing wave structures in reactors with gas-phase oxidation but also lays the groundwork for broader applications in reaction-diffusion systems [20-22]. Improved reactor design and operation, with implications for a wide range of industries, can be achieved by considering feedback mechanisms and external conditions [23; 24]. Future research avenues include exploring specific feedback mechanisms, dynamic control strategies, and experimental validation of theoretical models. investigating the potential integration of advanced computational techniques, such as machine learning algorithms, could offer a powerful tool for predicting and optimizing standing wave structures in complex reaction-diffusion systems, further enhancing the precision and efficiency of reactor operations.

Conclusions

The approach proposed in this study, specifically the use of a mathematically developed method, highlights the intricacies of establishing dynamic regimes with standing wave structures in the system. The research yielded novel and compelling insights into the impacts of external conditions, such as heat dissipation, excited particles, and changes in the surface properties of reaction vessels, often manifesting as feedback mechanisms on the dynamic behavior of chain reaction systems. A particularly noteworthy aspect explored in this work is the influence of oscillation phenomena in the near-surface layer on the overall reactor process.

The problem was addressed by considering the stationary process in a reactor with a changing radius, as in the case of a reactor with spherical symmetry. When the concentration of CH_3CO_3 radicals minimizes due to interaction with excited molecules of formaldehyde, it is assumed that the reactor radius decreases by the penetration depth of excited formaldehyde molecules due to diffusion. It becomes evident that localized feedback near the reactor walls can lead to the formation of standing wave structures within the reactor. From the presented material, it can be inferred that the registration of radical wave structures in the reactor, especially when feedback is present due to the inhibition of the reaction by intermediate or final excited reaction products, can significantly contribute to understanding dynamic regimes and assessing their efficiency and safety. Areas with maximum radical concentrations exhibited more intense reaction emissions, and therefore, the registration of such patterns can provide a striped representation.

This approach offers valuable information about the nature of feedback mechanisms in the reactor. The investigation of dynamic regimes and the evaluation of their efficiency and safety can benefit significantly from the registration of radical wave structures in the reactor. Future research directions could involve exploring different reactor geometries, varying external conditions, and expanding the understanding of the intricate interplay between feedback mechanisms and the formation of standing wave structures. This work lays the foundation for further studies in the field, providing a basis for refining reactor design and optimizing processes in chemical engineering applications.

Acknowledgements

None.

Conflict of Interest

None.

References

[1] Lin C, Jiang J, Ruan H, Ma X. Investigation of non-uniform oxidation based on a mechanochemical phase field model with nonlinear reaction kinetics and large inelastic deformation. *npj Mater Degrad*. 2023;7:57. DOI: 10.1038/s41529-023-00376-z.

[2] Sargsyan G, Evinyan M, Gukasyan P, Sargsyan H. Modeling of hydrocarbons and hydrogen oxidation in the presence of surface-active centers water-negative halogen ion in terms of the formation of weak shock waves. *J Contemp Phys*. 2022;57:297-302. DOI: 10.1134/S1068337222030148.

[3] Abrahamyan T, Haroyan H, Hambaryan D, Parsamyan H, Babajanyan A, Lee K, *et al*. Surface-standing-wave formation via resonance interaction of a finite-length conductive rod with microwaves. *J Phys D Appl Phys*. 2022;55:445001. DOI: 10.1088/1361-6463/ac8e14.

[4] Kretschmer S, Heermann T, Tassinari A, Glock P, Schwille P. Increasing MinD's membrane affinity yields standing wave oscillations and functional gradients on flat membranes. *ACS Synth Biol.* 2021;10(5):939–949. DOI: 10.1021/acssynbio.0c00604.

[5] Villar-Sepúlveda E, Champneys AR. General conditions for Turing and wave instabilities in reaction-diffusion systems. *J Math Biol*. 2023;86:39. DOI: 10.1007/s00285-023-01870-3.

[6] Gaskins D, Soohoo J, Dolnik M, Epstein I. Birth and death of invading standing waves in the BZ-AOT reaction-diffusion system. *Israel Journal of Chemistry*. 2018;58(6–7):776–780. DOI: 10.1002/ijch.201700142.

[7] Sargsyan GN, Yessayan RS, Vardanyan IA. Analysis of heterogeneous homogeneous model, describing oscillations in system CH_3CHO+O_2. *Appl Catal A*. 2000;203(2):285–291. DOI: 10.1016/S0926-860X(00)00488-9.

[8] Berenstein I, Beta C. Spatiotemporal chaos arising from standing waves in a reaction-diffusion system with cross-diffusion. *J Chem Phys.* 2012;136(3):034903. DOI: 10.1063/1.3676577.

[9] Lim S. Mechanisms underlying sharpening of visual response dynamics with familiarity. *Neurosci.* 2019;8:e44098. DOI: 10.7554/eLife.44098.001.

[10] Hu H, Li X, Fang Zh, Fu X, Ji L, Li Q. Inducing and modulating spiral waves by delayed feedback in a uniform oscillatory reaction-diffusion system. *Chem Phys.* 2010;371:60–65. DOI: 10.1016/j.chemphys.2010.04.004.

[11] Lansdell B, Ford K, Kutz JN. A reaction-diffusion model of cholinergic retinal waves. *PLOS Comput Biol*. 2014;10(12):e1003953. DOI: 10.1371/journal.pcbi.1003953.

[12] Hamik CT, Steinbock O. Excitation waves in reaction-diffusion media with non-monotonic dispersion relations. *New J Phys.* 2003;5:58.1–58.12.

[13] Hata S, Nakao H, Mikhailov AS. Sufficient conditions for wave instability in three-component reaction–diffusion systems. *Prog Theor Exp Phys*. 2014;1:013A01. DOI: 10.1093/ptep/ptt102.

[14] Regenauer-Lieb K, Hu M, Schrank C, Chen X, Clavijo SP, Kelka U, *et al*. Cross-diffusion waves resulting from multiscale, multi-physics instabilities: Theory. *Solid Earth*. 2021;12:869–883. DOI: 10.5194/se-12-869-2021.

[15] Cuiñas D, Berenstein I, Carballido-Landeira J, Muñuzuri A. Transition from traveling to standing waves as a function of frequency in a reaction-diffusion system. *J Chem Phys.* 2008;128:244907. DOI: 10.1063/1.2946697.

[16] Hamster C, van Heijster P. Waves in a stochastic cell motility model. *Bull Math Biol*. 2023;85(8):70. DOI: 10.1007/s11538-023-01164-1.

[17] Bianchi F, Kurtén Th, Riva M, Mohr C, Rissanen MP, Roldin, P, *et al*. Highly oxygenated organic molecules (HOM) from gas-phase autoxidation involving peroxy radicals: A key contributor to atmospheric aerosol. *Chem Rev*. 2019;119(6):3472–3509. DOI: 10.1021/acs.chemrev.8b00395.

[18] Li, BW, He Y, Li LD, Yang L, Wang X. Spiral wave chimeras in reaction-diffusion systems: Phenomenon, mechanism and transitions. *Commun Nonlinear Sci Numer Simul.* 2021;99:105830. DOI: 10.1016/j.cnsns.2021.105830.

[19] Xu Z, Ren Y, Deng X, Xu M, Chai W, Qian X, *et al*. Recent developments on gas-phase volatile organic compounds abatement based on photocatalysis. *Adv Energy Sustainability Res*. 2022;3(11):2200105. DOI: 10.1002/aesr.202200105.

[20] Salo V, Valiev R, Lehtola S, Kurtén Th. Gas-phase peroxyl radical recombination reactions: A computational study of formation and decomposition of tetroxides. *J Phys Chem*. 2022;126(25): 4046–4056. DOI: 10.1021/acs.jpca.2c01321.

[21] Cardona, AL, Gibilisco, RG, Rivela, CB, Blanco MB, Patroescu-Klotz I, Illmann N, *et al*. Kinetics, product distribution and atmospheric implications of the gas-phase oxidation of allyl sulfides by OH radicals. *Chemosphere*. 2022;288(2):132546. DOI: 10.1016/j.chemosphere.2021.132546.

[22] Subramanian S, Murray SM. Pattern selection in reaction diffusion systems. *Phys Rev E.* 2021;103 (1–1):012215. DOI: 10.1103/PhysRevE.103.012215.

[23] Sargsyan G, Gukasyan P, Sargsyan H, Poveda R. Diffusion flames and a semi-empirical method for estimating the distribution of hydrogen molecules in propane flames. *Sci Herald Uzhhorod Univ Ser Phys*. 2023;53:42–52. DOI: 10.54919/physics/53.2023.42.

[24] Bobyr SV. Development and application of a simple model for calculating the quantum diffusion parameters of rubidium, hydrogen, and deuterium atoms. *Sci Herald Uzhhorod Univ Ser Phys*. 2021;49:19–25.

Поява стоячих хвильових структур у реакційному середовищі під час дифузійного розвитку ланцюгової реакції

Гарнік Норайрович Саргсян

Кандидат фізико-математичних наук, старший дослідник
Інститут хімічної фізики ім. А.Б. Налбандяна Національної академії наук Республіки Вірменія
0014, вул. Паруйра Севака, 5/2, м. Єреван, Республіка Вірменія
https://orcid.org/0000-0002-4832-0623

Анатолій Миколайович Сільвейстр

Доктор педагогічних наук, професор
Вінницький державний педагогічний університет імені Михайла Коцюбинського
21001, вул. Острозького, 32, м. Вінниця, Україна
https://orcid.org/0000-0002-3633-3910

Михайло Вікторович Лисий

Кандидат фізико-математичних наук, доцент
Вінницький національний технічний університет
21021, Хмельницьке шосе, 95, м. Вінниця, Україна
https://orcid.org/0000-0002-5155-966X

Микола Олексійович Моклюк

Кандидат педагогічних наук, доцент
Вінницький державний педагогічний університет імені Михайла Коцюбинського
21001, вул. Острозького, 32, м. Вінниця, Україна
https://orcid.org/0000-0002-8717-5940

Грач'я Паргевович Саргсян

Кандидат фізико-математичних наук, старший дослідник
Інститут хімічної фізики ім. А.Б. Налбандяна Національної академії наук Республіки Вірменія
0014, вул. Паруйра Севака, 5/2, м. Єреван, Республіка Вірменія
https://orcid.org/0009-0006-4188-158X

Анотація

Актуальність. Розуміння динамічної поведінки радикалів у реакторах, які зазнають газофазного окислення органічних речовин, має вирішальне значення для оптимізації конструкції реактора та безпеки в промисловості.

Мета. Це дослідження має на меті з'ясувати появу структур стоячих хвиль під впливом механізмів зворотного зв'язку в реакторах із циліндричною та сферичною симетрією, використовуючи математичні принципи, що керують поширенням коливань і ударних хвиль у ланцюгових реакціях, керованих дифузією.

Методологія. Матеріали та методи дослідження включали комп'ютерне моделювання з використанням MATHCAD 2001i та порівняльний аналіз експериментальних даних, отриманих у реакторних експериментах. Розрахункове моделювання виявило яскраві утворення структур стоячої хвилі в реакторах під впливом механізмів зворотного зв'язку.

Результати. Вплив зворотних зв'язків у реакторах з циліндричною та сферичною симетрією суттєво сприяв утворенню різноманітних структур стоячої хвилі концентрацій радикалів у зоні реакції. Було виявлено, що ці структури були в основному непомітними візуально і могли спостерігатися лише тоді, коли реакція супроводжувалася інтенсивним випромінюванням світла. Ці візуальні представлення служили переконливим доказом складної взаємодії між кінетикою реакції та ефектами зворотного зв'язку. Дослідження наголошує на важливості розуміння та прогнозування основних причин нестабільності, що в кінцевому підсумку підвищує надійність і безпеку реакторів у різних галузях промисловості. Результати продемонстрували кореляцію між конкретними механізмами зворотного зв'язку та просторовим розподілом структур стоячої хвилі.

Висновки. Отримані моделі обчислень, представлені в цій статті, надають переконливі докази, що підтверджують можливість формування структури стоячої хвилі в реакторах під впливом механізмів зворотного зв'язку. Дослідження розкрило потенціал для точного налаштування параметрів реактора для впливу на формування та стабільність цих структур. Отримані результати стали значним кроком до більш повного розуміння динамічних режимів у реакторах, що має наслідки для конструкції реактора, експлуатації та протоколів безпеки. Уявлення, отримані в результаті розкриття структур стоячих хвиль, на які впливають механізми зворотного зв'язку, пропонують цінні можливості для оптимізації конструкції реактора та безпеки експлуатації, що призводить до більш ефективних і стійких процесів.

Ключові слова: окиснення; зворотний зв'язок; моделювання динамічних режимів; радикали; коливальні явища; стаціонарний процес

Scientific Herald of Uzhhorod University
Series "Physics"

Journal homepage: https://physics.uz.ua/en
Issue 54, 47–66
Received: 14.09.2023. Revised: 04.12.2023. Accepted: 18.12.2023

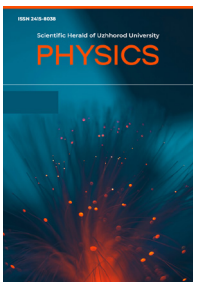

UDC 677.027.1:677.017.6
PACS: PACS 68.60.Dv
DOI: 10.54919/physics/54.2023.47

Examination of the influence of hydrothermal treatment of textile materials on their physical and mechanical properties and development of innovative technology

Salikh Tashpulatov*
Doctor of Technical Sciences, Professor
Tashkent Institute of Textile and Light Industry
100059, 5 Shohjahon Str., Tashkent, Uzbekistan
Jizzakh Polytechnic Institute
130100, 4 I. Karimov Str., Jizzakh, Uzbekistan
https://orcid.org/0000-0001-5483-2644

Dilrabo Bakhriddinova
PhD in Technical Sciences, Associate Professor
Tashkent Textile and Light Industry Institute
100059, 5 Shohjahon Str., Tashkent, Uzbekistan
https://orcid.org/0000-0003-2083-4902

Shakhlo Nutfullaeva
Postgraduate Student
Bukhara Engineering Technological Institute
200100, 15 Q. Murtazaev Str., Bukhara, Uzbekistan
https://orcid.org/0009-0001-8739-4705

Lobar Nutfullaeva
PhD in Technical Sciences, Associate Professor
Bukhara Engineering Technological Institute
200100, 15 Q. Murtazaev Str., Bukhara, Uzbekistan
https://orcid.org/0000-0001-6982-3185

Mukhlisa Muminova
Master, Assistant
Bukhara Engineering Technological Institute
200100, 15 Q. Murtazaev Str., Bukhara, Uzbekistan
https://orcid.org/0009-0003-8299-9662

Abstract

Relevance. Investigation in the field of textile materials and the effect of processing on their properties, is relevant, as it helps to develop more effective processing methods and increase the resistance of textile materials to the influence of various factors, which is important for both manufacturers and consumers.

Suggested Citation:
Tashpulatov S, Bakhriddinova D, Nutfullaeva D, NutfullaevaL, Muminova M. Examination of the influence of hydrothermal treatment of textile materials on their physical and mechanical properties and development of innovative technology. *Sci Herald Uzhhorod Univ Ser Phys.* 2023;(54):47–66. DOI: 10.54919/physics/54.2023.47

*Corresponding author

Purpose. The purpose of the study was to examine the effect of hydrothermal processing of textile materials on their physical and mechanical properties, develop a technology for the production of clothing using a new method (device) of press equipment for hydrothermal processing of composite material.

Methodology. The analysis method was used during the study, and an experiment was also conducted in which the temperature of the steam that did not fall below 160°C was used when processing the selected fabric samples, and the temperature of the working bodies of the press for forming the back was at least 110°C.

Results. As a result, the influence of hydrothermal treatment on the properties of textile materials was examined in detail and established. Having analysed the existing method of hydrothermal treatment using a vacuum unit, it was established that the conventional method of treatment leads to a substantial decrease in fabric thickness, breaking load and air permeability. It was also noted that during the hydrothermal treatment of the material, it is exposed under the influence of pressure. This leads to densification and flattening of the threads inside the material, creating flat areas, which causes adverse changes in the physical and mechanical characteristics of the fabric.

Conclusions. These factors indicate a potential deterioration in the quality and durability of textile products, which can increase the percentage of defects and negatively affect consumer satisfaction. This study also points to the prospects of using a vacuum installation in hydrothermal treatment, which allows preserving the desired properties of materials, improving the quality of the final products. The practical importance of the results of this study lies in the possibility of improving the quality of textile products and reducing the damage to materials, which is important for ensuring longer operation of textile products and increasing consumer satisfaction.

Keywords: atom; moulding of products; fabric structure; fibre deformation; vacuum installation; breaking load; breathability

Introduction

The textile industry is one of the modern world's most dynamically developing and important production areas. Textile materials are used in various fields, ranging from the fashion industry to medical applications. However, to meet the ever-growing demand for textile products, manufacturers face constant challenges in the quality and performance of materials.

Hydrothermal (wet-heat) treatment of textile materials is an effective method that allows improving and optimising the properties of these materials substantially. This includes reducing the material consumption, metal and energy consumption in production, increasing product strength, durability, and reliability. Consequently, such technologies contribute to reducing the weight and cost of structures, which makes them more competitive in the market. In addition, hydrothermal treatment increases technological productivity while maintaining the flexibility and versatility of the process. These factors are important for the textile industry, as they improve product quality and make production more efficient.

The improvement of technology and equipment for wet-heat treatment (WHT) is an urgent task in the textile industry. It is based on the use of moulding properties of various materials, such as fabric, nonwovens, leather, fur, knitwear. This approach allows achieving a high degree of stability in the configuration of clothing parts, which in turn contributes to improving the quality and durability of textiles, reducing the number of seams and improving overall production efficiency.

According to S. Samieva *et al.* [1], hydrothermal treatment is a complex process that affects many physical and mechanical properties of textile materials. In particular, this process can cause changes in the thickness of the fabric, breathability, and other characteristics of the material. The greatest attention was paid to optimising the parameters of hydrothermal treatment to ensure the preservation or even improvement of the quality of textiles.

S. Mahkamova *et al.* [2] state that hydrothermal treatment by repeated washing of textile materials can have both positive and negative effects on the basic properties of the material, depending on the conditions of use. It was emphasised that properly configured parameters of hydrothermal treatment can strengthen some textile product characteristics, such as durability and elasticity. Therewith, uncontrolled or excessive processing can cause undesirable changes in the structure of the material, which will negatively affect its quality and durability.

S. Makhkamova & Z. Valieva [3] in their study drew attention to the importance of finding optimal conditions for hydrothermal treatment that will maximise the potential of this process and minimise its negative consequences. In the study, the work on the selection of optimal parameters to preserve the physico-mechanical properties of textile materials during hydrothermal treatment by washing was conducted [3].

According to a study by D. Kurbanov [4], hydrothermal treatment of textile materials can have a substantial impact on their physical and mechanical

properties. The researcher drew attention to the fact that this process can change the material's structure, leading to its more compact organisation. This, in turn, can lead to an improvement in some characteristics, such as strength and resistance to wear.

However, in the study by N. Murodova [5] also noted that improper hydrothermal treatment, namely multiple washes or the use of uncontrolled parameters, can cause the opposite effect. In particular, excessive exposure to moisture and heat can lead to deformation and loss of material properties. This study also emphasised the importance of careful monitoring and adjustment of hydrothermal treatment conditions to achieve the desired results and minimise negative consequences.

Since the studies mentioned above did not pay due attention to the improvement of the hydrothermal treatment process, this study aimed to develop a new clothing production method. This method involves using a vacuum installation, which can contribute to the preservation or improvement of the physical and mechanical properties of materials.

Materials and Methods

The study was conducted at the company "Maxpress Industry" (Uzbekistan). The materials used during the study included woollen fabrics for men's jackets designed for autumn, for seasonal and summer – polyester and viscose fabrics. Adhesive materials that have a textile base were used to ensure the preservation of the shape of various parts of clothing, such as, for example, backs. These materials are presented by various companies, such as HYMO from Japan, Kufner from Germany, Iskoj from Russia, DANELLI from China, and Camela from Poland.

In the course of the study, the hydrothermal treatment process was conducted on a special vacuum forming device developed using a polymer composition instead of adhesive gasket materials (Fig. 1-3, Table 1).

Figure 1. General view of the bottom cushion of the vacuum installation made of composite material
Source: compiled by the authors

Table 1. Technical characteristics of the bottom cushion of the vacuum installation

No.	Technical specifications	
1	Length, mm	A-700; B-580
	Width, mm	A-330; B-440
	Height, mm	A-73; B-53; B-95
	Wall thickness, mm	6
	Weight, kg	3.7
2	Thermal resistance, °C	325
3	Mechanical resistance, MPa	34
4	Material of the working body	composite material

Source: compiled by the authors

The improvement of the technological scheme was conducted based on investigating the mechanism of surface formation of both flat and volumetric sections of the back of clothing and methods of fixing them. Experiments were conducted on a press to form the back of the brand UPP1617KI, manufactured by the German company "Malkan", to develop an improved technology that gives the details of clothing shape stability using a vacuum installation.

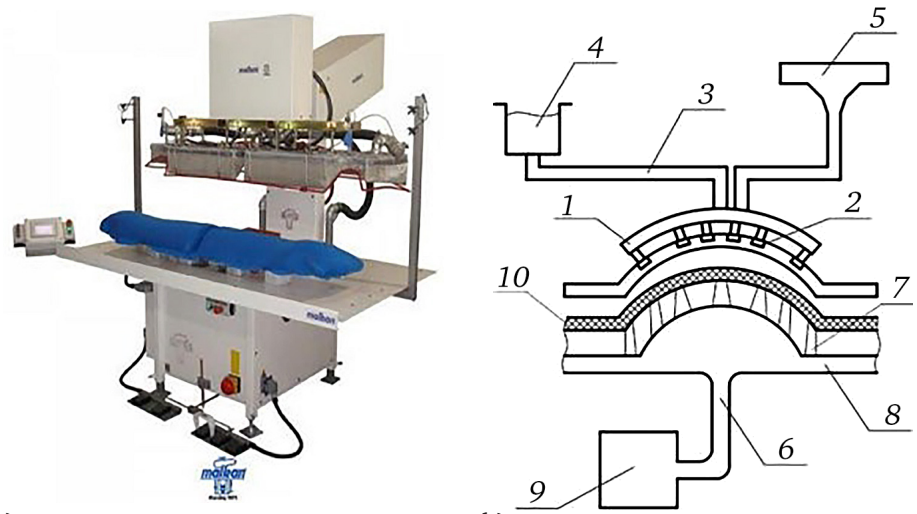

a) b)

Figure 2. Press for processing the back of a men's jacket UPP1617KI (Malkan) with a bottom cushion of a vacuum installation

Note: a) appearance; b) block diagram of the equipment: 1 – upper cushion, 2 – nozzles for PC and warm air supply, 3 – pipeline, 4 – PC container, 5 – hair dryer, 6 – vacuum chamber, 7 – perforation, 8 – lower cushion, 9 – compressor, 10 – semi-finished product (processed fabric)

Source: compiled by the authors

Figure 3. The process of testing the method of shaping in the production conditions of "Maxpress Industry"

Source: compiled by the authors

When processing semi-finished products, the surface temperature of the working bodies was maintained at least 110°C and the temperature of the steam used for processing was at least 160°C, the back of the semi-finished product was placed on the lower working bodies of the press in accordance with the established procedure. Then, the deformation of the back of the product was conducted through a press, and then drying and stabilisation of a given shape were conducted.

Experiments were conducted with various fabric samples, as indicated in Table 2, to estimate the diameters of the inlet holes that should be created in the lower cushion of the device. The fabric samples had dimensions of 250×50 mm and were secured with clips in accordance with the "strip" technique. Uniaxial stretching of materials was conducted on a special breaking machine Autograph AG-1 (Shimadzu, Japan).

Table 2. Characteristics of costume fabrics

No.	Name of the fabric	Surface density g/m²	Fibrous composition, %	Mechanical characteristics			
				Breaking load, N		Breaking elongation, %	
				Base	Warp and weft	Base	Warp and weft
1	Tweed (Art. 89-05)	374.4	10% wool 20% 70% PE	970	680	19	9
2	Corduroy (Art.06535)	250.5	35% 65% PE	1010	755	18	9
3	Costume "Euro" (Art.180703)	315.9	20% 80% PE	750	550	21	14
4	Christmas tree "Spruce" (Art. 11684)	164.7	20% viscose 80% PE	739	608	20	14
5	Diagonal Blue (Art.VT-468)	173.9	90% PE 10% viscose	898	709	22	12

Source: compiled by the authors

The calculation of pressure losses caused by local resistances was conducted using the Weisbach equation (1):

$$h_m = \zeta(v^2/2g) = \zeta h_v, \quad (1)$$

where: $h_v = v^2/2g$ – the high-speed pressure.

The pressure losses were calculated using the Borda formula, which was derived from the equations of D. Bernoulli and the law of conservation of momentum (2):

$$h_m = [(1/(\varepsilon - 1)]^2(v_2^2)/2g) = \zeta(v_2^2)/2g), \quad (2)$$

where: $\zeta = \left(\frac{1}{\varepsilon} - 1\right)^2$ – the coefficient of resistance, in relation to speed (in a section of a narrow section of the pipeline); $\varepsilon = F_c/F_2$ – compression ratio, determined by the ratio of the area of the compressed section F_c to the area of the pipe in the section F_2.

The compression ratio during operation was calculated using the formula proposed by A.D. Altshul (3):

$$\varepsilon = 0.57 + [0.043/(1.1\text{-}n)], \quad (3)$$

where: $n = F_2/F_1$ – the ratio of pipe areas in narrow and wide sections.

The value of the local resistance coefficient was determined by the formula (4):

$$\varepsilon_{conf} = C_c\zeta = C_c\left(\frac{1}{\varepsilon} - 1\right)^2, \quad (4)$$

where: C_c – the compression ratio.

Using the analysis method, the results of experiments in laboratory conditions were also evaluated to determine the degree of influence of pressure and humidity on the properties of textile materials. This analysis allowed understanding what changes occur in the properties of the material under such influences. As part of the theoretical part of the study, this method was used to analyse the physical and mechanical properties of the material before and after wet-heat treatment and to examine the material's abrasion resistance. It allowed identifying changes in the properties of the material caused by the technological process of the WHT and drawing conclusions about its impact on textiles.

Using the statistical method in this study, various indicators of the properties of textile materials were compared before and after wet-heat treatment. This method allowed assessing the degree of changes in the thickness of the fabric, breaking load, breathability, and abrasion resistance and to make a statistically substantial comparison between the samples of the material before and after the WHT.

Results

According to the current technology, mechanical pressure, superheated process steam, and a certain temperature for a certain time are used to achieve a given shape of textile-made clothing parts. As a result of the influence of these factors on a semi-finished textile material, its structure changes, which leads to a deterioration of its properties. This, in turn, leads to a decrease in the overall quality of the final clothing. For example, when forming a mould using mechanical pressure, the threads that make up the textile material are subjected to undesirable loads that lead to microscopic damage (Fig. 4-6).

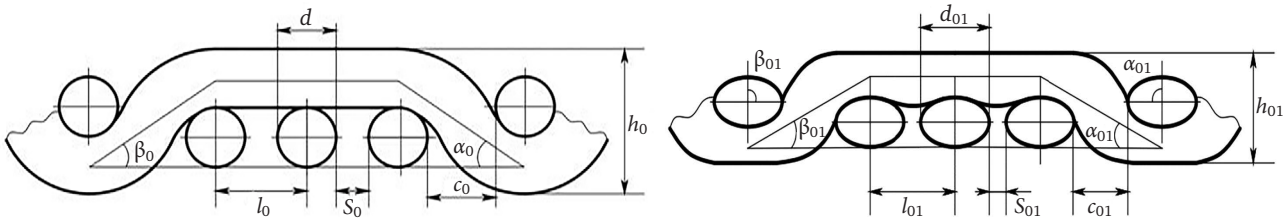

a) b)

Figure 4. Scheme of changing the cross-section of fabric threads before (a) and after (b) hydrothermal treatment (WHT)

Note: d – the initial diameter of the thread and d_{01} – after the WHT; h_0 – the initial thickness and h_{01} – after the WHT; l_0 – the initial distance between the axes of the threads and l_{01} – after the WHT; S_0 – the distance between the edges of the threads and S_{01} – after the WHT; c_0 – the distance between the threads where the thread bends in the phase of passage and c_{01} – after the WHT; α_0, β_0 – axial tilt angles of the thread in the passage phase and α_{01}, β_{01} – after the WHT

Source: compiled by the authors

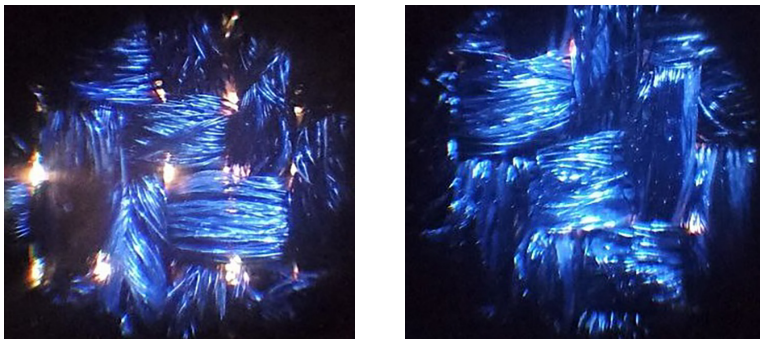

a) b)

Figure 5. Micrograph of textile material before (a) and after (b) the WHT

Source: compiled by the authors

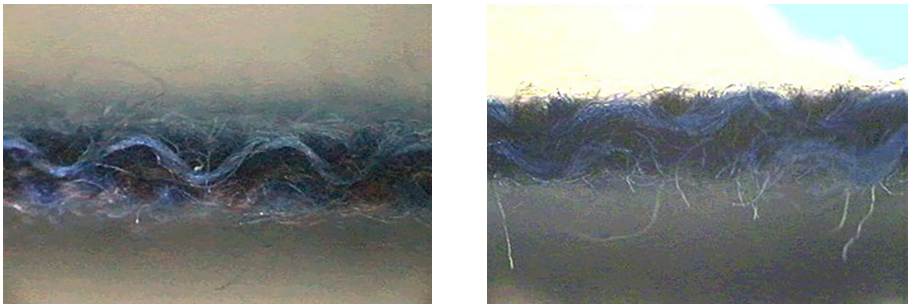

a) b)

Figure 6. Micrographs of the fabric section before (a) and after (b) pressing and WHT

Source: compiled by the authors

As a result of such damages, the original physical, mechanical, hygienic, and geometric characteristics of the material are violated. These characteristics may include thickness, density, breaking load, breaking elongation, stiffness, breathability, vapour permeability. Such changes in the material can negatively affect its quality and ability to perform its functional tasks. For example, this can lead to a decrease in strength, increased breathability or loss of hygiene of textile products [6, 7]. The above-mentioned WHT method showed the need for technology development to improve the quality of the product and the stability of the clothing part, reduce the damage to the structure of the textile material of the product part by using a fundamentally new working body of technological equipment. The cyclogram of the work of the press UPP1617KI of the company "Malkan" in combination with steaming and pressing is shown in Figure 7, which also describes the technological process of WHT and shaping. The temperature of the working surface of the pillows should be maintained at the level of $Tw \geq 110°C$.

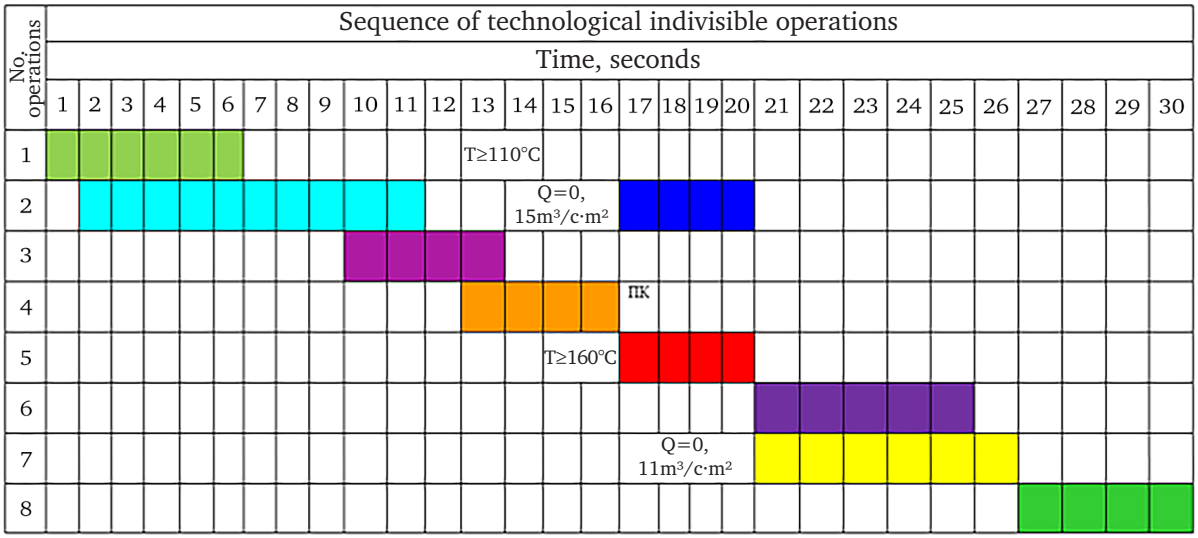

Figure 7. The cyclogram of control and operation of automated equipment of the ironing vacuum installation of the WHT for the formation and fixing of the shape of the part of the back of a man's jacket

Note: 1 – preparation and laying of the product on the bottom cushion ($T_{bot.} \geq 110$°C; 2 – switching on vacuum-suction ($Q = 0.15$ m³/(cm²)) in the lower cushion and the formation of a shape by deforming the mesh structure of the fabric of the part; 3 – lowering the upper cushion and stopping within 2-3 cm of the semi-finished product; 4 – applying a polymer composition to the specified areas of the deformed part; 5 – steaming with superheated steam at a temperature of 1600°C using the upper cushion over the entire surface of the part with the vacuum suction turned on (Q = 0.15 m³/(cm²)) until the end of the technological process; 6 – lifting the upper cushion and returning to its original position; 7 – stabilisation and drying of a given shape by vacuum suction through the lower cushion with parameters Q = 0.11^{m3}/(cm²); 8 – removal of the semi-finished product
Source: compiled by the authors

The semi-finished product is placed on the bottom cushion along the upper and lower points of the back-rest line. A semi-finished part is placed on the lower forming cushion. Then, vacuum deformation of the part is conducted through the lower pillow, and the upper pillow is lowered and stopped before reaching 2-3 cm to the semi-finished product. Then, a polymer composition is applied to the specified local areas, and after the end, superheated steam is applied through the upper cushion. After that, the upper pillow is lifted and returned to its original position, then stabilisation and drying of the given shape by vacuum suction through the lower pillow and removal of the semi-finished product. The process of vacuuming in a limited technological volume in the lower cushion consists in reducing the air (gas) pressure to values below atmospheric, as described in L. Nutfullaeva *et al.* [8].

The level of gas rarefaction is determined by the ratio of the average free path $\bar{\lambda}$, which is associated with mutual collisions of gas molecules in a given medium. Depending on this ratio, vacuum degrees are distinguished, such as ultra-high (when $\bar{\lambda}$, substantially larger than the particle size r), high (when $\bar{\lambda}$, larger than the particle size, but not by much), medium (when $\bar{\lambda}$, approximately equal to the particle size), and low (when $\bar{\lambda}$, substantially smaller than the particle size). The average length $\bar{\lambda}$, over which molecules can move freely, given the variety of their velocities during mutual collisions, is defined as (5):

$$\bar{\lambda} = \frac{1}{\sqrt{2} n_o \delta}, \quad (5)$$

where: n_o –number of molecules (in cm³); δ – cross-section for the interaction of molecules.

In the collision of particles formed by molecules with $d \approx 10^{-8}$ cm, the determination of δ is conducted by (6):

$$\delta = \pi d^2. \quad (6)$$

To analyse the efficiency of a vacuum installation, it is important to have information about the characteristics of different vacuum levels (Table 3). It is necessary to analyse the average free path of $\bar{\lambda}$ air molecules (1) and analyse it by comparing it with the dimensions of clothing elements to determine what level of vacuum is necessary for the formation of clothing parts. In the case of a vacuum level, n_o in 1 m³ is in the range from 10^{22} to 10^{19}, the average free path length $\bar{\lambda}$ is in the range from 0.00225 to 2.25 m. This value is comparable to (r) of the installation for creating a vacuum for the purpose of forming clothing parts, that is, at an average vacuum level $\bar{\lambda}$ less than or approximately equal to the size of the device ($\lambda \leq r$).

Table 3. Parameters of different vacuum levels

Characteristics	Vacuum level			
	Low	Medium	High	Ultra-high
Pressure (mmHg)	760-1	$1\text{-}10^{-3}$	$10^{-3}\text{-}10^{-7}$	Less than 10^{-8}
Number of molecules n_o, m^3	$10^{25}\text{-}10^{22}$	$10^{22}\text{-}10^{19}$	$10^{19}\text{-}10^{13}$	Less than 10^{13}
Dependence of the coefficients of thermal conductivity and internal friction	There is no dependency	The dependency is calculated based on λ/D	Direct dependence on pressure	Practically absent

Source: compiled by the authors

Many holes are provided in the lower cushion of the installation to create the shape of clothing parts using vacuuming. These holes can have various shapes, which are selected considering the air dynamics and the need to provide the best conditions for fabric deformation [9]. Therefore, to create a vacuum in a closed technological space limited by the contour of the lower cushion, it is necessary to maintain the pressure at the level of $p = 1 - 10^{-3}$ mmHg, which corresponds to the average vacuum level. Vacuuming is achieved by removing air from a closed, sealed space using a vacuum pump. In this device, air jets pass through holes of different shapes (Fig. 8): they can taper to the lower surface like conical confusers (Fig. 8a), expand to the lower surface (Fig. 8b) or have a cylindrical shape (Fig. 8c).The movement of air jets or other gases through such holes is calculated according to the principles of hydrodynamics.

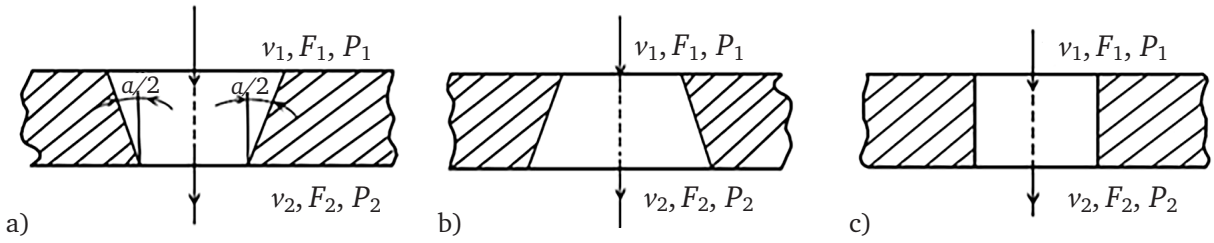

Figure 8. Types of perforations and their effect on aerodynamic parameters
Note: v – air velocity; F – cross-sectional area; p – pressure
Source: compiled by the authors

In most cases, the small changes in the basic physical properties of air and gases encountered in technology, such as density, viscosity, and temperature, when moving at low speeds and pressures (close to atmospheric), are so insubstantial that they can be neglected. This allows applying the basic principles of hydrodynamics to the analysis of aerodynamic processes [10].

A real liquid has a viscosity, and therefore, substantial resistance forces arise, including both internal and external friction. These forces lead to irreversible losses of pressure energy. Such losses are usually called linear pressure losses (h_{tr}). In addition, there are pressure losses on local resistances (h_m), which arise due to the specific features of geometry, design, and technology of moving or transporting a liquid or gas flow. Based on this, losses on any of the taken sites are defined as (7):

$$h_{nom} = h_{mp} + h_m. \quad (7)$$

When analysing energy losses in the movement of a liquid or gas, the impact of local resistances, which are caused by several factors, is considered. First, a change in the cross-section, including extensions and constrictions, substantially affects the flow. In addition, the curvature of the air channels, such as the flow turns, contributes to energy losses. Branching and merging of streams can also provide additional resistance to movement. Especially important in aerodynamic calculations is the consideration of local resistances, which are associated with the design features of the system [11].

The calculation of pressure losses caused by local resistances is conducted using the Weisbach equation (1) or by determining through the pressure loss Δp_m (kgf/m²) in the local resistance (8):

$$\Delta p_m = (\gamma v^2/2g), \quad (8)$$

where: ζ – the coefficient measured in experiments and embodies the loss of pressure as a percentage of the velocity pressure.

In the case of a sharp narrowing of the duct, the air flow is compressed first, and then its expansion. The main pressure losses with such a narrowing occur in the expansion area. Table 4 contains the values of ζ depending on the ratio of the areas n between the narrow section and the wide section F_2 of the F_1 pipe.

Table 4. Values of ζ depending on n

$n = F_2/F_1$	0	0.1	0.2	0.3	0.4	0.5	0.6	0.7	0.8	1
Z	0.41	0.4	0.38	0.36	0.34	0.3	0.23	0.2	0.16	0

Source: compiled by the authors

The change in the rate of flow during compression occurs in the case of a gradual narrowing of the pipeline, which is called a confuser, as shown in Figure 9. The coefficient ζ for the confuser is calculated also considering the coefficient C_c (4). The value of the correction factor C_c depends on the taper angle α of the confuser. When conducting aerodynamic calculations, a graph showing the dependence of C_c on α can be used.

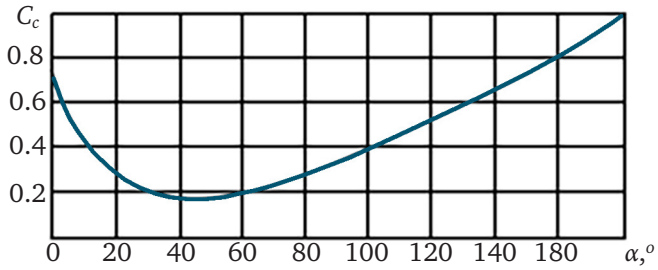

Figure 9. The dependence of the corrective compression ratio C_c on the taper angle
Source: compiled by the authors

With an increase in the velocity in the confuser, some transformation of the pressure in the flow into kinetic energy occurs.

The pressure loss due to a sudden expansion of the flow is also calculated using the Borda formula (9):

$$h_m = \zeta(v_1^2)/2g), \quad (9)$$

where: $\zeta = (1 - V_2)/V_1)^2$; $v_1^2/2g$ – pressure in a narrow section.

Also, the coefficient of local resistance ζ can be expressed as follows:

$$\zeta = \left(1 - \frac{F_1}{F_2}\right)^2 = \left[1 - \left(\frac{d_1}{d_2}\right)^2\right]. \quad (10)$$

In the case of the expression of the coefficient ζ relative to the velocity head (in a wide section), the following is obtained (11):

$$h_m = \left(\frac{V_1}{V_2} - 1\right)^2 (v_2^2/2g) = \left(\frac{F_2}{F_1} - 1\right)^2 (v_2^2/2g). \quad (11)$$

When analysing the pressure loss resulting from the resistances in the diffuser, a special correction factor known as the softening factor (C_m) is considered. The value of this coefficient depends on the angle of expansion (α) of the diffuser (Table 5).

In the diffuser, some part of the kinetic energy is converted into pressure energy. A general formula is used that considers the local resistance coefficient (ζ) to calculate the pressure loss associated with local resistances in the diffuser, considering the softening coefficient (C_m) (12):

$$h_m = C_m[(v_1 - v_2)^2/2g]. \quad (12)$$

Table 5. Values of the softening coefficient C_m depending on the opening angle α

α,°	C_m
8	0.16
15	0.35
30	0.8
60	0.95

Source: compiled by the authors

When analysing the aerodynamics of the passage of air through various configurations of holes, it becomes evident that a smooth narrowing of the cross-section from the inlet to the outlet, made in the form of a confuser in the lower part of the material forming device, is preferable. This is explained by the fact that in the process of creating a vacuum in the technological space, the air is sucked from a larger section (the upper part of the perforation) to a smaller section (the lower part of the perforation). According to the equation of D. Bernoulli and the mass conservation equation ($Q = V_1{*}F_1 = V_2{*}F_2 = \text{const}$), when a

liquid (or gas) moves in a horizontal pipe with different sections, the velocity of the liquid is higher in the narrowing areas, and the pressure is higher in wider areas where the velocity is lower.

Thus, positioning the deformable fabric in accordance with Figure 10 brings great benefits: it provides a tighter fit to the lower surface of the device since it increases the area that is exposed to atmospheric pressure during vacuuming; it also creates a pressure difference between the upper and lower parts of the pillow, and the hole in the lower part has a smaller diameter. This distribution of contact between the fabric and the working surface of the pillow contributes to a more efficient fabric moulding process, making it more favourable and intensive.

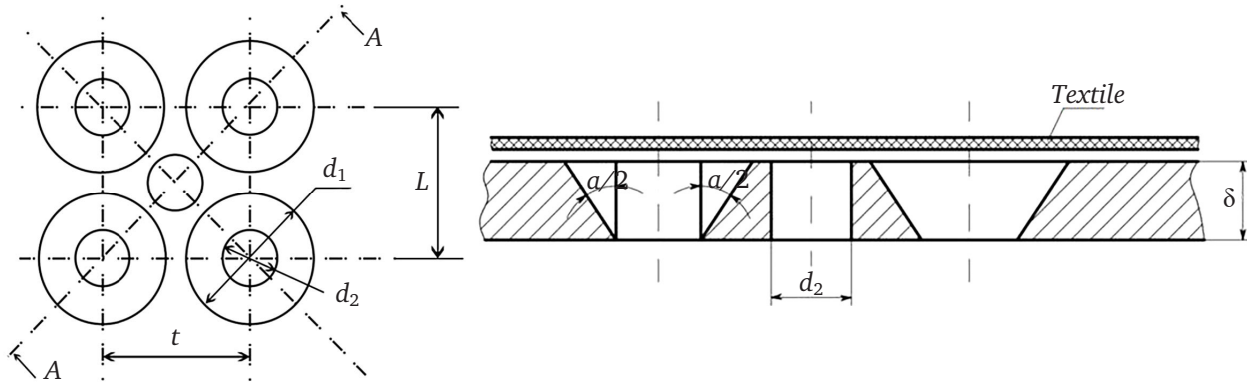

Figure 10. An elementary cell containing holes inside the thickness δ in the lower cushion of the device for forming three-dimensional parts of clothing using the vacuum method
Note: α – taper angle; t – distance between the perforations; d_1, d_2 – diameters of the inlet and outlet holes, respectively
Source: compiled by the authors

Since air is considered a compressible fluid in this context, the equation of D. Bernoulli, used for the flow of an ideal liquid, can be successfully used in the case of any gas flow with minor pressure changes [12]. In particular, with small differences in temperature between the transported air and the environment, it is possible to consider the difference in geometric altitude levels, and the equation of D. Bernoulli can be represented as (13):

$$\frac{P_1}{\gamma}+\frac{V_1^2}{2g}=\frac{P_2}{\gamma}+\frac{V_2^2}{2g}=\text{const, m}. \quad (13)$$

Which can also be presented in a more convenient form for calculations (14):

$$p_1+\frac{\gamma V_1^2}{2g}=p_2+\frac{\gamma v_2^2}{2g}=\text{const, kgf/m}^2. \quad (14)$$

For real gases, an additional term is added to equation (14), which considers the pressure losses Δp, associated with overcoming hydraulic resistances (3). Thus, if the pressure is measured in Pascals, equation (14) changes as follows (15):

$$p_1+\frac{\gamma v_1^2}{2}=p_2+\frac{\gamma v_2^2}{2}+\Delta p, \quad (15)$$

where: v_1, p_1 – velocity and pressure of the gas (in the initial part); v_2, p_2 – velocity and pressure at the outlet of the pipeline; γ – volume weight or density of a gas, measured in kg/m³.

In aerodynamic calculations for ordinary air, a standard value of γ is often used, equal to 1.2 kg/m³. For a gas pipeline of any configuration, the pressure loss due to friction ($\Delta p = \Delta p_f$) over a section of length l can be calculated using the Darcy formula, applied to circular sections (16):

$$\Delta p_f=\frac{\lambda}{d}*\frac{\gamma V^2}{2}*l, \text{Pa}, \quad (16)$$

where: λ – coefficient describing the friction pressure loss along the section of length l; d – diameter of the duct, m.

For approximate calculations, a value of λ equal to 0.02 can be used. According to equation (3), it can be argued that the loss of friction pressure is proportional to the length of the duct (and the thickness of the bottom cushion). It is important to consider that the pressure losses caused by friction are inversely proportional to the size of the hole. In addition, Δp increases non-linearly as the air velocity increases, having a parabolic dependence. Thin-sheet steel was used for most of the ducts, and its absolute roughness is $k = 0.1$ mm.

However, if the ducts are made of other materials, then to account for changes in the specific resistance to friction C_f and λ/d, it is necessary to introduce a correction factor β (17):

$$\beta=(kV)^{0.25}, \quad (17)$$

where: k – roughness value of the inner surface of the duct, mm; V – air velocity, m/s.

Based on the physical and mechanical properties of the fabric used to form the parts of clothing, it is possible to pre-estimate the diameters of the inlet holes that should be created in the lower cushion of the device. As can be seen from the data presented in Table 2, the average values of the maximum load required for the rupture of the considered fabrics along the base and weft are 873/660 N, respectively. Therefore, the specific tearing load R_t, expressed in newtons for each millimetre of the length of the material, is equal to 17.5/13.2 N/mm on the basis/weft, respectively. The maximum tearing load (R_{st}), considering the circumference (πd), will be equal to the average specific tearing load (18):

$$R_{st} = R_t * \pi d, \text{N}. \quad (18)$$

The ultimate tensile stress σ_{st} at which fabric destruction occurs is defined as (19):

$$\sigma_{st} = \frac{R_{st}}{F}, \text{N/mm}^2, \quad (19)$$

where: $F = \pi/4$ – size of the hole; d – diameter, mm.

Given (18), the following is obtained (20):

$$\sigma_{st} = \frac{R_t * \pi d * 4}{\pi / d^2} = \frac{R_t * 4}{d}, \quad (20)$$

therefore (21):

$$d = \frac{4 * R_t}{\sigma_{st}} \text{ mm}. \quad (21)$$

For average stress parameters at break (26.55 N/mm^2) and specific breaking loads both on the base and on the weft (15.36 N/mm^2), the minimum diameter of the inlet is (22):

$$d = \frac{4 * 15.36}{26.55} = 2.3 \text{ (mm)}. \quad (22)$$

Therefore, when creating perforations in the form of a confuser, it is established that the diameter of the outlet is 2 mm, and the upper hole is 4 mm (considering technical requirements). It is necessary to compare the surface dimensions necessary to create an element of clothing with the interval between the holes (t) to determine the number of such perforations located in the unit cell. For this purpose, a structurally set pitch of 6 mm is assumed, which allows placing an additional hole d_2 with a diameter of 2 mm in the centre of this cell.

It is possible to make an approximate calculation of the loss of air pressure, which is sucked through the perforations, using the described system. For a specific example, hole sizes such as 4 and 2 mm will be assumed. The depth of the holes corresponds to the thickness of the bottom cushion and is 6 mm. With such data, the taper angle α is approximately 20°. In case of sudden narrowing, equation (6) is used to calculate the pressure loss, which requires the determination of the coefficients ζ and ε (local resistance and compression). The formula (3) is used to determine the coefficient ε, where $n = F_2/F_1$ – the ratio between the areas of holes in a narrow section and a wide section (23-25):

$$F_1 = 12.56 \text{ mm}^2; F_2 = 3.14 \text{ mm}^2, \quad (23)$$

$$\varepsilon = 0.57 + [0.043/(1.1 - 3.14/12.56)] = 0.62, \quad (24)$$

$$\zeta = \left(\frac{1}{\varepsilon} - 1\right)^2 = \left(\frac{1}{0.62} - 1\right)^2 = 0.376. \quad (25)$$

For the final determination of the value of the local resistance coefficient ζ of the confuser, a correction factor C_c is considered, which depends on the taper angle α of the confuser. At α = 20°, the value $C_c = 0.3$ can be assumed. In this case, according to the formula (4), the following value (26) is obtained:

$$\varepsilon_{\text{conf}} = C_c \zeta = C_c \left(\frac{1}{\varepsilon} - 1\right)^2 = 0.3 * 0.376 = 0.113. \quad (26)$$

Having information about the air flow velocity in a narrow section, it is possible to calculate the pressure loss in accordance with equation (6). Therefore, for the successful application of the method of forming clothes, it is necessary to cut perforations with the shape of a confuser in the lower cushion of the device. The confuser hole, in accordance with aerodynamic principles, ensures a close fit of the material to the working surface of the cushion, as it increases the area on which the vacuum acts during vacuuming. This results in a higher pressure at the top of the cushion due to the larger size of the opening compared to the outlet openings. The size of the perforations was also calculated, considering the maximum breaking load of the deformed fabric. The obtained results indicate the need to create a moderate vacuum, providing a pressure within 1-10^{-3} mmHg, to form clothing elements with the specified dimensions.

The results of experiments conducted on textile materials after hydrothermal treatment under mechanical pressure indicate a loss of these properties of the material at an average level of 15-21%. Based on this, it can be concluded that to improve the processing standards at which the physical-mechanical, and hygienic properties of various textile materials are preserved, improvement of the formation method is required. This method should exclude the negative impact on the clothing parts group from the equipment's working elements, such as matrices and punches. One of the disadvantages of existing devices is their fixed shape of the matrix and punch. It is necessary to change the matrix and punch to create a variety of clothing parts or replace them, which leads to additional costs and reduced productivity.

In the process of manufacturing sewing parts, fabrics or textile materials and bags are subjected to various physical influences: stretching, compression, and moulding. The above factors should be aimed at changing the actual structure of the fabric, thread, and fibres to give a given shape. As a result of these technological influences, the geometric parameters of the threads that make up the fabric and some of the physical and mechanical properties of textile materials naturally change. If the fabric is pressed and the fibres of the thread are plasticised with heated steam, then such a surface differs more than the surface of the fabric that has not been pressed and wet-heat treated.

Experiments conducted in laboratory conditions have shown that the air permeability index for samples before exposure to pressure and moisture is on average, 67.16 cm^3/cm^2s (Table 6) [13]. This indicator, after applying pressure and moisture with a mass of 5 kg, decreases to a value of 46.98 cm^3/cm^2s; after pressing with a 10 kg press, the device shows 43.74 cm^3/cm^2s; after a press load of 15 kg, air permeability decreases to 40.77 cm^3/cm^2s; after 20 kg of load, air permeability reduced to 38.01 cm^3/cm^2s. It follows that after applying pressure paired with moisture, the air permeability index decreases by 36.95%.

Table 6. Indications of the breathability of the fabric after presses of various weights

Load, m	0	5 kg	10 kg	15 kg	20 kg
Costume fabric	67.16	46.98	43.74	40.77	38.01

Source: compiled by the authors

This can be explained by the fact that in the process of exposure to pressure and moisture, the threads of the fabric flatten, i.e., under the influence of pressure and moisture, acting as a plasticiser, the intermolecular bonds of the fibres of the threads weaken. As a result, the transverse shape and geometric parameters of the threads change, i.e. a circular cross-section of the thread turns into an oval one. This can be compared by the distance between the two threads decreases, and the distance between the central points of the threads increases in their diameter and in the width of the fabric section itself, and thereby the surface coverage of the fabric with threads increases.

Considering that polymer compositions are effective when fixing a given shape of clothing parts, experimental tests were conducted in this part of the study for samples with a polymer coating before and after wet-heat treatment and pressing. In these samples, there was also a decrease in air permeability. Thus, in the samples before pressing, the readings on average are:

1. In a fabric with a 0.5 cm wide strip with a polymer coating from the initial indicator of 16.008 cm^3/cm^2s, after a press load of 5 kg, breathability decreases to 15.054 cm^3/cm^2s; after 10 kg of press load, breathability decreases to 13.85 cm^3/cm^2s; after 15 kg, breathability has a value of 12.7 cm^3/cm^2s; after 20 kg of pressing load, this indicator is 11.7 cm^3/cm^2s; it follows that the breathability of fabric with a 0.5 cm wide strip of coating is reduced by 16.9%.

2. In a fabric with a 1 cm wide strip with a polymer coating, the initial air permeability index is 18.368 cm^3/cm^2s. Further, after pressing with 5 kg of load, the indicator decreases to 17.138 cm^3/cm^2s; after 10 kg of load, the air permeability has a value of 16.182 cm^3/cm^2s; after 15 kg of press load, the air permeability decreases to 15.369 cm^3/cm^2s; after pressing with 20 kg of load, the indicator is 14.597 cm^3/cm^2c. This indicator decreased by 13.9% compared to the initial value.

3. In a fabric with a 2 cm wide strip with a polymer coating, the initial air permeability data reaches 21.39 cm^3/cm^2s, after a press load of 5 kg, the air permeability decreased to 21.02 cm^3/cm^2s; after 10 kg of the press, the air permeability reaches 20.72 cm^3/cm^2s; after 15 kg of the press, the air permeability decreases by 19.68 cm^3/cm^2s; after a pressing load of 20 kg, air permeability decreases by 19.2 cm^3/cm^2s, which, in total, reduces air permeability from the initial value by 5.8%.

When exposed to high humidity and heat during wet-heat treatment, the bonds between the molecules of the material are weakened and destroyed, and the structure of the material is reshaped in accordance with the deformation of the fibres. After removing moisture (by drying) and lowering the temperature of the material, the bonds between the macromolecules are restored, that is, the deformation of the fibres, threads, and, consequently, the entire material is fixed. However, this fixation of the deformation is temporary; when wearing clothes, the reverse relaxation occurs, and part of the fixed deformation disappears with time. The speed of this reverse relaxation process depends on how similar the conditions of use of the products are to the conditions of wet-heat treatment and wearing of the product, and the closer they coincide, the more firmly the deformation is fixed. The process of restructuring the fibre structure during wet-heat treatment also depends on the chemical composition of the material, its supramolecular structure, and the type of intermolecular bonds [14]. Relaxation processes were traced and investigated in the laboratory to substantiate these processes. From the experimental data obtained, it can be seen that the main relaxation of the examined fabric after wet-heat treatment occurs within 1 hour, totalling in 36.4%.

After two hours, relaxation is 2.7%, after three hours – 0.2%, after four, five and six hours – 0.02%.

To identify the relationship of the WHT process with physical-mechanical properties, for example, with the breaking load, experimental tests were conducted using a device that determines the breaking load index of fabrics and other textiles. The results of the tests and the analysis of the comparative indicators of the breaking load before and after the WHT are shown in the graph (Fig. 11). Experiments conducted in the laboratory have shown that the breaking load of fabrics before wet-heat treatment in the direction of the warp threads is obtained on average 190.074 N, in the direction of the weft threads – 164.996 N, and after wet-heat treatment and pressing, the breaking load index for the warp thread of the material on average decreases to 177.82 N, for the weft thread – 150.256 N. Considering this as a percentage, the index of the breaking load of fabrics after WHT and pressing in the fractional direction of the material decreases by 6.5%, and the breaking load in the transverse direction of the fabric decreases by 8.94%. It follows from this that the breaking load of the examined fabric decreased by an average of 7.72%. This naturally negatively affects the quality indicators of manufactured clothing, in particular, leads to rapid wear of clothing.

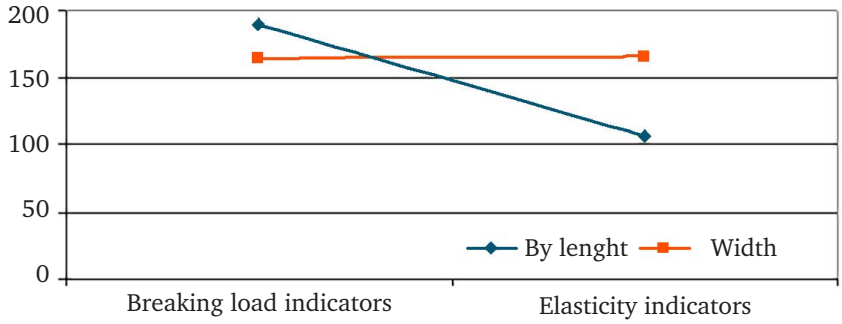

Figure 11. Graph of the impact of the WHT and pressing on the indicators of the breaking load of the material
Source: compiled by the authors

In the next part of the study, experimental tests were conducted on the effects of existing and developed methods of wet-heat treatment on the thickness of the fabric, breaking load, surface density, breathability, stiffness [15]. The results of a comparative assessment of the impact of the conventional and developed WHT method, and the results of the study are presented in Figures 12-16. From the data presented in Figure 12, it can be seen that if the reference thickness value is 1.7 mm, then under the influence of the existing WHT, the fabric thickness index decreases by 32.9% compared to the reference value. When using a vacuum installation in WHT, the thickness of the fabric remains unchanged. This is observed in all examined variants of the textile material.

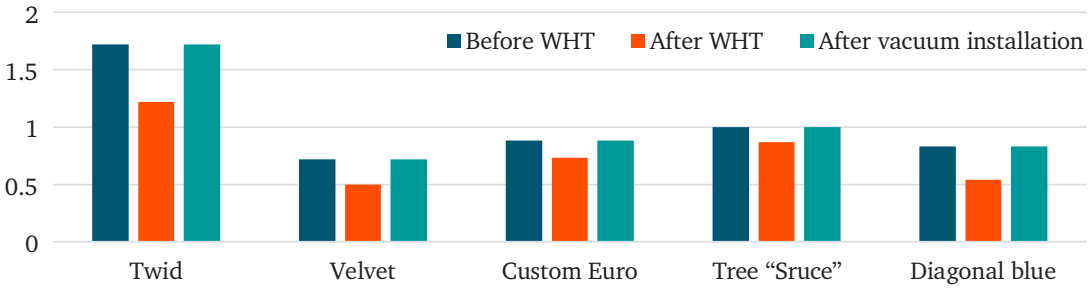

Figure 12. The influence of existing and developed methods of WHT on the indicators of the thickness of the fabric of the examined samples
Source: compiled by the authors

Figure 13 shows the data of experimental tests, with a control value of the breaking load of 845 N, samples under the influence of the existing WHT, this indicator decreases by 21.41% compared with the control value. This is observed in all examined variants of textile material, where the decrease in this indicator is from 17.43 to 33.33% of the control. During the WHT using a vacuum installation, the breaking load indicator remains unchanged.

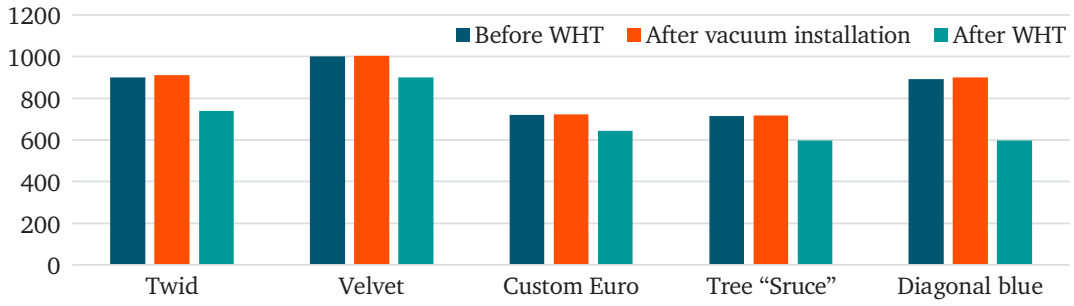

Figure 13. Influence of the existing and developed methods of WHT on the breaking load of the examined samples
Source: compiled by the authors

From the data presented in Figure 14, it can be seen that the surface density index for the control sample and processed according to the existing and proposed technology remains unchanged.

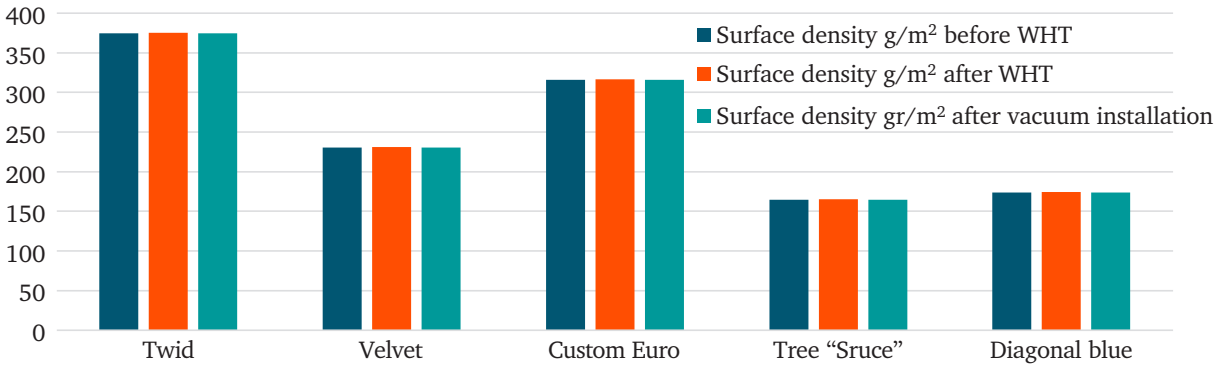

Figure 14. The effect of existing and developed WHT methods on the surface density of fabric
Source: compiled by the authors

From the experimental data presented in Figure 15, it can be seen that if the control value of air permeability is 187.32 cm^3/cm^2s, then in samples under the influence of the existing WHT, this indicator decreases by 12% compared to the control value. This is observed in all considered variants of the textile material, where the decrease in the air permeability index is from 7.17 to 31.53% compared to the control. When using a WHT vacuum installation, the air permeability index remains unchanged [16].

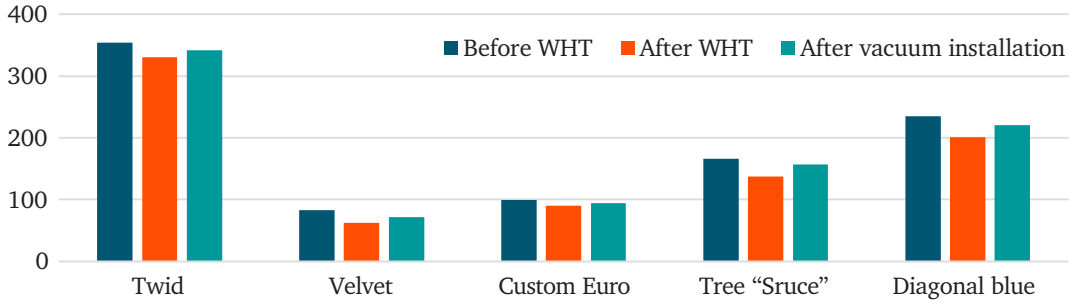

Figure 15. The influence of existing and developed methods of WHT on the breathability of the examined fabrics
Source: compiled by the authors

From the data of experimental tests of the stiffness index of samples presented in Figure 16, it can be seen that if the control stiffness value is 51.36, then this indicator is 22.51% higher for samples under the influence of the existing WHT than for the control sample. This is observed in all examined variants of the textile material, where the increase in the stiffness index is from 14.1 to 28.9% compared to the control.

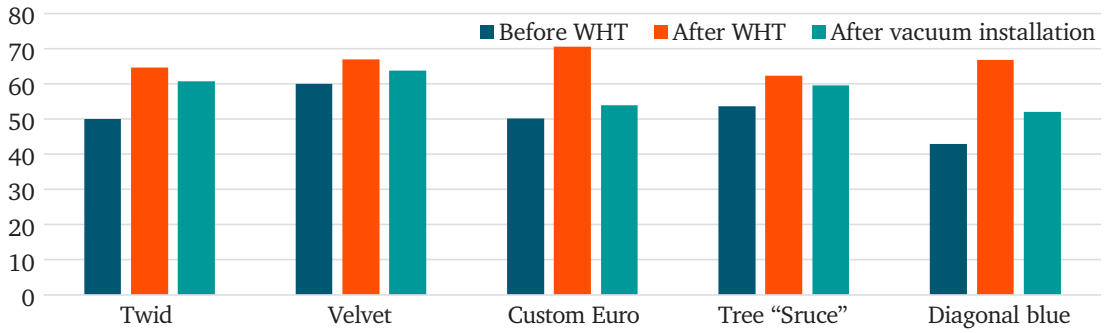

Figure 16. The influence of existing and developed methods of WHT on the stiffness of the fabric of the examined samples
Source: compiled by the authors

Based on the above examination, a comparative graph of the complex of indicators of the textile materials' properties has been developed for an objective assessment of the influence of the existing method of hydrothermal treatment of a vacuum installation and that proposed by the authors (Fig. 17).

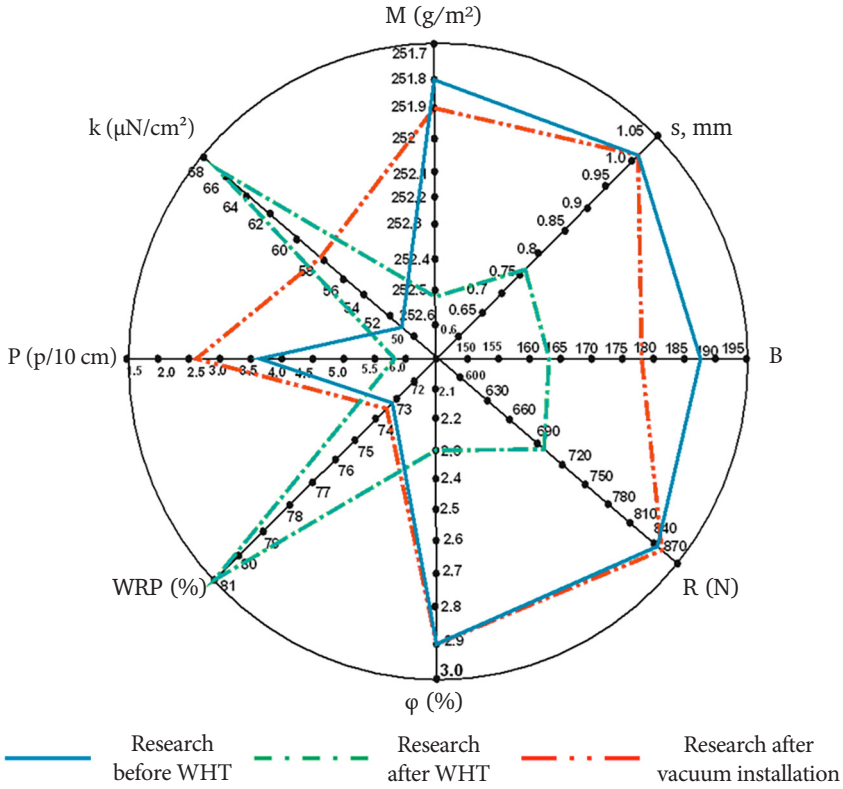

Figure 17. Comprehensive assessment of costume fabrics
Note: k – stiffness (μN/cm^2); P – density (p/10 cm); WRP – water-repellent properties (%); φ – humidity (%); R – breaking load (N); B – breathability; s – thickness (mm); M – mass of material (g/m^2)
Source: compiled by the authors

Thus, summarising the results of the data obtained, according to a comparative assessment of the effects of the existing and proposed methods of WHT of sewing parts, it can be stated that when processing textile material with the existing WHT method, the indicators of fabric thickness, breaking load, and breathability decrease on average by 32.9%, 21.41%, and 22.51%, respectively. Considering the importance of such properties of textile materials as fabric thickness, breaking load, and breathability for ensuring the quality of manufacturing of clothing parts, it can be concluded that the use of a vacuum installation allows maintaining the specified properties of the materials used [17].

Based on the theoretical and experimental examinations conducted, factors were identified, and assumptions were substantiated about the negative impact of the technological process of wet-heat treatment in the aggregate of moulding and pressing on the fabric in the manufacture of sewing parts. It was determined that during the WHT process, the fabric is subjected to pressure, while the threads in the fabric will flatten, flat areas will appear, thereby negatively affecting the physical and mechanical properties of the fabric. Experiments conducted in laboratory conditions have shown that the air permeability index for samples without polymer application and before exposure to pressure and moisture is on average 67.16 cm^3/cm^2s. It follows from this that after applying pressure paired with moisture, that is, after pressing, the air permeability index in sewing products decreases by 36.95%.

The influence of the WHT process on the physical and mechanical parameters of the fabric has been established. Thus, the breaking load and the elasticity index of fabrics before wet-heat treatment are also substantially reduced. It follows that the breaking load of the examined fabric decreased by an average of 7.72%, leading to rapid wear of individual sections of clothing parts. The strength indicators of fabrics to abrasion were examined and it was identified that the strength of the fabric to abrasion decreases after wet-heat treatment by about 15%, which leads to a decrease in the quality indicators of garments.

Discussion

It is difficult to overestimate the importance of the examinations of the effect of hydrothermal treatment on the properties of textile materials since they allow a better understanding of what changes occur in materials during processing and how these changes can affect the quality and durability of the finished textile products. One of the key aspects of such examinations is to determine the optimal parameters of hydrothermal treatment, which will preserve or even improve the physical and mechanical properties of the material. This is important for manufacturers of clothing and textiles, as it allows reducing the percentage of defects and improving the quality of products.

Studies on the effects of hydrothermal treatment of textile materials have long-term implications for both industry and consumers of textile products. Understanding the impact of hydrothermal treatment allows developing more innovative processing methods that consider important aspects of preserving the quality of the material. It also allows enterprises to save resources as optimised processing methods help to reduce energy consumption and raw material costs. An important factor is that the examinations of the hydrothermal treatment process can have an impact on the development of new materials and innovative textiles. Understanding how changes in the structure and properties of materials affect their functionality allows creating products that better meet the needs of modern society.

In the study by Z. Haitang & C. Shan [18] it was observed that after applying pressure paired with moisture, the air permeability index in sewing products can substantially decrease, reaching 30%. This fact indicates that hydrothermal treatment can have a negative impact on the breathability of textile materials and requires more detailed research and finding ways to improve the processing process to minimise the loss of breathability. Evaluating the results obtained by the researchers and this study, the use of a vacuum installation can help maintain the specified properties of the materials used, including fabric thickness, breaking load, and breathability. This is especially important in the clothing manufacturing process, where the quality and characteristics of materials play a key role. However, it is important to conduct additional research and testing to confirm the effectiveness of the vacuum installation and determine the optimal parameters of its application. Such research can contribute to the development of improved technologies and processes for processing textile materials, which, in turn, will increase the quality and durability of the finished textile products.

In the study by Y. Yang *et al.* [19] it was established that after the wet-heat treatment process, the breaking load of the textile fabric is substantially reduced. This observation indicates a potential decrease in the strength of the material after hydrothermal treatment, which can increase the risk of damage, shorten the service life of textiles, and reduce their quality and durability. Such results emphasise the importance of careful control and optimisation of the WHT process to minimise losses in strength and preserve the durability of materials and, consequently, the quality of finished products. In addition, these factors indicate the need to search for new processing methods or the use of improved technologies that could preserve the physical and mechanical properties of textile materials to a greater extent. Effective management of the WHT process can contribute to prolonging the service life of textile products, improving their characteristics, and, as a result, meeting the needs of consumers.

R. Mathangadeera *et al.* [20] in their study noted that after wet-heat treatment, the strength of the fabric is substantially reduced, thereby worsening the overall quality of textiles. These findings highlight the importance of careful control and management of the hydrothermal treatment process to ensure the quality of the final products. Notably, using a vacuum installation provides a potential solution to minimise the negative effects of hydrothermal treatment. The process of vacuuming allows for better retention of the properties of textile materials, which in the end, can

contribute to the preservation of the quality and durability of textile products.

In the study by R. Vinayagamoorthy [21], special attention was paid to the damage of textile fibres during hydrothermal treatment. Studies have shown that humidity and elevated temperature, accompanied by this process, can weaken intermolecular bonds in fibres, which leads to their destruction and deformation. This observation indicates the need for careful monitoring and optimisation of hydrothermal treatment conditions to prevent damage to fibres and ensure the safety of textile materials. This once again confirms the importance of research aimed at developing more effective methods of hydrothermal treatment and improving technologies that would preserve the physical and mechanical properties of textile materials during processing.

A. Kumar *et al.* [22] noted that after hydrothermal treatment, fabric thickness indicators can substantially decrease. This fact indicates potential changes in the structure of the material, such as compaction and compression of fibres, which can lead to a decrease in the thickness of the fabric. Reducing the thickness of the material can affect its thermal insulation, protective properties, the appearance, and comfort. Notably, these changes in thickness may be undesirable in some applications where maintaining the original thickness of the material is important. Thus, the results obtained in this study and those of other researchers emphasise the importance of careful control and optimisation of hydrothermal treatment processes, considering the thickness and other properties of the material. This can help preserve the quality and productivity of textiles and contribute to the more efficient use of these materials in various fields, including the textile industry, medicine, and sports applications.

K. Pandey *et al.* [23] noted that the use of new methods of processing textile materials may require additional attention to the technological aspects and control of the hydrothermal treatment process. This means the need to train personnel and create more complex systems to ensure the stability and reliability of the production process. This study, in addition to the paper of the above-mentioned researchers, confirms the need for the development and introduction of new methods and technologies in the hydrothermal processing of textile materials to improve their physical and mechanical properties and the overall quality of the final products. Both studies emphasise the need to improve processing processes to meet the needs of the textile industry for high-quality and durable materials.

Analysing the above-mentioned studies, the potential of research in the field of textile materials processing is great and represents an important step in improving production processes [24]. The relationship between materials' physical and mechanical properties and processing conditions implies that further research may lead to the development of more efficient and sustainable processing methods. Understanding the processes occurring in textile materials as a result of hydrothermal treatment allows optimising this process considering specific requirements and goals, such as maintaining the strength, thickness, and breathability of materials. Achieving this optimisation is of great importance for various industries where the quality and characteristics of textiles are important for comfort and safety [25]. Deeper research in this area can contribute to the development of new processing methods and innovative technologies that will combine high productivity and minimal impact on the properties of materials. Such findings can improve the quality of textile products, reduce production losses, and create more sustainable and efficient textile materials. Ultimately, studies of the effect of hydrothermal treatment of textile materials on their physical and mechanical properties not only contribute to the expansion of scientific knowledge in this field but also have direct application, providing improvement in the quality and functionality of textile products in everyday life and industry.

Conclusions

As a result of the conducted examination, which includes a number of experiments, it was established that the process of hydrothermal treatment can have a substantial impact on the properties of textile materials. A comparative analysis of the existing and proposed WHT methods allowed identifying substantial changes in the indicators of fabric thickness, breaking load, and breathability. On average, it was noted that the use of the existing WHT method leads to a decrease in these indicators by 32.9%, 21.41%, and 22.51%, respectively. This indicates a potential loss of quality of textile materials when using the conventional method. Additionally, the study identified the negative impact of the technological process of wet-heat treatment on the fabric structure.

It was noticed that the fabric is subjected to pressure as a result of pressing. This leads to the flattening of the threads and the formation of flat areas, negatively affecting the material's physical and mechanical properties and reducing its strength. As a result of a series of experiments, it was established that the impact of WHT is accompanied by a substantial decrease in the air permeability of the fabric and can negatively affect the comfort and functionality of textiles. The breaking load and elasticity index also decrease after processing, which increases the risk of wear and reduces the quality of garments. Potential problems associated with conventional WHT methods were identified and the importance of further research in the field of improving processing processes was highlighted.

The introduction of innovative methods, such as the use of a vacuum installation, can help maintain

the desired properties of materials and improve the quality of finished products. Areas for further research in this area may also include the development of special recommendations for optimal parameters of hydrothermal treatment and the analysis of the effects of treatment on various types of textile materials and their durability in real operating conditions. The practical importance of this study lies in the fact that the introduction of innovative methods will allow creating better textile products while preserving their characteristics and, ultimately, will contribute to meeting the needs of customers.

Acknowledgements
None.

Conflict of Interest
None.

References
[1] Samieva SH, Dzhuraeva TS, Asadova SS. Innovative technologies in the garment industry. Bukhara: Bukhara Engineering and Technology Institute; 2020.
[2] Mahkamova SF, Yuldasheva MT, Usanov MM. Influence of fibre composition on physical and mechanical properties of suit fabrics. 2020 [cited 2023 Oct 21]. Available from: http://rep.vstu.by/bitstream/handle/123456789/13997/s_61_64.pdf?sequence=1 .
[3] Makhkamova SF, Valieva ZF. Influence of wet-heat treatment on the degree of destruction of operational properties of fabrics of different fibre composition. 2019 [cited 2023 Oct 22]. Available from: http://www.rep.vstu.by/bitstream/handle/123456789/12215/Innov_2019_284-287.pdf?sequence=1&isAllowed=y.
[4] Kurbanov D. Development of textile industry in industrial production. *World Sci Res J*. 2023;15(1):58–63. http://www.wsrjournal.com/index.php/wsrj/article/view/2630.
[5] Murodova NS. Strategies of development of textile industry in Uzbekistan. *J Interdiscip Innovations Sci Res Uzb*. 2022;1(9):353–357.
[6] Younesi S, Ezazshahabi N. Tensile characteristics and stress relaxation analysis of woven fabrics in terms of fabric direction. *J Text Inst*. 2020;111(3):453–466. DOI: 10.1080/00405000.2019.1642711.
[7] Choi M, Kim Y, Park S, Ka D, Kim T, Lee S, *et al*. Functionalized polyurethane-coated fabric with high breathability, durability, reusability, and protection ability. *Adv Funct Mater*. 2021;31(24):2101511. DOI: 10.1002/adfm.202101511.
[8] Nutfullaeva LN, Artikbaeva NM, Bakhriddinova DA, Shin IG, Tashpulatov SS, Murodov TB. Investigation of formation conditions package and ensuring pillarity of pillows from composite materials. *Technol Text Ind*. 2019;2:95–101.
[9] Bakhriddinova DA. The process of technology forming in volume areas of outer clothing details using a device for vacuuming a closed technological space. *Thematic J App Sci*. 2022;6(1):145–151.
[10] Bhatti MM, Marin M, Zeeshan A, Abdelsalam SI. Recent trends in computational fluid dynamics. *Front Phys*. 2020;8:593111. DOI: 10.3389/fphy.2020.593111.
[11] Khlapuk M, Bezusyak O, Volk L, Zhang Z. Theoretical research of friction factor in hydraulically smooth pipes. *E3S Web Conf*. 2021;280:10009. DOI: 10.1051/e3sconf/202128010009.
[12] Wenbin YI, Qingchang M, Hui D, Chong W, Zhihong Z, Jiannong GU. Several issues in Bernoulli equation's instructional design. *Mech Eng*. 2021;43(6):967–972.
[13] Korovnikova NI, Dubina OM, Oliynyk VV. Properties of synthetic fibres with reduced flammability. 2020 [cited 2023 Oct 25]. Available from: http://repositsc.nuczu.edu.ua/bitstream/123456789/12101/1/Korovnikova_31_01_2020.doc.
[14] Zhang S, Gu W, Yao S, Lu S, Zhou S, Wu Z. Partitional decoupling method for fast calculation of energy flow in a large-scale heat and electricity integrated energy system. *IEEE Trans Sustainable Energy*. 2020;12(1):501–513. DOI: 10.1109/TSTE.2020.3008189.
[15] Lenko KA, Yasinskaya NN, Skobova NV, Lisovsky DL. Investigation of the effect of enzymes in the application composition on the properties of cotton fabrics. *Bull Namangan Inst Eng Technol*. 2021;1:82–84.
[16] Prajapatil DG, Kandasubramanian B. A review on polymeric-based phase change material for thermoregulating fabric application. *Polym Rev*. 2020;60(3):389–419. DOI: 10.1080/15583724.2019.1677709.
[17] Rakhmatullina ER, Lisanevich MS, Galimzyanova RYu, Khakimullin YuN. The effect of radiation sterilization on the stress-strain properties of non-woven materials -based on polypropylene. *Mat Sci Forum*. 2020;992:403–8. DOI: 10.4028/www.scientific.net/msf.992.403.
[18] Haitang Z, Shan C. Ergonomic performance research and evaluation method of cycling clothes. *J Phys Conf Ser*. 2021;1790:012022. DOI: 10.1088/1742-6596/1790/1/012022.
[19] Yang Y, Chen L, Naveed T, Zhang P, Farooq A. Influence of fabric structure and finishing pattern on the thermal and moisture management properties of unidirectional water transport knitted polyester fabrics. *Text Res J*. 2019;89(10):1983–1996. DOI: 10.1177/0040517518783349.

[20] Mathangadeera RW, Hequet EF, Kelly B, Dever JK, Kelly CM. Importance of cotton fiber elongation in fiber processing. *Ind Crops Prod*. 2020;147:112217. DOI: 10.1016/j.indcrop.2020.112217.
[21] Vinayagamoorthy R. Influence of fibre pretreatments on characteristics of green fabric materials. *Polym Polym Compos*. 2021;29(7):1039-1054. DOI: 10.1177/0967391120943461.
[22] Kumar A, Sharma M, Vaish R. Durable antibacterial cotton fabric via spray-coating of photocatalytic MoS2. *Mater Chem Phys*. 2022;290:126658. DOI: 10.1016/j.matchemphys.2022.126658.
[23] Wang Y, Li Z, Cao Y. Design of an environmentally friendly leather-like fabric based on thermoplastic polyurethanecoveredyarn.*JPhysConfSer*.2022;2256:012032.DOI:10.1088/1742-6596/2256/1/012032.
[24] Tsysar MO, Zakora AP, Babak AM, Ivakhnenko SO, Zanevsky OO. Dependence of the static strength of type Ib single crystal diamonds with octahedral habit on their size. *Sci Herald Uzhhorod Univ Ser Phys*. 2021;50:25–30.
[25] Molodetska TI. Investigation of the stress-strain state of the bending process of coated materials. *Sci Herald Uzhhorod Univ Ser Phys*. 2021;50:15–24.

Дослідження впливу гідротермічної обробки текстильних матеріалів на їх фізико-механічні властивості та розробка інноваційної технології

Саліх Шукурович Ташпулатов
Доктор технічних наук, професор
Ташкентський інститут текстильної та легкої промисловості
100059, вул. Шохжахон, 5, м. Ташкент, Узбекистан
Джизакський політехнічний інститут
130100, вул. І. Карімова, 4, м. Джизак, Узбекистан
https://orcid.org/0000-0001-5483-2644

Ділрабо Аманбаївна Бахріддінова
Кандидат технічних наук, доцент
Ташкентський інститут текстильної та легкої промисловості
100059, вул. Шохжахон, 5, м. Ташкент, Узбекистан
https://orcid.org/0000-0003-2083-4902

Шахло Нуруллаївна Нутфулаєва
Аспірант
Бухарський інженерно-технологічний інститут
200100, вул. К. Муртазаєва, 15, м. Бухара, Узбекистан
https://orcid.org/0009-0001-8739-4705

Лобар Нуруллаївна Нутфулаєва
Кандидат технічних наук, доцент
Бухарський інженерно-технологічний інститут
200100, вул. Каюма Муртазаєва, 15, м. Бухара, Узбекистан
https://orcid.org/0000-0001-6982-3185

Мухліса Собірівна Мумінова
Магістр, асистент
Бухарський інженерно-технологічний інститут
200100, вул. Каюма Муртазаєва, 15, м. Бухара, Узбекистан
https://orcid.org/0009-0003-8299-9662

Анотація

Актуальність. Дослідження у сфері текстильних матеріалів, а також впливу обробки на їх властивості мають актуальність, оскільки допомагають розробляти ефективніші методи обробки та підвищувати стійкість текстильних матеріалів до впливу різних факторів, що важливо як для виробників, так і для споживачів.

Мета. Метою дослідження було вивчити вплив гідротермічної обробки текстильних матеріалів на їх фізичні та механічні властивості, а також розробити технологію виробництва одягу з використанням нового способу (пристрою) пресового обладнання гідротермічної обробки з композитного матеріалу.

Методологія. При проведенні дослідження використовувався метод аналізу, а також був проведений експеримент, в якому при обробці відібраних зразків тканини використовувалася температура пари, яка не опускалася нижче 160°С, температура на робочих органах преса для формування спинки становила не менше 110°С.

Результати. В результаті було детально вивчено та встановлено вплив гідротермічної обробки на властивості текстильних матеріалів. Проаналізувавши існуючий метод гідротермічної обробки з використанням вакуумної установки, виявлено, що традиційний спосіб обробки призводить до істотного зниження товщини тканини, розривного навантаження та повітропроникності. Також було зазначено, що під час гідротермічної обробки матеріалу відбувається його експонування під впливом тиску. Це призводить до ущільнення та сплющування ниток усередині матеріалу, створюючи плоскі ділянки, що спричиняє несприятливі зміни у фізико-механічних характеристиках тканини.

Висновки. Ці фактори свідчать про потенційне погіршення якості та довговічності текстильних виробів, що може підвищити відсоток браку та негативно позначитися на задоволеності споживачів. Дане дослідження також вказує на перспективи використання вакуумної установки в гідротермічній обробці, що дозволяє зберегти бажані властивості матеріалів, покращуючи якість кінцевих продуктів. Практичне значення результатів цього дослідження полягає у можливості покращення якості текстильних виробів та зниження ступеня пошкодження матеріалів, що важливо для забезпечення більш тривалої експлуатації текстильної продукції та підвищення задоволеності споживачів

Ключові слова: формоутворення виробів; структура тканини; деформація волокон; вакуумне встановлення; розривне навантаження; повітропроникність

Scientific Herald of Uzhhorod University
Series "Physics"

Journal homepage: https://physics.uz.ua/en
Issue 54, 67–79
Received: 31.07.2023. Revised: 06.11.2023. Accepted: 18.12.2023

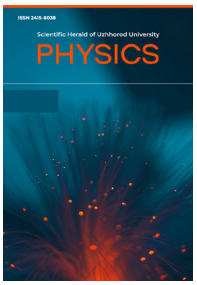

UDC 53.087
PACS 61.66
DOI: 10.54919/physics/54.2023.67

Crystal structure of barium manganese vanadate $BaMnV_2O_7$

Viktor Zavodyannyi*
PhD in Physical and Mathematical Sciences, Associate Professor
Kherson State Agrarian and Economic University
25031, 5/2 Universytetskyi Ave., Kropyvnytskyi, Ukraine
https://orcid.org/0000-0002-8224-8215

Mykola Voloshyn
PhD in Technical Sciences, Associate Professor
Kherson State Agrarian and Economic University
25031, 5/2 Universytetskyi Ave., Kropyvnytskyi, Ukraine
https://orcid.org/0000-0003-0467-1963

Valentina Zubenko
PhD in Technical Sciences, Associate Professor
Kherson State Agrarian and Economic University
25031, 5/2 Universytetskyi Ave., Kropyvnytskyi, Ukraine
https://orcid.org/0000-0002-8401-755X

Ruslan Teliuta
PhD in Technical Sciences, Associate Professor
Central Ukrainian National Technical University
25006, 8 Universytetskyi Ave., Kropyvnytskyi, Ukraine
https://orcid.org/0000-0002-4923-1227

Serhii Kvitka
PhD in Technical Sciences, Associate Professor
Dmytro Motornyi Tavria State Agrotechnological University
69600, 66 Zhukovskyi Str., Zaporizhzhia, Ukraine
https://orcid.org/0000-0001-9234-9274

Abstract

Relevance. The development of materials with excellent dielectric properties is crucial for modern telecommunications. The value of this study lies in the importance of examining these properties in the context of expanding possibilities for high-frequency applications in modern telecommunication technologies, including 4G and 5G communication.

Purpose. The purpose of this study is to investigate the crystal structure of the compound $BaMnV_2O_7$ and its dielectric properties.

Suggested Citation:
Zavodyannyi A, Voloshyn M, Zubenko V, Teliuta R, Kvitka S. Crystal structure of barium manganese vanadate $BaMnV_2O_7$. *Sci Herald Uzhhorod Univ Ser Phys.* 2023;(54):67–79. DOI: 10.54919/physics/54.2023.67

*Corresponding author

Methodology. To achieve the set purpose, methods of analysis, experimentation, comparison, and computer modelling were used. Within this study, the material of low-temperature co-fired ceramics (LTCC) was thoroughly examined, known for its high efficiency as moisture protection.

Results. A structural model for the compound $BaMnV_2O_7$ was proposed and investigated. In particular, it was found that the radius of Mn^{2+} (0.75 Å) is almost identical to the radius of Zn^{2+} (0.68 Å), confirming the similarity of the crystal structures of $BaMnV_2O_7$ and $BaZnV_2O_7$. The main results showed that pyrovanadate has a monoclinic symmetry and has a spatial symmetry group P121/c1 (14), characterised by lattice parameters: a = 5.6221(5) Å, b = 15.271(1) Å, c = 9.7109(8) Å, β = 123.702(3)°. The divergence factor was 9.05, indicating the model's correspondence to experimental data. Additionally, the density of the compound was calculated, amounting to 4.2699 g/cm^3.

Conclusions. Experimental data confirmed the presence of interatomic distances within 1.33-3.47 Å. The minimum interatomic distance in the compound structure is 1.33 Å between oxygen (O5) and vanadium (V2) atoms. The maximum interatomic distance is 3.47 Å observed between oxygen (O1) and (O2) atoms. With characteristics such as low dielectric permittivity (εr~8.9) and a high quality factor coefficient (Qu×f 31362 GHz), the compound $BaMnV_2O_7$ exhibits excellent microwave dielectric properties. The practical value of the obtained results lies in the potential development and improvement of materials with high dielectric properties, such as $BaMnV_2O_7$, for their application in telecommunication technologies, contributing to the development of more compact and reliable components for electronics

Keywords: X-ray structural analysis; dielectric properties; Bragg-Brentano geometry; Rietveld method; resonator

Introduction

Since 2013, there has been a rapid development of cellular communication, which requires materials with exceptional dielectric characteristics. Properties such as high quality factor, low temperature coefficient of resonant frequency, and excellent relative dielectric permittivity are critical for the further development of this area. In this context, low-temperature co-fired ceramics (LTCC) emerge as one of the promising materials. The ability to sinter at temperatures below 1000°C and the use of more readily available materials, such as copper, make LTCC technology particularly attractive. In addition, ceramics offer cost-effectiveness and ease of manufacturing devices, moisture tightness, and reliability even under significant temperature fluctuations. For instance, in radar systems, active phased array antennas consisting of receiver-transmitter modules are employed for optimisation and size reduction. L.O. Roman [1] notes that the miniaturisation of such devices led to the adoption of LTCC multilayer board technology.

It is essential to highlight that this technology also allows for the creation of complex multilayer boards. O.A. Nemyrovych [2] mentions that during LTCC technology, metallisation occurs through screen printing on an unfired ceramic sheet. The sheets are assembled into a stack, rolled on rollers, and sintered at temperatures up to 950°C, allowing the use of materials like silver or copper. The thickness of the resulting conductors is approximately 10 micrometres, roughly corresponding to three skin depths at 1 GHz. LTCC technology is particularly suitable for manufacturing planar high-Q inductors, resonators, and planar resistors. In the work of D.I. Varvaruk [3], the PBA 313 01/2 is investigated, representing an edge cascade for a Bluetooth communication system. It utilises ball grid array (BGA) connectors, and all individual components are located on one side of the board. This board is manufactured using LTCC technology and consists of 6 layers of this ceramic and 7 metal layers, confirming the possibility of creating multilayer boards. Moreover, Ye.M. Yashchyshyn [4] indicates that the advantages of LTCC include the ability for three-dimensional system integration, high control of technological parameters to ensure high repeatability, flexibility regarding the number of layers and types of materials, achieving minimal line and gap widths (on the order of 50 microns), the possibility of integrating passive and distributed elements, and mounting integrated circuits.

Many materials are considered for potential use in LTCC. However, vanadates attract special attention because they exhibit important properties that can be useful for high-frequency applications. For example, T.M. Hrychanovska & I.Yu. Protsenko [5] note that VO_2 films undergo a phase transition with increasing temperature, accompanied by a significant decrease in specific resistance. This property allows their use as thermoresistors for effective thermal protection at high temperatures. According to S.V. Khalameida *et al.* [6], the use of a V_2O_5 wet gel and hydrothermal treatment allowed obtaining magnesium pyro- and orthovanadates. Samples obtained

by microwave-assisted hydrothermal treatment are characterised by a high specific surface area and a developed porous structure.

Pyrovanadates are known for their complex crystalline structure, including atoms of chemical elements arranged in a specific lattice. These characteristics of the crystalline structure influence its physical and electronic properties and determine the magnetic and dielectric characteristics of the compound. However, information about the crystalline structure of $BaMnV_2O_7$ is not yet fully revealed, and the parameters of the lattice microstructure remain unknown. Therefore, the analysis of LTCC ceramic properties, including its crystalline structure, is especially relevant and crucial for developing modern telecommunications technologies. The purpose of this study is to analyse the crystalline structure and dielectric characteristics of the $BaMnV_2O_7$ compound. The high dielectric permittivity under certain conditions and frequencies makes the compound an interesting material for use in telecommunications technologies, where having materials with high dielectric properties for manufacturing resonators, filters, and other components is crucial.

Materials and Methods

To achieve the purpose of this study, various methods were employed, including analysis, comparison, experimental investigations, and computer modelling. All measurements and analyses were conducted under specialised laboratory conditions, where necessary temperature and humidity parameters were ensured. The obtained results underwent further scrutiny, and their reliability was subjected to additional verification and analysis.

The analysis method allowed for a detailed examination and breakdown of experimental and computational data to reveal the peculiarities of the crystalline structure of the $BaMnV_2O_7$ compound. During the comparative analysis, properties of $BaMnV_2O_7$ were juxtaposed with other materials exhibiting high dielectric characteristics, providing insights into its potential applications. For the experiments, $BaMnV_2O_7$ samples were prepared according to detailed protocols, involving synthesis and purification to obtain pure material for further investigations. Experimental measurements of dielectric properties and other physical parameters of the $BaMnV_2O_7$ compound provided specific data for analysis and justification of material properties. For the analysis, the diffraction spectrum of the compound was utilised using the PDF-2 No. 044-0245 database, containing theoretical and experimental data of powder diffractograms collected under conditions of radiation on a copper filter with Bregg-Brentano geometry [7]. The spectrum was analysed using the HighScore Plus 3.0 programme (Netherlands) to ensure its correspondence to a single-phase state of the $BaMnV_2O_7$ compound. Indexing of the diffraction spectrum was performed to determine the crystalline structure of the $BaMnV_2O_7$ compound. The built-in TREOR module in this programme was used to index the diffraction spectrum. Furthermore, using the structural model for the β-$BaZnV_2O_7$ phase, refinement of microstructural parameters was conducted using the Rietveld method and the HighScore Plus 3.0 programme. Key characteristics of the crystal structure of pyrovanadate were obtained.

Using computer modelling allowed for a detailed analysis of the crystalline structure and properties of $BaMnV_2O_7$ using modern computational technologies. The combination of these diverse methods provided a comprehensive understanding of the $BaMnV_2O_7$ compound, including its crystalline structure and physical characteristics. Specific protocols for result analysis were developed for each of the methods used. This included processing diffraction patterns, phase identification, determination of crystalline structure parameters, and more. To confirm the reliability and accuracy of the obtained results, series of repeated experiments were conducted, and the obtained data were compared with literature sources. Considering the large amount of data, a statistical analysis was performed to confirm the results and determine the degree of their deviation.

The study paid special attention to the analysis of the crystalline structure and physical properties of the $BaMnV_2O_7$ compound. The combination of methods, including X-ray structural analysis, computer modelling, and other spectroscopic and physical methods, provided an opportunity to gain a comprehensive understanding of the crystalline structure and physical properties of the $BaMnV_2O_7$ compound.

Results

It follows from the literature that vanadates have satisfactory microwave dielectric properties and can be used as microwave LTCC ceramics [8]. Microwave dielectric ceramics are an important class of materials for the production of electronic devices, especially high-frequency and microwave devices. It is characterised by high permittivity and low losses, which allow effectively using these materials for transmitting signals in the high-frequency range. In addition, it is important to note that vanadates can be integrated into LTCC technology. This means that they can be used as components of the material used for the manufacture of microwave devices by co-heating at low temperatures.

$BaMnV_2O_7$ is also a promising material for use in LTCC technology. Given that the radius Mn^{2+} (r = 0.75 Å) is close to Zn^{2+} (r = 0.68 Å), a crystal structure similar to the $BaZnV_2O_7$ compound should be expected [6]. This similarity in crystal structures is due to the close values of the sizes of Mn^{2+} and Zn^{2+} atoms, which leads to similar ways of ordering

them in the crystal lattice of both compounds. This pyrovanadate has two polymorphic modifications, i.e. it can exist in two different crystal structures under the same temperature and pressure conditions. Crystal structure of low-temperature β-$BaZnV_2O_7$ crystallises in monoclinic syngony, spatial symmetry group (PGS) $P2_1/n$, grid parameters a = 5.573 A^0, b = 15.175 A^0, c = 7.429 A^0, β = 96.45^0. The data show that there is a certain degree of irregularity in the crystal lattice, but simultaneously, there is a plane of symmetry. The microstructural parameters are shown in Table 1 and indicate small-scale features of the material's crystal structure. Small-scale features indicate details and relationships between atoms or other components in the crystal structure of a material.

Table 1. Microstructural parameters of β-$BaZnV_2O_7$

Atom	Wyck	X/a	y/b	z/c
Ba	4e	-0.2830(1)	0.28596(3)	0.4471(7)
Zn	4e	-0.2077(2)	0.05006(6)	0.3676(1)
V1	4e	-0.2525(2)	0.36597(8)	0.6654(2)
V2	4e	-0.2052(2)	0.56203(8)	0.7105(2)
O1	4e	-0.246(1)	0.2824(4)	0.5224(8)
O2	4e	-0.256(1)	0.4716(4)	0.5530(8)
O3	4e	-0.229(1)	0.6604(4)	0.617(1)
O4	4e	0.077(1)	0.5527(4)	0.8214(9)
O5	4e	-0.414(1)	0.5542(4)	0.8681(8)
O6	4e	-0.494(1)	0.3553(4)	0.7904(9)
O7	4e	0.005(1)	0.3609(4)	0.8099(9)

Source: compiled by the authors

The structure of β-BaZnV was taken as the initial model of the crystal structure$_2O_7$. Selection of the initial model of the β-$BaZnV_2O_7$ crystal structure in the examination of $BaMnV_2O_7$ is based on several reasons. First, both compounds have the same composition and arrangement of atoms, which may indicate the similarity of their crystal structures. Secondly, the ability to use an already examined model simplifies the analysis and comparison of the properties of a new compound. Furthermore, if β-$BaZnV_2O_7$ was the subject of previous research, the availability of known data facilitates the analysis of $BaMnV_2O_7$. In addition, the affinity of the components Ba, Mn, V, Zn, and O emphasised the similarity of the structures of these compounds.

As a result of the conducted analysis of the structural characteristics of the $BaMnV_2O_7$ compound, it was established to crystallise in monoclinic syngony and have a P121/c1 spatial symmetry group [14]. Monoclinic syngony indicates that the crystal structure of the compound has irregularity, which manifests itself in the form of uneven sides and angles in a parallelogram that restricts the base region. In this case, the main axes of the crystal are not mutually perpendicular, and therefore, the connection exhibits symmetry with respect to only one plane. In the $BaMnV_2O_7$ crystal lattice, the plane of symmetry inequalities is present, as in β-$BaZnV_2O_7$. The specific lattice parameters are: a=5.6221(5)A0, b = 15.271(1)A0, c = 9.7109(8) A0 at β = 123.702(3)0. The specified lattice parameters (a, b, c, and β) determine the geometric dimensions and angles between the lattice vectors. The values a, b, and c represent the lengths of the axes, and β determines the angle between a and c. Table 2 shows the microstructural parameters for detailed analysis.

Table 2. $BaMnV_2O_7$ microstructural parameters

Atom	Wyck	s.o.f.	x	y	z
Ba1	4e	1	0.403(2)	0.2068(4)	0.6468(8)
V1	4e	1	0.930(3)	0.1236(9)	0.130(2)
V2	4e	1	0.954(4)	0.948(1)	0.240(2)
Mn1	4e	1	0.595(4)	0.442(1)	0.874(2)
O1	4e	1	0.81(1)	0.220(3)	0.079(4)
O2	4e	1	0.84(1)	0.823(4)	0.724(7)
O3	4e	1	0.92(1)	0.855(3)	0.107(5)
O4	4e	1	0.73(1)	0.960(3)	0.276(5)
O5	4e	1	0.825(8)	0.523(3)	0.570(5)
O6	4e	1	-0.107(9)	0.190(3)	0.311(4)
O7	4e	1	0.825(9)	0.103(3)	0.340(3)

Source: compiled by the authors

Important experimental data for the characterisation of crystalline materials are the values of interplanetary distances. Interplanetary distances indicate the distances between atoms and molecules located on different planes of the crystal lattice [9]. The intensity, i.e. the strength of the diffraction signal that is recorded during the crystal examination, also depends on the structural features of the crystal, such as the position of atoms and their interplanetary distances. The divergence factor (R-factor) is 9.05, and the calculated density is 4.2699 g/cm^3. If the interplanetary distances differ by 0.03A_0, the diffraction lines are taken as one. The values of interplanar distances and intensities calculated using this model are shown in Table 3. This position was considered when analysing the crystal structure, and according to these data, the $BaMnV_2O_7$ structure is represented.

Table 3. Values of interplanar distances and intensities calculated for the structure of the $BaMnV_2O_7$ compound

$2\theta_{cal}$	$2\theta_{obs}$	d_{cal}	d_{obs}	I_{cal}	I_{obs}	H	K	L
11.5723	11.574(5)	7.64064	7.63951	4.46	3.16	0	2	0
13.3377	13.344(4)	6.63302	6.62968	2.87	4.17	0	1	-1
16.7107	-	**5.301**	-	0.21	-	0	2	-1
16.7107	-	**5.301**	-	0.21	-	0	2	1
16.853	-	**5.25656**	-	0.08	-	1	1	-1
18.9506	18.957(5)	4.67918	4.67769	1.12	3.18	1	0	0
19.6453	19.650(6)	4.51526	4.51408	5.99	3.06	1	2	-1
19.8285	19.839(6)	4.47395	4.47163	2.17	3.03	1	1	0
20.8258	-	**4.2619**	-	0.8	-	1	0	-2
21.1981	21.19(1)	4.18788	4.18901	1.24	1.06	0	3	-1
21.6308	21.619(4)	4.10508	4.10738	5.05	4.23	1	1	-2
22.2635	22.263(2)	3.98983	3.98994	15.34	13.12	1	2	0
23.2727	23.266(5)	3.81905	3.82015	0.21	3.05	0	4	0
23.6007	23.610(8)	3.7667	3.76525	2.1	1.83	1	3	-1
23.891	23.892(2)	3.72159	3.72138	16.5	15.85	1	2	-2
24.1616	24.1646(6)	3.68052	3.68007	64.23	66.81	0	0	2
24.8641	24.8607(5)	3.5781	3.57858	45.96	88.96	0	1	-2
25.8398	25.845(4)	3.44516	3.44451	6.34	4.14	1	3	0
26.269	-	**3.38984**	-	1.86	-	0	4	-1
26.269	-	**3.38984**	-	1.86	-	0	4	1
26.8685	-	**3.31555**	-	0.26	-	0	2	-2
26.8685	-	**3.31555**	-	0.26	-	0	2	2
27.267	27.264(1)	3.26799	3.26834	23.26	17.78	1	3	-2
28.2674	28.277(1)	3.15457	3.1535	100	99.98	1	4	-1
28.2908	28.279(1)	3.15201	3.15325	89.19	100	1	1	1
29.933	29.9314(8)	2.98271	2.98287	22.35	38.38	0	3	-2
30.1852	30.184(1)	2.95837	2.95847	15.33	19.83	1	4	0
30.8755	30.8743(9)	2.89378	2.89389	33.11	30.7	1	1	-3
31.4309	-	**2.8439**	-	3.42	-	1	4	-2
31.9536	31.9486(9)	2.79856	2.79899	29.52	28.9	2	0	-2
32.8753	32.892(2)	2.72218	2.72086	9.27	8.24	1	3	1
33.7987	33.782(4)	2.64988	2.65113	0.65	4.22	0	4	-2
35.1563	35.2(1)	2.5506	2.55051	16.78	9.58	1	3	-3
35.1795	35.18(7)	2.54898	2.54864	0.36	9.47	2	2	-1
35.8705	-	**2.50144**	-	0.06	-	2	1	-3
36.463	36.478(3)	2.46214	2.46118	5.07	6.2	1	4	1
37.0835	37.111(2)	2.42236	2.4206	3.33	11.92	0	1	-3
37.347	37.357(1)	2.40587	2.40527	10.02	22.98	0	6	-1
38.5105	38.5(1)	2.33582	2.33571	0.36	5.52	0	2	-3
38.5587	38.55(4)	2.33301	2.33359	11.01	5.51	1	4	-3
38.5875	38.60(4)	2.33133	2.33041	0.75	3.53	1	0	2
38.8313	38.82(1)	2.31725	2.31781	0.52	2.54	1	6	-1

Table 3. Continued

$2\theta_{cal}$	$2\theta_{obs}$	d_{cal}	d_{obs}	I_{cal}	I_{obs}	H	K	L
38.9206	38.950(5)	2.31214	2.31049	2.74	9.56	2	1	0
39.0525	39.071(4)	2.30464	2.3036	12.96	11.68	1	1	2
39.9081	39.927(7)	2.25718	2.25616	0.01	2.12	2	4	-2
40.861	40.821(2)	2.20671	2.2088	2.32	8.28	2	4	-1
41.561	41.538(5)	2.17115	2.17232	2.28	3.22	1	0	-4
41.9985	41.991(3)	2.14954	2.14989	2.88	6.16	1	1	-4
42.593	42.587(1)	2.1209	2.1212	2.98	15.92	1	5	-3
42.8215	42.815(3)	2.11011	2.11041	9.66	8.79	2	1	-4
43.2112	43.2(1)	2.09198	2.09297	2.74	6.23	0	7	1
43.2895	43.2(1)	2.08838	2.0918	0.7	6.22	1	2	-4
43.8265	43.81(6)	2.06403	2.0648	5.92	11.25	0	4	-3
43.8394	43.84(5)	2.06345	2.0633	0.4	10.4	2	5	-2
45.3733	45.4(1)	1.99719	1.99787	0.43	9.68	1	6	1
45.3754	45.38(6)	1.9971	1.99672	14.34	9.38	1	3	-4
46.1501	46.156(3)	1.96536	1.96513	0.04	5.21	2	3	-4
46.5094	46.509(4)	1.95102	1.95103	0.9	4.18	2	5	-3
47.4955	47.501(6)	1.91279	1.91259	5.44	9.45	0	5	-3
47.5903	47.54(2)	1.9092	1.91124	2.55	4	0	8	0
49.1616	49.159(8)	1.85179	1.85188	0.01	6.18	3	1	-3
49.2685	49.25(2)	1.84802	1.84853	0.42	3.01	0	8	-1
49.4989	49.501(1)	1.83995	1.83990	16.11	28.86	0	0	4
50.4662	50(1)	1.80693	1.807	2.23	7.04	1	8	-1
50.4805	50(1)	1.80645	1.80699	3.1	7.04	1	7	1
51.0418	51.04(9)	1.7879	1.78791	3.47	5.42	1	1	3
51.6071	51.07(9)	1.76963	1.78686	0.19	5.42	1	5	-4
51.6547	51.6(1)	1.76812	1.76867	0.11	1.24	3	0	-4
51.6701	51.7(3)	1.76763	1.76745	1.48	1.13	1	8	0
52.1158	52.102(5)	1.75355	1.75397	1.29	3.2	1	7	-3
52.8668	52.846(5)	1.7304	1.73103	0.73	3.15	0	3	-4
53.1268	53.139(4)	1.72254	1.72217	0.09	4.13	3	2	-4
53.1345	54.717(4)	1.72231	1.67619	0.25	4.06	2	6	0
54.928	54.928(3)	1.67024	1.67023	1.3	6.05	3	3	-4
55.3854	55.343(7)	1.65752	1.65868	0.12	5.94	0	4	-4
55.3854	55.5(1)	1.65752	1.65442	0.12	3.41	0	4	4
55.5197	55.54(7)	1.65383	1.65333	2.84	3.41	2	7	-3
56.1183	56.129(4)	1.6376	1.63732	3.03	4.03	2	5	1
56.3901	56.388(2)	1.63035	1.6304	1.78	8.09	0	7	-3
57.0776	57.10(4)	1.61233	1.61182	0.01	1.25	1	3	-5
57.1508	57.18(1)	1.61044	1.60961	4.32	2.88	2	0	2
57.5574	57.520(5)	1.60003	1.60099	2.02	4.95	2	4	-5
57.7379	57.71(9)	1.59546	1.59616	0.5	3.46	2	7	0
57.7448	57.75(4)	1.59528	1.59524	0.07	3.16	1	9	0
58.4963	58.507(5)	1.57657	1.5763	0.28	3.15	1	9	-2

Source: compiled by the authors

However, not all lines meet this criterion. Lines that do not meet this criterion are shown in bold in Table 3. As can be seen from the calculation table, such diffraction lines have a low intensity and, therefore, may not be detected in the diffraction spectrum. All observed strong lines coincide with the lines calculated using this structural model. In addition, the discrepancy factor is less than 10% and is 9.05%. The R-factor is one of the criteria used to evaluate the suitability of a structural model for experimental data [10]. It indicates a correspondence between the measured data and those obtained using the model.

A low R-factor (less than 10%) indicates that the structural model correctly describes the experimental data, so it can be assumed that the proposed structural model of the crystal structure of a given compound is correct. Ultimately, Zn and Mn are similar in their properties and can have a similar structure for the $BaZnV_2O_7$ compound. Table 4 shows the interatomic distances for the $BaMnV_2O_7$ structural model.

Table 4. Interatomic distances of the $BaMnV_2O_7$ compound structural model

Ba1		V1		V2		Mn1	
- O6	2.77(3)	- O2	1.47(6)	- O5	1.33(4)	- O7	1.63(6)
- O6	2.78(5)	- O1	1.58(4)	- O4	1.47(7)	- O4	2.07(6)
- O2	2.80(6)	- O6	2.00(5)	- O3	1.79(5)	- O2	2.77(8)
- O2	2.83(8)	- O7	2.26(5)	- O7	2.76(5)	- O6	2.87(6)
- O4	2.84(5)	- O5	2.30(4)	- V1	2.83(2)	- V2	2.91(2)
- O1	2.88(6)	- O3	2.68(6)	- Mn1	2.91(2)	- V1	3.27(2)
- O3	2.99(4)	- V2	2.83(2)	- O7	3.29(4)	- V2	3.31(3)
- O1	3.19(3)	- O5	3.18(5)	- Mn1	3.31(3)	- O5	3.31(3)
- O1	3.25(6)	- Mn1	3.27(2)			- O4	3.32(4)
- O7	3.27(4)	- O4	3.28(6)			- Mn1	3.45(3)
- O3	3.30(5)						
O1		**O2**		**O3**		**O4**	
- V1	1.58(4)	- V1	1.47(6)	- V2	1.79(5)	- V2	1.47(7)
- O6	1.88(6)	- O6	1.7(1)	- O5	1.92(6)	- Mn1	2.07(6)
- O2	1.89(6)	- O1	1.89(6)	- O6	2.67(6)	- O5	2.18(8)
- Ba1	2.88(6)	- O7	2.5(1)	- V1	2.68(6)	- O7	2.24(7)
- O7	2.88(6)	- Mn1	2.77(8)	- O4	2.79(8)	- O3	2.79(8)
- O6	3.00(7)	- Ba1	2.80(6)	- Ba1	2.99(4)	- Ba1	2.84(5)
- O3	3.02(8)	- Ba1	2.83(8)	- O1	3.02(8)	- O7	3.04(4)
- O3	3.10(5)	- O3	3.03(9)	- O2	3.03(9)	- O5	3.07(5)
- Ba1	3.19(3)	- O3	3.19(9)	- O1	3.10(5)	- V1	3.28(6)
- Ba1	3.25(6)	- O1	3.47(7)	- O2	3.19(9)	- Mn1	3.32(4)
- O7	3.47(6)			- Ba1	3.30(5)		
- O2	3.47(7)						
O5		**O6**		**O7**			
- V2	1.33(4)	- O7	1.45(7)	- O6	1.45(7)		
- O3	1.92(6)	- O2	1.7(1)	- Mn1	1.63(6)		
- O4	2.18(8)	- O1	1.88(6)	- O4	2.24(7)		
- V1	2.30(4)	- V1	2.00(5)	- V1	2.26(5)		
- O5	2.93(7)	- O3	2.67(6)	- O2	2.5(1)		
- O7	3.06(6)	- Ba1	2.77(3)	- V2	2.76(5)		
- O4	3.07(5)	- Ba1	2.78(5)	- O1	2.88(6)		
- V1	3.18(5)	- Mn1	2.87(6)	- O4	3.04(4)		
- O5	3.22(6)	- O1	3.00(7)	- O5	3.06(6)		
- Mn1	3.31(3)			- Ba1	3.27(4)		
				- V2	3.29(4)		
				- O1	3.47(6)		

Source: compiled by the authors

Minimum interatomic distance is 1.33A^0 O5-V2. Maximum interatomic distance is 3.47A^0 O1-O2. Interatomic distances are key crystal structure parameters and determine atoms' relative position in the crystal lattice. In crystal lattices, the atoms are arranged in an ordered manner, forming various structural elements, such as cubes, tetrahedra, and octahedra [11]. The distances between these structural elements determine interatomic distances. For example, interatomic distances indicate the distances between atoms for metal crystal lattices. In the context of the $BaMnV_2O_7$, interatomic distances indicate the distances between barium (Ba), manganese (Mn), vanadium (V), and oxygen (O) atoms in the crystal lattice. The interatomic distances between these atoms affect the electronic structure and, consequently, the conductivity of the compound. These distances are important for understanding the properties of a material, such as

magnetic, electronic, and dielectric, because of their effect on electron motion. In addition, interatomic distances indicate possible interactions between atoms in a compound that affect its properties and behaviour under various conditions.

In metals, electrons in the outer shell of atoms, known as "free electrons", can separate from atoms and move freely along the crystal lattice. If the interatomic distances in the metal crystal decrease, the electrons will have less space to move. This can increase the effective concentration of free charge carriers since the electrons will interact more with each other. As a result, the conductivity of the material may increase. In contrast, if the interatomic distances increase, the electrons will have more space to move. This can lead to a decrease in the effective concentration of free charge carriers and, accordingly, to a decrease in conductivity. According to this, if the interatomic distances in $BaMnV_2O_7$, the electrons in the manganese and vanadium sublattices decrease, they will have less space to move. This can lead to an increase in the effective concentration of free charge carriers, which will make the material a better conductor. In contrast, if the interatomic distances increase, the electrons will have more space to move. This can lead to a decrease in the effective concentration of free charge carriers and, accordingly, to a decrease in conductivity [12].

In the crystal structure of the $BaMnV_2O_7$ compound, two Ba+2 arrangements are observed, each of which has special bonds with oxygen and vanadium atoms and different configurations of Mn atoms. In Figure 1, Ba+2 is bound to four oxygen atoms O1, O2, O4, O6, and in another modification, the atom has a different arrangement of O1, O2, O2, and O3. O4, O6. The Vanadium atom also has two locations. V1 forms triangular bonds with oxygen atoms O1, O6. Another arrangement of V2 forms an irregular tetrahedron with oxygen atoms O3, O4, and O5. Two Mn atoms form triangular bonds with oxygen atoms O4, O7, the other arrangement of the manganese atom has a bond with the oxygen atom O7.

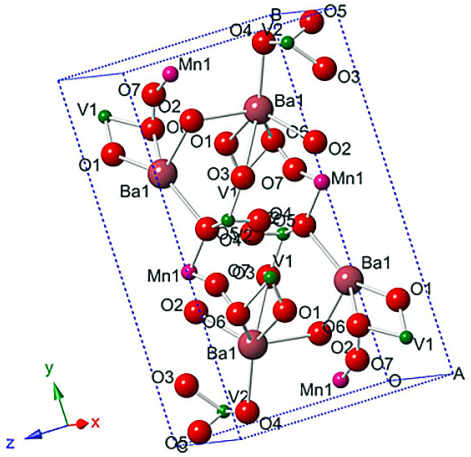

Figure 1. Image of the crystal structure of the $BaMnV_2O_7$ compound
Source: compiled by the authors

In further analysis of the crystal structure of the $BaMnV_2O_7$, this structure affects the electronic and electrical properties of the material. For example, the arrangement of Ba^{+2} atoms and their bonds with oxygen and vanadium atoms can determine the efficiency of charge transfer in a material. It is also important to consider that different configurations of Mn atoms can affect the magnetic properties of the compound. The arrangement of Ba^{+2} atoms and their bonds with oxygen and vanadium atoms can affect the efficiency of charge transfer in a material through two main mechanisms: changes in the valence or degree of ionisation of atoms and changes in the electronic structure. In the specific case of a $BaMnV_2O_7$ compound, the arrangement of Ba^{+2} atoms affects the location and structure of charge carriers in the material. This leads to a change in its electrical conductivity.

As for Mn atoms, their different configurations can affect the magnetic properties of the compound. The orientation and spin structures of the atoms determine the magnetic properties of a material. Changes in the crystal structure and arrangement of Mn atoms lead to changes in magnetic properties, such as magnetic susceptibility, magnetic separation coefficient, and spin resonance frequency. These aspects of magnetic properties may be the subject of additional experiments to understand better the physical mechanisms that determine the magnetic behaviour of the $BaMnV_2O_7$ compound. The application of $BaMnV_2O_7$ in LTCC ceramics can open up new opportunities for the production of high-frequency devices with excellent stability and efficiency. $BaMnV_2O_7$ shows substantial potential for application in LTCC due to its satisfactory microwave dielectric properties. The main characteristics of

the compound, such as its low permittivity (er ~ 8.9), high quality factor (Qu×f 31362 GHz) and excellent thermal stability, make it an attractive candidate for use in the manufacture of microwave devices.

However, on the dielectric characteristics of $BaMnV_2O_7$, various factors can influence understanding, which is important for optimising the characteristics of the material. For example, changes in the crystal structure. Since the permittivity of a material depends on the internal lattice and the location of atoms, any changes in the crystal structure can affect the dielectric properties. The presence of impurities or irregularities in the crystal structure can affect the conductivity and dielectric properties. If defects in the crystal structure (for example, gaps in the lattice, inconsistencies in the atomic arrangement) or impurities are present, the conductivity and dielectric properties are changed. Defects can be charged, which also affects electrical behaviour. In addition, microscopic features such as grain boundaries and inclusions also change electrical behaviour. Dielectric properties often change with temperature changes. Thermal exposure can lead to changes in the crystal structure and dielectric parameters. As the temperature rises, the atoms move and change their position in the lattice, affecting the electrical properties. Material processing also plays an important role in the manufacture of devices [13].

In many cases, LTCC ceramics are used to make RF electronics components, and $BaMnV_2O_7$ can be an important material for optimising such devices. This material can be particularly valuable for developing new telecommunications and microwave technologies components, where low losses and high frequency stability are critical factors. The results obtained create prospects for further research and possible implementation of $BaMnV_2O_7$ in the telecommunications technology industry, including modern 5G networks.

Discussion

LTCC ceramic is an important material in modern technologies for the production of microwave appliances. It allows manufacturing devices with high dielectric properties and low signal loss at high frequencies. However, the use of LTCC ceramics has some drawbacks. One of the main disadvantages is the physico-chemical incompatibility of many thick-film materials with LTCC sheets, which makes them difficult to use simultaneously. In the study by H. Birol et al. [14], it is indicated that chemical problems occur due to the interaction of the glass phase in the tape and thick films, while physical problems are usually associated with the discrepancy between the shrinkage of the tape and the paste for screen printing. This is observed microscopically and macroscopically in chemical diffusion (using microscopy and spectroscopic analysis) or deformed structures (warping, stratification, twisting), respectively. In addition, deformations such as warping, conductor inflating, and peeling can occur during the ceramic sintering process. This clearly affects the quality of devices manufactured using this technology. In addition, the compatibility of LTCC materials with other components of electronic devices can cause certain difficulties. Since they can have different thermal expansion coefficients, this can cause mechanical stresses and affect the reliability of the device in general.

Despite some of the shortcomings of LTCC ceramics, intensive research is being conducted to optimise it and find new compounds that can be applied in electronics and telecommunications technologies. Among the representatives of LTCC ceramics, a number of vanadates can be distinguished, the dielectric properties and crystal structure of which are intensively examined. One of the most interesting alternatives is pyrovanadate ceramics, which has already attracted the attention of researchers for its unique properties and potential applications in modern technologies. In the study of Y.T. Huang *et al.* [16], it was reported that the results of a study of the dielectric properties and crystal structure of $SrCo1\text{-}xMgxV_2O_7$ (x = 0-0.09) LTCC ceramics. It is indicated that the $SrCoV_2O_7$ compound crystallises in monoclinic syngony with the spatial symmetry group P21/c (14). Due to its dielectric properties, this compound is promising as a microwave dielectric ceramic. Microwave dielectric ceramics have specific dielectric properties at high frequencies, especially in the microwave range. $NaCa_4V_5O_{17}$ ceramics manufactured using LTCC technology (at temperatures of 780-860°C), attracts attention as a potential candidate for use in the production of microwave devices. The results, provided in study by C. Yin *et al.* [17], demonstrate that the compound crystallises in triclinic syngony, and has promising dielectric properties (permittivity εr = 9.72, Q-factor Q×f = 51000 GHz, and temperature coefficient of resonant frequency τf = -84 · 10-6 1/°C) and can be used in multilayer electronic devices.

Authors A.N. Unnimaya *et al.* [18] reported the results of the examination of $Mg_4V_2O_9$ ceramics, which show high efficiency in the microwave range and also demonstrate good chemical compatibility. It is indicated that by its properties, the compound can be used for the fairing designs of terahertz (THz) antenna arrays. According to experiments of D. Zhou *et al.* [19], microwave dielectric ceramics $(1\text{-}x)BiVO_4\text{-}xTiO_2$ (x = 0.4, 0.5, 0.55, and 0.60) in low-temperature firing was obtained by the conventional solid-phase reaction method. According to the results of the study, ceramics can be used as a substrate for physically and electrically small dielectric microstrip antennas. In the study by E.K. Suresh *et al.* [20], the dielectric properties of a16v18o61 ceramics (a = Ba, Sr, Ca) were measured using a vector network analyser, which showed

high-quality coefficients in the absence of load. Together with 0.4 $BaTa_2V_2O_{11}$-0.6 $Ba_2BiV_3O_{11}$ composite material, potential high-frequency compounds.

Given the importance of microwave ceramics in modern technologies, especially in the context of 4G cellular communication and its further development in 5G, it is important to consider its properties and potential for optimising and improving high-frequency signal transmission. Results of the examinations of the $BaMnV_2O_7$ LTCC indicate the high potential of this material as a microwave dielectric ceramic, in particular, due to its low sintering temperature and impressive microwave dielectric characteristics, indicating possible use in modern and future communication systems. Notably, the examined compound $BaMnV_2O_7$ fits in with the general trend of pyrovanadates in terms of crystal features. Regularities in the crystal features and dielectric properties of $BaMnV_2O_7$, consist in their similarity in terms of interatomic distances and the base crystal structure. This indicates a certain conservatism of the pyrovanadate group in these aspects. However, it should be considered that individual differences may occur due to the influence of valence and the location of atoms in the structure. In comparison with the results of studies of other compounds, it can be noted that $BaMnV_2O_7$ has close interatomic distances characteristic of pyrovanadates. The atoms' arrangement and coordination are also similar to other vanadates examined. Additional research, in particular, dielectric studies, allows a better understanding of the properties of these compounds and their potential applications.

Common dielectric properties include parameters that characterise the ability of a material to conduct or block the flow of electric charge when exposed to an electric field. These include characteristics such as permittivity, Q-factor, loss of dielectric properties. The overall dielectric properties of a material are determined by its chemical composition, crystal structure, microstructure, and other factors. In the case of pyrovanadates like $BaMnV_2O_7$ their dielectric properties may affect their suitability for specific applications, particularly in telecommunications technologies. A study by X. Jiang *et al*. [21] showed that microwave dielectric $BaMnV_2O_7$ LTCC ceramics have high performance. For example, its permittivity (εr) is about 8.9, and the quality factor (Qu×f) is 31362 GHz. The temperature resistance is also -54.9 ppm/°C at a sintering temperature of 950°C [22]. These properties make $BaMnV_2O_7$ LTCC a promising material for use in 5G polarisation converters [23]. Compared to other materials, $BaMnV_2O_7$ LTCC is identified to be competitive. For example, $CA_3MgSi_2O_8$ ceramics have an εr of about 5.3, Qu×f reaches 60000 GHz, and τf is -15 ppm/°C, as reported by H. Barsegar-Bafrooei *et al.* [24]. In addition, the dielectric properties of ceramics Bi1.5 Mg0.8 Cu0.2 V1.5 O7 and Bi1.5 Mg0.2 Cu0.8 V1.5 O7 were examined, characterised by low permeability and higher losses according to M. Shivalingayya & R.L. Raibagkar [25].

Summarising, $BaMnV_2O_7$ LTCC exhibits excellent microwave dielectric characteristics that can be compared to or even surpass other materials used in 5G technologies [26; 27]. In particular, the high-temperature modification of $BaMnV_2O_7$ may have the potential to solve problems related to high-frequency bands in telecommunications systems [28]. Further research is needed to better understand the possibilities and potential applications of the materials under study. In particular, it is important to investigate the possibility of optimising the manufacturing processes and properties of $BaMnV_2O_7$ LTCC ceramics. This will expand the scope of its application and improve efficiency in telecommunications technologies. It is also important to consider that a detailed study of the crystal structure and properties of materials is a key stage for their successful implementation in microwave devices and 5G equipment.

Conclusions

The diffraction spectrum of the $BaMnV_2O_7$ compound was used in this study from the 2009 PDF-2 database No. 044-0245. The spectrum was captured using copper-filtered radiation with the Breg-Brentano shooting geometry and was single-phase. The HighScore Plus 3.0 programme (Netherlands) was used to analyse the crystal structure. The structural model proposed for $BaMnV_2O_7$ compound corresponds to the β-$BaZnV_2O_7$ type. This compound belongs to a monoclinic syngony with a spatial symmetry group P121/c1 (14). Using this model, specific values of the lattice constants were determined: a = 5.6221(5) Å, b = 15.271(1) Å, c = 9.7109(8) Å, and angle β = 123.702(3). The microstructural parameters that have been determined provide additional information about the orientation of crystal grains in the compound. The general trend of vanadates indicates that the $BaMnV_2O_7$ compound exhibits good dielectric properties that can make it attractive for use in telecommunications technologies, in particular, in microwave devices.

The analysis performed allows understanding how the crystal structure affects the dielectric properties of the compound, which is important for its further improvement and optimisation. In the course of the study, LTCC ceramics were considered. Although the material has its advantages, such as cost-effective device manufacturing, tightness and mechanical strength, disadvantages, such as physicochemical incompatibility with other materials and the possibility of deformation during sintering, have been identified. The detected characteristics of $BaMnV_2O_7$ open up opportunities for its use in high-frequency applications, this is an important element of modern

communication technologies. This opens up broad prospects for further research in this area. Opportunities to use the results also include the development of more compact and reliable components for electronics and the introduction of $BaMnV_2O_7$ in high-frequency applications where good dielectric characteristics of the material are important. Further research may be of great importance for developing and improving materials in the telecommunications and electronics industries.

Acknowledgements
None.

Conflict of Interest
None.

References
[1] Roman LO. X-band transceiver module. In: Materials of the II All-Ukrainian Scientific and Technical Conference of Students and Postgraduates "Radio Electronics in the XXI Century". Kyiv: National Technical University of Ukraine "Igor Sikorsky Kyiv Polytechnic Institute"; 2019:80–1.
[2] Nemyrovych OA. Temperature and frequency properties of piezoelectric crystals germano- and silicosillenites. Kyiv: National Technical University of Ukraine "Igor Sikorsky Kyiv Polytechnic Institute"; 2019. 91 p.
[3] Varvaruk DI. Development of a graphical interface and BlueTooth connection module multimedia touch keyboard. Ivano-Frankivsk: King Danylo University; 2021. 111 p.
[4] Yashchyshyn YeM. Pecularities of practical use of the terrahertz range. *ICT*. 2022;1(03):16–27.
[5] Hrychanovska TM, Protsenko IYu. Dimensional impurity effects in the crystal structure of vanadium and titanium thin films. *Visnyk Sumy State Univ Phys Mat. Mech*. 2004;10:41–50.
[6] Khalameida SV, Sydorchuk VV, Skubiszewska-Zięba J, Leboda R, Zazhigalov VO. Physical-chemical and photocatalytic properties of V-Mg oxide compositions synthesized by different methods. *Chem Phys Technol Surface*. 2013;4(1):47–54.
[7] International Centre for Diffraction Data. PDF-2 data bases for 2009. 2009. Available from: https://www.icdd.com/pdf-2/.
[8] Li F, Li Y, Wang S, Zhang J, Tang T, Liao Y, *et al.* Improved co-substituted zinc vanadate ceramics based on LTCC for enhanced polarization converters. *J Alloys Compd.* 2022;921:166089. DOI: 10.1016/j.jallcom.2022.166089.
[9] Zhang RZ, Seth S, Cumby J. Grouped representation of interatomic distances as a similarity measure for crystal structures. *Dig Discov*. 2023;2:81–90. DOI: 10.1039/D2DD00054G.
[10] Thomas JC, Natarajan AR, Van der Ven A. Comparing crystal structures with symmetry and geometry. *npj Comput Mater*. 2021;7:164. DOI: 10.1038/s41524-021-00627-0.
[11] Lin Y, Yan K, Luo Y, Liu Y, Qian X, Ji S. Efficient approximations of complete interatomic potentials for crystal property prediction. In: Proceedings of the 40th International Conference on Machine Learning. Honolulu: JMLR; 2023:21260-87.
[12] Ahmad MA, Olule LJA. Meshed stacked LTCC antenna for space application. *IEEE Access*. 2022;10:29473–81.
[13] Sadeghi M. Analysis and design of a mm-wave wideband LTCC patch antenna for 5G Applications. Calgary: University of Calgary; 2022. DOI: 10.11575/PRISM/40568.
[14] Birol H, Maeder T, Ryser P. Materials compatibility issues in LTCC technology and their effects on structural and electrical properties. In: 1st International Conference on Ceramic Interconnect and Ceramic Microsystems Technologies (CICMT); 2005:300–9.
[15] Birol H. Fabrication of low temperature co-fired ceramic (LtCC)-based sensor and micro-fluidic structures. Lausanne: EPFL; 2007.
[16] Huang YT, Huang CC, Hsu TH, Huang CL. Ultra-low temperature sintering and microwave dielectric properties of Mg-substituted $SrCoV_2O_7$ ceramics. *J Asian Ceram Soc*. 2022;10(1):188–95. DOI: 10.1080/21870764.2022.2031535.
[17] Yin C, Li C, Yang G, Fang L, Yuan Y, Shu L, Khaliq J. $NaCa_4V_5O_{17}$: A low-firing microwave dielectric ceramic with low permittivity and chemical compatibility with silver for LTCC applications. *J Eur Ceram Soc*. 2020;40(2):386–90. DOI: 10.1016/j.jeurceramsoc.2019.09.029.
[18] Unnimaya AN, Suresh EK, Ratheesh R. Crystal structure and microwave dielectric properties of new alkaline earth vanadate $A_4V_2O_9$ (A=Ba, Sr, Ca, Mg and Zn) ceramics for LTCC applications. *Mater Res Bull*. 2017;88:174–81. DOI: 10.1016/j.materresbull.2016.12.026.
[19] Zhou D, Guo D, Li WB, Pang LX, Yao X, Wang DW, Reaney IM. Novel temperature stable high-ε r microwave dielectrics in the Bi_2O_3-TiO_2-V_2O_5 system. *J Mater Chem C*. 2016;23:5357–62. DOI: 10.1039/C6TC01431C.

[20] Suresh EK, Prasad K, Arun NS, Ratheesh R. Synthesis and microwave dielectric properties of $A_{16}V_{18}O_{61}$ (A = Ba, Sr and Ca) ceramics for LTCC applications. *J Electron Mater*. 2016;45:2996–3002. DOI: 10.1007/s11664-016-4388-6.
[21] Jiang X, Li Ch, Su C, Wei Z, Fang L. Low temperature firing and microwave dielectric properties of $BaCaV_2O_7$ ceramics. *Ceram Int*. 2015;41(3B):5172–76. DOI: 10.1016/j.ceramint.2014.12.001.
[22] Wang Y, Zuo R. A novel low-temperature fired microwave dielectric ceramic $BaMg_2V_2O_8$ with ultra-low loss. *J Eur Ceram Soc*. 2016;36(1):247–51. DOI: 10.1016/j.jeurceramsoc.2015.09.011.
[23] Peng S, Li C, Tang C, Liu S, Huang S, Qiu L, Deng L. Crystal structures and microwave dielectric properties of novel $MgCu_2Nb_2O_8$ ceramics prepared by two-step sintering technique. *Materials*. 2022;15(22):8053. DOI: 10.3390/ma15228053.
[24] Barzegar-Bafrooei H, Liu B, Su W, Song KX. $Ca_3MgSi_2O_8$: Novel low-permittivity microwave dielectric ceramics for 5G application. *Mater Lett*. 2020;263:127248. DOI: 10.1016/j.matlet.2019.127248.
[25] Shivalingayya M, Raibagkar RL. Microstructure and dielectric studies of bismuth vanadate based LTCC. *Indian J Sci Res*. 2017;8(1):77–80.
[26] Bizan MS, Naseri H, Pourmohammadi P, Melouki N, Iqbal A, Denidni TA. Dual-band dielectric resonator antenna with filtering features for microwave and mm-wave applications. *Micromachines*. 2023;14(6):1236. DOI: 10.3390/mi14061236.
[27] Bataiev YM, Bataiev MM, Kornienko OA, Lavrynenko OM, Pavlenko OYu. EPR-spectral, magnetic, and ionic features of CeO2, Yb2O3, Yb2O3-CeO2 powders and ceramics based on reo oxides. *Sci Herald Uzhhorod Univ Ser Phys*. 2021; 49:9–18.
[28] Chobal I, Chobal O, Myslo Yu, Petryshynets I, Rizak V. Elastic-plastic properties of Li2B4O7 determined by nanoindentation. *Sci Herald Uzhhorod Univ Ser Phys*. 2023;53:53–63. DOI: 10.54919/physics/53.2023.53.

Кристалічна структура пірованадата $BaMnV_2O_7$

Віктор Володимирович Заводянний
Кандидат фізико-математичних наук, доцент
Херсонський державний аграрно-економічний університет
25031, просп. Університетський, 5/2, м. Кропивницький, Україна
https://orcid.org/0000-0002-8224-8215

Микола Миколайович Волошин
Кандидат технічних наук, доцент
Херсонський державний аграрно-економічний університет
25031, просп. Університетський, 5/2, м. Кропивницький, Україна
https://orcid.org/0000-0003-0467-1963

Валентина Олександрівна Зубенко
Кандидат технічних наук, доцент
Херсонський державний аграрно-економічний університет
25031, просп. Університетський, 5/2, м. Кропивницький, Україна
https://orcid.org/0000-0002-8401-755X

Руслан Васильович Телюта
Кандидат технічних наук, доцент
Центральноукраїнський національний технічний університет
25006, просп. Університетський, 8, м. Кропивницький, Україна
https://orcid.org/0000-0002-4923-1227

Сергій Олексійович Квітка
Кандидат технічних наук, доцент
Таврійський державний агротехнологічний університет імені Дмитра Моторного
69600, вул. Жуковського, 66, м. Запоріжжя, Україна
https://orcid.org/0000-0001-9234-9274

Анотація

Актуальність. Розробка матеріалів з відмінними діелектричними властивостями є важливою для сучасних телекомунікацій. Актуальність даної роботи полягає у важливості вивчення цих властивостей

в контексті розширення можливостей для високочастотних додатків у сучасних телекомунікаційних технологіях, включаючи 4G і 5G зв’язок.

Мета. Метою даного дослідження є вивчення кристалічної структури сполуки $BaMnV_2O_7$ і її діелектричних властивостей.

Методологія. Для досягнення поставленої мети використовувалися методи аналізу, експерименту, порівняння і комп’ютерного моделювання. У рамках даного дослідження було ретельно вивчено матеріал низькотемпературної спільнообпалювальної кераміки (LTCC), який відзначається високою ефективністю у якості захисту від вологи.

Результати. Була запропонована і досліджена структурна модель для сполуки $BaMnV_2O_7$. Зокрема, виявлено, що радіус Mn^{2+} (0.75 Å) майже ідентичний радіусу Zn^{2+} (0.68 Å), що підтверджує подібність кристалічних структур $BaMnV_2O_7$ та $BaZnV_2O_7$. Основні результати показали, що пірованадат має моноклінну сингонію та має просторову групу симетрії P121/c1 (14), характеризуючись такими параметрами решітки: a = 5.6221(5) Å, b = 15.271(1) Å, c = 9.7109(8) Å, β = 123.702(3)°. Фактор розбіжності склав 9.05, що свідчить про відповідність моделі експериментальним даним. Крім того, була розрахована густина сполуки, яка становить 4.2699 г/см^3.

Висновки. За допомогою експериментальних даних було підтверджено наявність міжатомних відстаней в межах 1.33-3.47 Å. Мінімальна міжатомна відстань в структурі сполуки становить 1.33 Å між атомами кисню (O5) та ванадію (V2). Максимальна міжатомна відстань складає 3.47 Å та спостерігається між атомами кисню (O1) та (O2). За характеристиками, такими як низька діелектрична проникність (εr∼8.9) та високий коефіцієнт якості (Qu×f 31362 ГГц), сполука BaMnV2O7 проявляє відмінні мікрохвильові діелектричні властивості. Практичне значення отриманих результатів полягає в можливості розвитку та вдосконалення матеріалів з високими діелектричними властивостями, таких як BaMnV2O7, для їх застосування в телекомунікаційних технологіях та сприяє розробці більш компактних та надійних компонентів для електроніки.

Ключові слова: рентгеноструктурний аналіз; діелектричні властивості; геометрія зйомки Брег-Брентано; метод Рітвельда; резонатор

Scientific Herald of Uzhhorod University
Series "Physics"

Journal homepage: https://physics.uz.ua/en
Issue 54, 80–95
Received: 29.08.2023. Revised: 01.12.2023. Accepted: 18.12.2023

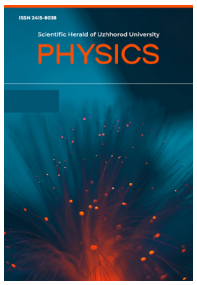

UDC 539
PACS 03.00
DOI: 10.54919/physics/54.2023.80

String theory and theory of everything: Review research

Abdimitalip Satybaldyev*
PhD in Technical Sciences, Associate Professor
Osh Technological University named after M. Adysheva
714018, 81 Isanov Str., Osh, Kyrgyzstan
https://orcid.org/0009-0006-2226-069X

Syrga Berdibekova
PhD in Pedagogical Sciences
Osh Technological University named after M. Adysheva
714018, 81 Isanov Str., Osh, Kyrgyzstan
https://orcid.org/0009-0004-1619-3537

Anarbek Attokurov
Postgraduate Student
Osh Technological University named after M. Adysheva
714018, 81 Isanov Str., Osh, Kyrgyzstan
https://orcid.org/0009-0009-0012-2271

Zhanargyl Igamberdieva
Postgraduate Student
Osh Technological University named after M. Adysheva
714018, 81 Isanov Str., Osh, Kyrgyzstan
https://orcid.org/0009-0000-3795-9408

Abstract

Relevance. Modeling is the primary tool for understanding the surrounding world, processes, and phenomena. The models currently used by humanity are essentially fragmentary (discrete) with certain variations of correlative generalizations. Therefore, humanity is constantly seeking mathematical formulations that can encompass the full picture of the Universe.

Purpose. The aim of the research is to analyze the evolution of the theoretical and modeling foundation of the physical picture of the world with the identification of promising research vectors that have the potential to form broad generalized models of the Universe, in other words, the theory of Everything.

Suggested Citation:
Hrechko Ya, Sereda I, Babenko Ie, Azarenkov M. String theory and theory of everything: Review research. *Sci Herald Uzhhorod Univ Ser Phys.* 2023;(54):80–95. DOI: 10.54919/physics/54.2023.80

*Corresponding author

Methodology. To achieve this goal, methods of systematization and generalization, meta-analysis, and meta-synthesis were employed. Since this study is a review and is intended to systematize and deepen knowledge, its structure is unconventional.

Results. The current model of the scientific landscape is described, based on which the dynamic vectors of development of the theoretical foundation of the Universe theory were determined. This allowed us to conclude the current state of the system of physical modeling as the main tool for the civilizational development of mankind. The research suggests that at the current stage of development of ideas about the physical picture of the world, M-theory is a potential model of the theory of Everything.

Conclusions. The practical significance of the research results indicates a potential mathematical and theoretical concept (among existing theories and models) that is relevant and adequate to modern ideas about cosmogony, phenomena, and the structure of the Universe. This can attract more attention to a certain direction of scientific research, not only among the professional community but also among the general public.

Keywords: standard model, quantum chromodynamics, quantum electrodynamics, quantum gravity, grand unified theory, M-theory

Introduction

The development and introduction of new technologies at the present stage of civilisational chronometry depend on the theoretical and modelling basis, which is equipped with an appropriate mathematical apparatus that allows to obtain forecasts of the dynamics of physical systems with a satisfactory level of correlation concerning natural and empirical observations of the real world. In this case, the most adequate models are those mathematical formulations that form the theoretical basis for a wider range of physical phenomena in a generalised, non-local form that allows obtaining local solutions for specific initial conditions. The problem that has been relevant throughout the development of modelling and constantly requires an appropriate solution is the deprivation of discreteness of individual models in terms of their application to the generalised landscape of the theory of the Universe.

Modelling, as the main tool for studying processes, phenomena, and objects, is based on the formation of concepts of certain algorithmic sequences that correlate to the conditions of regularities revealed by natural-empirical or logical-observational methods from the real world. The formation and study of models based on the relevant mathematical apparatuses allow to establish the level of adequacy of perception of the surrounding reality, as reported in the study by S. Raczynski [1].

As noted by S. Hawking and L. Mlodinov (as interpreted by A.F. van Biezen [2]), theoretical models, as the main scientific tool for studying the world and reality, to meet the criteria of completeness and efficiency, must meet three main requirements: first, to have an appropriate mathematical apparatus, second, to describe natural phenomena and processes in the widest possible application with the possibility of obtaining individual solutions for specific initial conditions of the modelled systems and processes, and (third requirement) must generate forecast and model results that should correlate with empirical data. Given the significant influence of the processes and results of modelling on scientific thought and the development of civilisation, it is reasonable to recognise that humanity is currently in the paradigm of model-dependent realism.

In the current state, humanity operates with theoretical models that are discrete in nature, as they describe individual processes and phenomena of external natural reality, and therefore, scientific thought is constantly in the process of searching for a single theory of Everything that can fully describe the essence and manifestations of the Universe. After the revolution in the scientific world (with far-reaching consequences in all spheres and branches of human activity and essence), which was caused by the fundamental works of A. Einstein, humanity, at the present stage, has not received scientific concepts that could explain the universal nature. Many theoretical statements and formulations have been created, but no scientific concepts have been formulated that satisfy the three conditions of completeness outlined above. However, in the landscape of scientific works, a concept has been formulated that currently has significant potential and claims to be a theory of Everything - the string theory and the *M*-theory (following S. Parekh [3]).

As T.A. Mohaupt [4] notes, the basic concepts of string theory were formed in 1914 and went through three iterations: zero - the creation of basic theoretical foundations and two string revolutions, which eventually led to the creation of a generalising concept – *M*-theory.

At the present stage, string theory is in the process of developing its mathematical apparatus and waiting for empirical confirmation (or refutation) of the hypotheses. Among the latest studies of string theory, it

is worth highlighting the studies of J. Gomis [5] (on the study of the limitations of bosonic string theory), S.P. De Alwis [6] (on the combination of string theory with Wilsonian effective field theory), S. Raucci [7] (on studies of non-super-symmetric strings, in particular, their vacuum states), S. Brahma [8] (on studies of the matrix model of the cosmogony of the Universe), S. Fumeron [9] (on studies of the topology of compactification spaces of additional dimensions of string theory), etc. Many studies and layers of hypotheses require systematisation and building a chronological vertical containing ordered and mutually consistent concepts, which in the future becomes a potential support structure for the development of the investigated sector of physics.

Thus, it can be stated that string theory is currently well developed and has a thorough mathematical apparatus, so the logical goal of the study is to assess the potential possibility of positioning string theory as a general mathematical model of the Universe – the theory of Everything. To achieve this goal, the Scopus database was searched for scientific sources using the keywords "Particle physics", "Theory of Everything", "Universe models", "Quantum gravity", "Extra-dimension", "Compactification", "Supersymmetry", "Gauge fields". Among the sources found, 35 were selected for meta-analysis, meta-synthesis, systematisation and generalisation [10]. Using the method of generalisation, the following conclusions were formulated.

String theory, M-Theory,and the quest for a unified theory of Everything

Currently, the scientific world has a generalised concept of the interaction of four fundamental forces (Fig. 1).

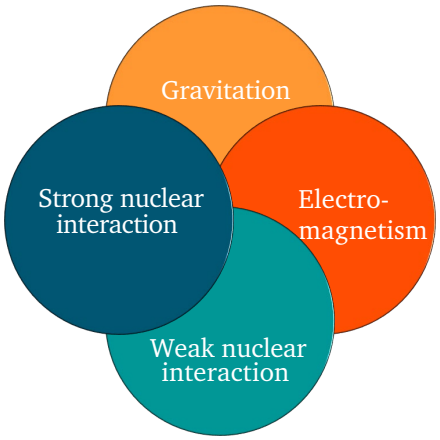

Figure 1. Conceptual diagram of fundamental interactions of the Universe

Source: [11]

Each of the fundamental interactions has a particle of the general class "gauge bosons", which transmits these forces (Fig. 2) [11]. The particle that provides the inert mass of the gauge bosons and the mechanism of spontaneous electroweak symmetry breaking was discovered by P.W. Higgs. This elementary particle is named after the inventor – the Higgs boson, which is de facto a quantum of the Higgs field [12].

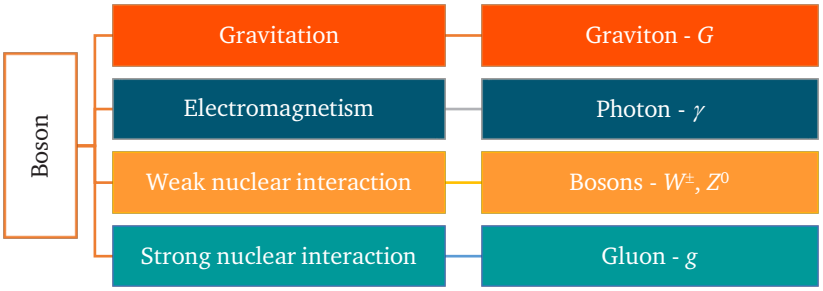

Figure 2. Conceptual diagram of gauge bosons for fundamental force transfer

Source: [11]

Matter also has corresponding elementary particles, which are part of the general class of fermions, consisting of three generations of quarks and leptons (Fig. 3).

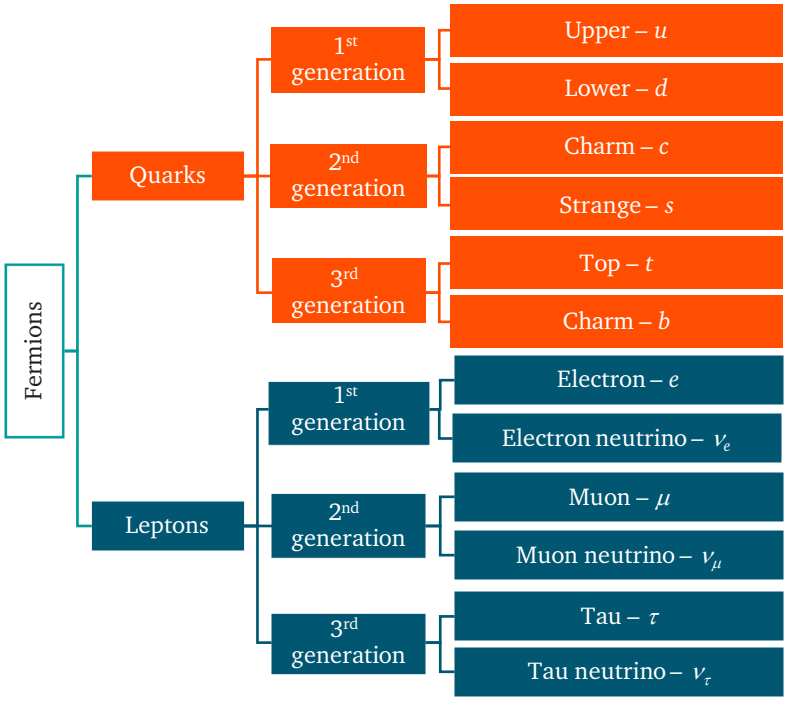

Figure 3. Conceptual diagram of matter fermions

Source: [13]

Classical physical theories are categorically limited in describing the interaction of fermions and bosons on the Planck scale, hence the introduction of quantum physics modelling, which adapts the corresponding fundamental interactions to the quantum level.

Thus, the very first fundamental interaction adapted to the quantum level was quantum electrodynamics (QED), a quantum field (relativistic) theory (formed in the 1940s) that was the first to harmonise quantum mechanics and A. Einstein's special theory of relativity. QED describes the mechanism of electromagnetic force transmission via bosons (in particular, the photon) between charged fermions (reacting to electromagnetic interaction: electrons and quarks). The QED model satisfies three conditions of conformity at once (with a very high level of correlation between empirical and model-predictive data) and has become a template for adapting other fundamental interactions to the quantum level [14].

The peculiarity of the first quantum field adaptation is the development by R.F. Feynman of a special mathematical apparatus based on a convenient graphical representation [15]. Feynman's mathematical apparatus greatly simplified the calculations and was used in other relativistic quantum field adaptations of classical force fields with the account of the boson-fermionic diversity (Fig. 4).

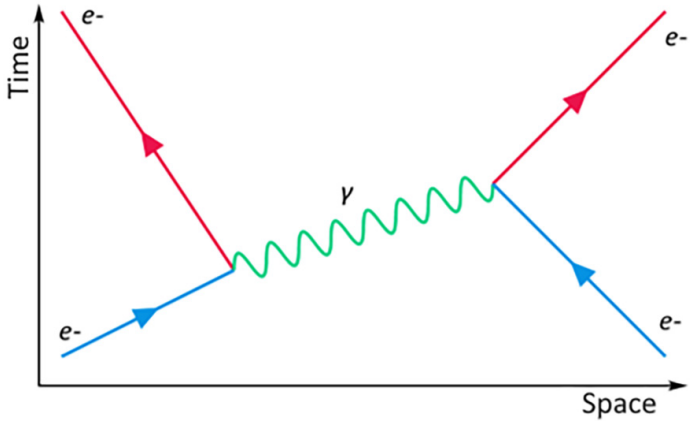

Figure 4. A simple computational case of Feynman's mathematical apparatus demonstrating the electromagnetic interaction between electrons via photon

Source: [15]

The graphically supplemented Feynmanian mathematical apparatus is more informative than the usual mathematical notation given for the calculated case (Fig. 4) - formula :

$$\bar{e} + \bar{e} \xrightarrow{\gamma} \bar{e} + \bar{e}. \quad (1)$$

The quantum principles underlying quantum field theories (in particular, the principles of quantum uncertainty by W.K. Heisenberg) allow to establish a single chronometry for tracing the motion of a particle, so R.F. Feyman formulated the principle of statistical summation of the contributions of all possible histories of particle motion [16] (Fig. 5).

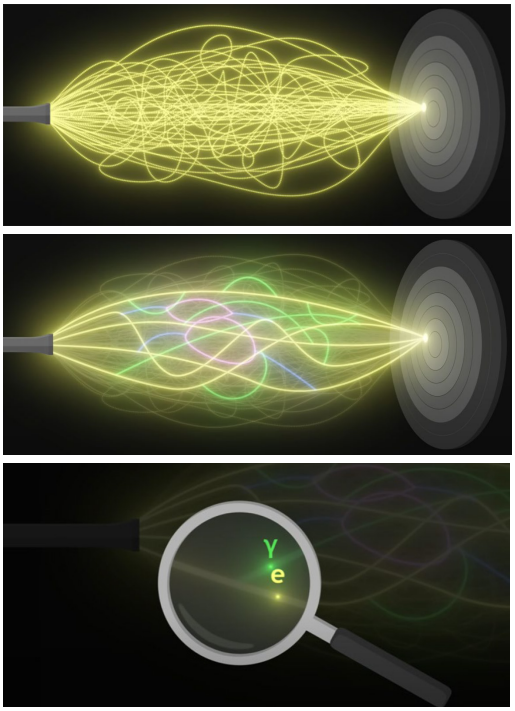

Figure 5. Visualisation of quantum variability based on the uncertainty principle
Source: [15]

Therefore, the summation of contributions from an infinite number of different chronometric trajectories of particles leads to an infinite result, which in turn requires the introduction of a new mathematical method – renormalisation. The renormalisation process involves subtracting values that are assumed to be equal to infinity and negative, so that, with careful mathematical calculation, the sum of the negative infinite values and the positive infinite values that appear in the theory almost balances out, excluding a small residual – the final observed values of mass and charge. Although this method is questionable from a mathematical point of view, the model predictions have a significant correlation with the empirical data [17].

The success of QED prompted further quantum adaptation of other fundamental interactions. Thus, in the 1960s, based on the studies of S.L. Glashow, S. Weinsberg, and M.A. Salam, the electroweak quantum theory was developed, combining QED with weak nuclear interaction. The electroweak interaction model predicted the existence of gauge bosons $W\pm$, Z_0, which are quanta of massless fields, gaining mass according to the Higgs mechanism. This model was empirically confirmed in 1973 at CERN – Conseil Européen pour la Recherche Nucléaire (neutral currents were detected) and in 1983 (based on the results of the international *UA1* and *UA2* experiments) [18].

The next quantum adaptation was made for the strong nuclear interaction, which resulted in the formation of the quantum field theory – quantum chromodynamics (QFT) in 1973, whose creators are D.D. Gross, F. Wilczek, and H.D. Politzer. Within the framework of QCD, thanks to the studies of S.L. Glashow, D. Iliopoulos, and L. Mayan, the concept of the structure of generations of quarks of matter fermions (Fig. 3) was formed. Quantum chromodynamics forms a model of the strong interaction between quarks (hadrons) via gluon fields [19]. The principle of interaction within QCD is also described using the Feynmanian mathematical apparatus (Fig. 6).

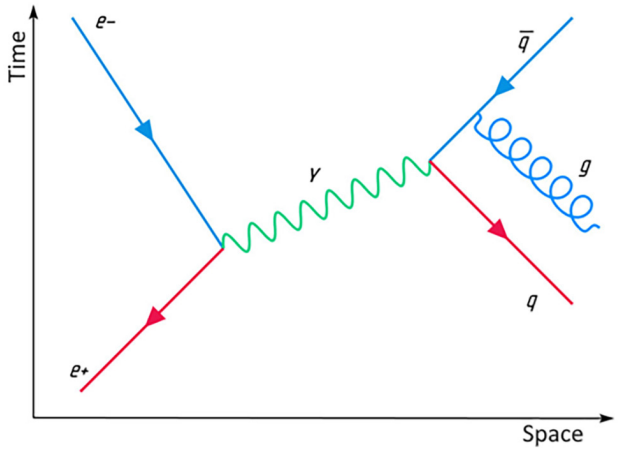

Figure 6. Feynman visualisation of QCD processes (one of the simplest cases): annihilation of an electron and a positron to form a quark from an antiquarian and a photon to emit a gluon
Source: [19]

Gluons in QCD have more bosonic variations than predicted by QCD modelling and were experimentally confirmed in 1979 at the *PETRA* facility. In 2000, thanks to the confirmation of the QCD modelling, a fundamentally new type of matter, the quark-gluon plasma, was discovered at CERN [20]. The quantum adaptation of the strong interaction is based on a more complex mathematical formulation than QED

and adopts the conditional mathematical concept of charge colour, and introduces such restrictions and conditions characteristic of this type of modelling as the confinement and asymptotic freedom, which were invented in the formulation and development of the mathematical apparatus of lattice QED [21].

A logical step in the quantum adaptation of fundamental interactions is the quantum gravity model. Even A. Einstein worked on this step in his time [22]. However, the corresponding model has not been formed yet, which is primarily due to the lack of understanding of the process of quantisation of the gravitational interaction: the Einstein energy-momentum tensor acquires the properties of a quantum operator, which implies the need to quantise the geometry of spacetime [23].

The success of the gauge model of the electroweak interaction led to the development of the Grand Unified Theory (GUT) in the 1970s, which described the three fundamental interactions without gravity. A significant drawback of the GUT model is the prediction of proton decay in $10^{>32}$ years, which seems unlikely since the age of the Universe is $10^{>10}$ years. Moreover, it has been experimentally established that the duration of proton decay can be even longer than predicted by the GUT model (more than $10^{>34}$ years) [24]. Thus, on the way to creating a unitary theory of the Whole, humanity has gone through several iterations (Fig. 7).

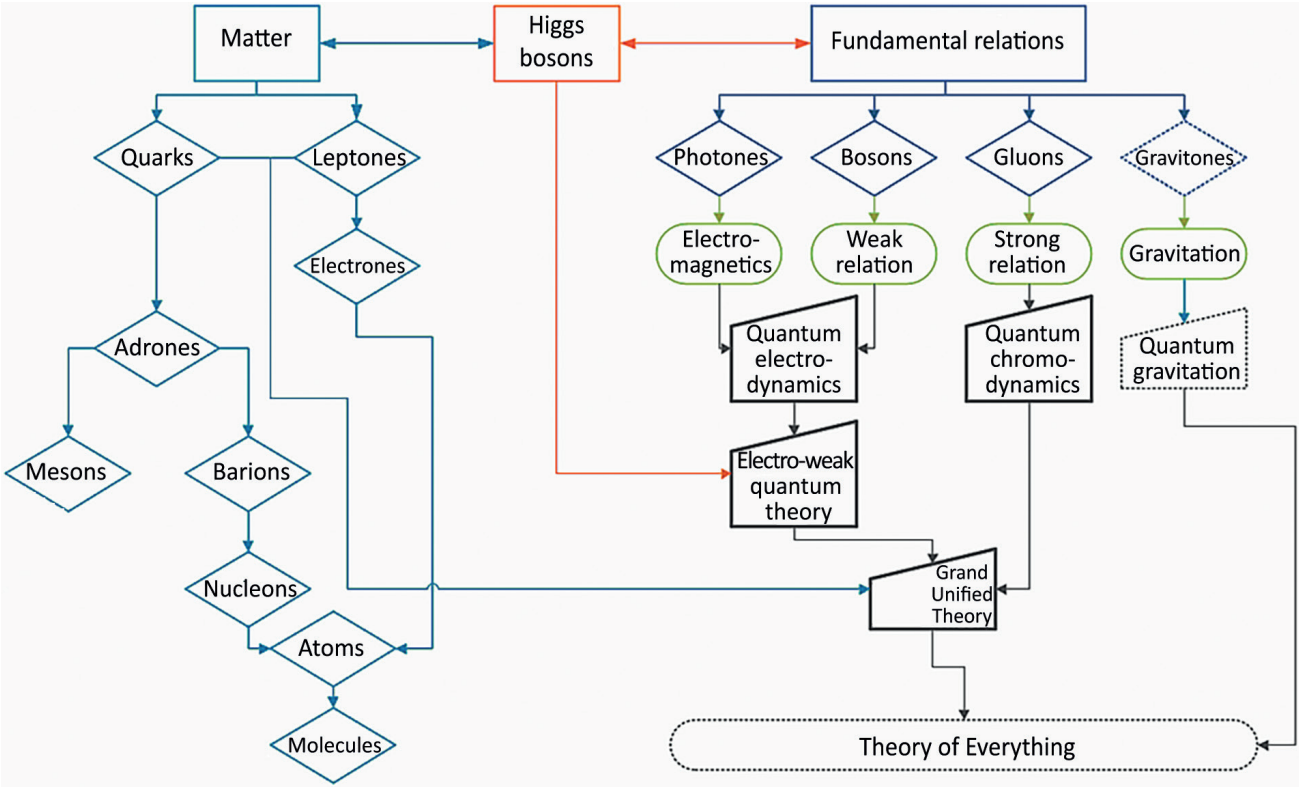

Figure 7. Conceptual diagram of the current state of the Universe modelling with indication of iterations of the development of model-theoretical representations
Note: dotted lines indicate hypothetical structural elements that require the formation of appropriate mathematical and theoretical formulations with subsequent empirical verification
Source: [24]

Experimental confirmation of the existence of the *t*-quark (1995), *b*-quark and tau-neutrino (2000) led to the formulation of a generalised theoretical concept, the Standard Model [13] (Fig. 8). The standard model allowed to systematise the boson-fermion interaction [13] (Fig. 9).

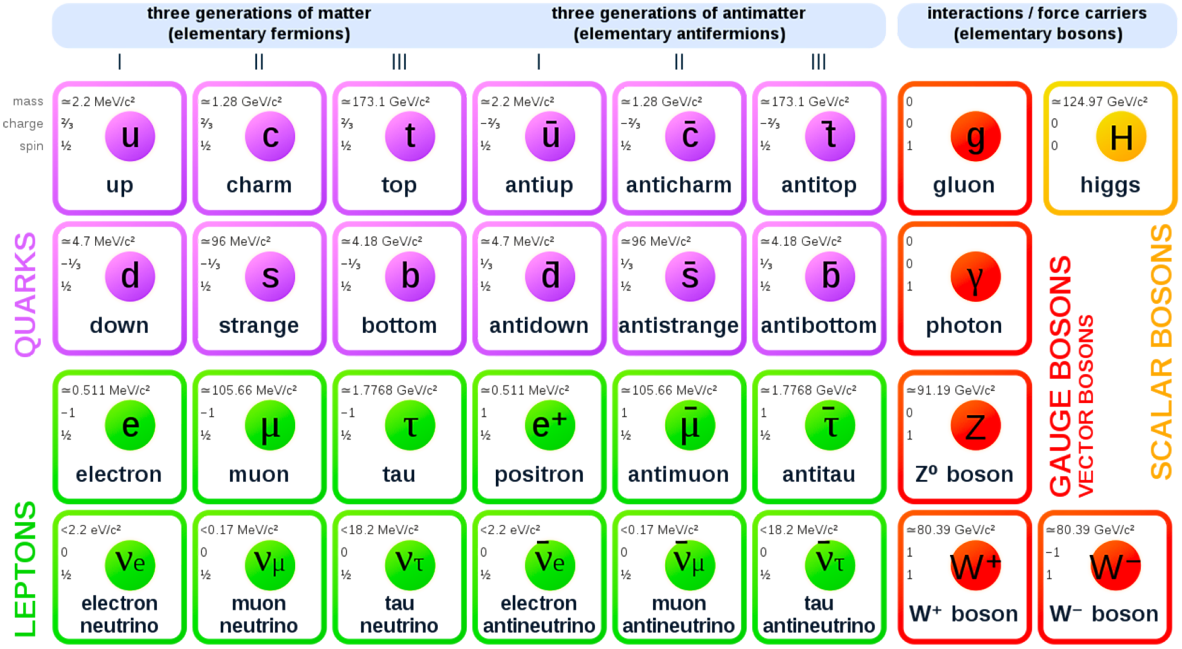

Figure 8. The generally accepted form of the Standard Model

Source: [13]

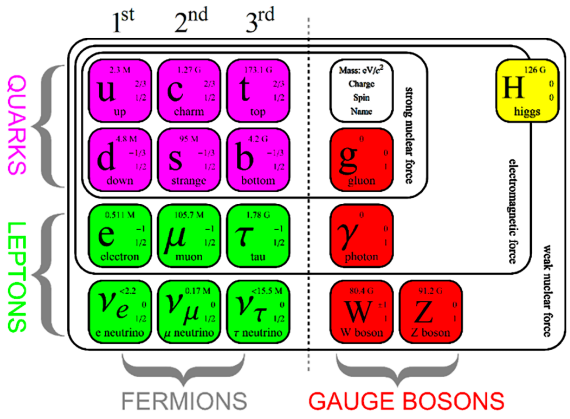

Figure 9. Interaction of bosons and fermions within the Standard Model

Source: [13]

The standard model is formed in compliance with the requirements of invariance of transformations, which form the basis of its mathematical apparatus in the form of local gauge symmetry for the bosonic interaction – formula (2) [25]:

$$SU(3) \times SU(2) \times U(1), \qquad (2)$$

where $SU(3)$ – symmetry group of 8 gluons of the strong interaction (Fig. 8);$SU(2)$ – symmetry group of 3 weak interaction bosons,W^+, W^-, Z^0; $U(1)$ – symmetry group for photons of electromagnetic interaction.

The Standard Model satisfies the conditions of completeness to a limited extent: the existence of gluons (since 1978), bosons W^+, W^-, Z^0 (1983) and H (Higgs boson) (2012) has been experimentally proven, but since 2021, quantum effects have been observed (*LHCb*, *Fermilab*, *CDF*), indicating the need to develop further iterations of modelling in search of a complete model of the Universe (physics beyond the Standard Model) [26].

The Standard Model, among other things (gauge hierarchy, 19 numerical constants, lack of explanations for high-energy physics phenomena, lack of explanations for dark matter and dark energy, etc.), from the point of view of the development of deterministic modelling, has a major drawback – the lack of quantum adaptation of gravitational interaction 13]. The inclusion of gravity in the Standard Model in mathematical modelling leads to the emergence of infinities. Even the application of the renormalisation methods used in QED and QCD does not eliminate the absurdi-

ty of mathematical formulations: the Feynmanian apparatus for gravity generates quantum infinities that cannot be eliminated by renormalisation within the framework of general relativity (GR) [13] (Fig. 10).

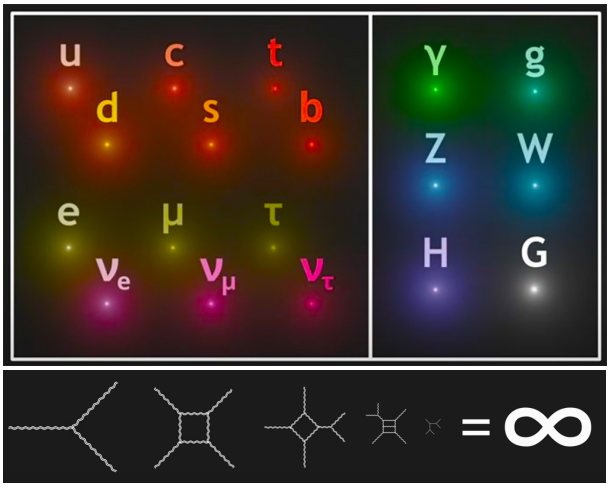

Figure 10. Visualisation of the problems of quantum adaptation of gravitational interaction and its combination with the provisions of the Standard Model

Source: [13]

Following the direction of the Standard Model, to solve the problem of quantum infinities in the mathematical modelling of gravitational interaction, several theoretical formulations have been developed using the principles of supersymmetry, a mathematical model that forms the union of boson-fermion fields by creating hypothetical partners for each of the standardised fundamental particles [27] (Fig. 11).

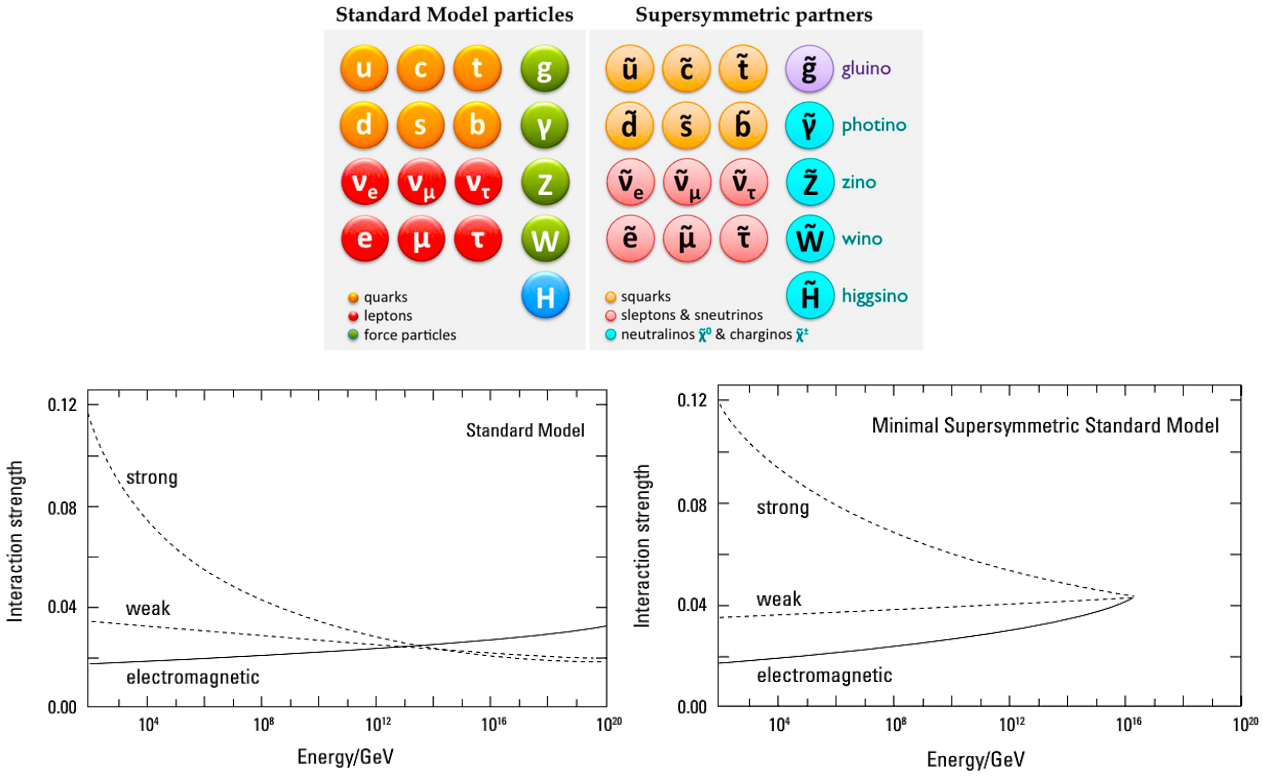

Figure 11. Conceptual diagram of boson-fermion supersymmetry with visualisation of symmetric principles on fundamental interactions (in comparison with the Standard Model)

Source: [27]

In the context of supersymmetric models, a mathematical formulation for supergravity was developed. Supergravity is a mathematical model (a gauge theory of local symmetry) that combines quantum field theories and GR [28]. Supersymmetry and supergravity had the potential to remove quantum infinities, since according to the Feynman rules, positive bosonic infinities annihilated with negative fermionic infinities. The complete calculation and construction of a full-fledged model of supergravity has proved to be an extremely difficult task that has not been solved. Also, no empirical confirmation of the existence of hypothetical supersymmetric boson-fermion partners has been obtained so far [28]. However, the principles of supersymmetry are reflected in a fundamentally new concept of a separate branch of the evolution of the modelling of the Universe – string theory [29]. The main postulate of string theory is that all fundamental particles (bosons and fermions) of the Standard Model (including gravitational interaction quanta) consist of the smallest (currently indivisible) elementary units – quantum strings [3] (Fig. 12). Following the string hypothesis, quantum strings vibrating on the Planck scale form all fundamental particles (fermions) and their interactions (bosons) [4] (Fig. 13).

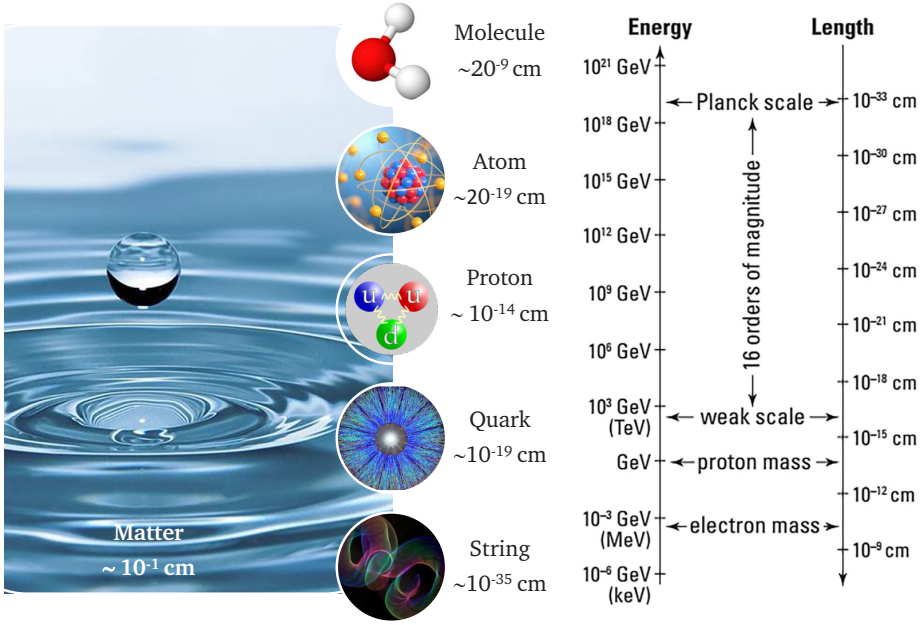

Figure 12. Conceptual scheme for comparing the scale of indivisibility of fundamental particles with the size-energy scale bar

Source: [3]

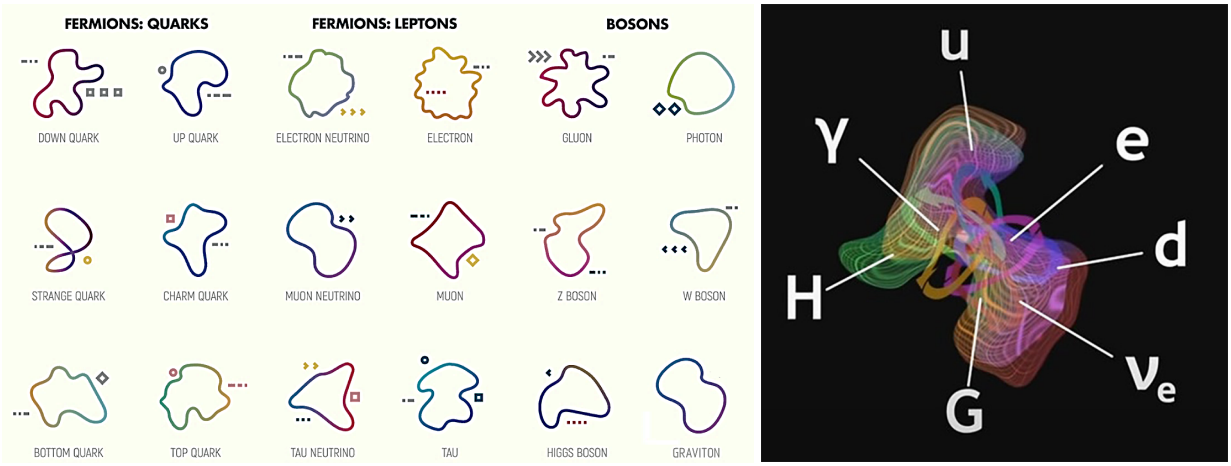

Figure 13. Visualisation of the string level of fundamental particles and fundamental interactions

Source: [4]

String theory combines the theoretical basis of quantum mechanics and Einstein's theory of relativity, and due to the full boson-fermion unification with the involvement of gravity in the model, it has the potential to form the theory of Everything (Fig. 7). A significant advantage of string theory modelling is the absence of the need to apply the renormalisation method and eliminate the problem of quantum infinities [3].

However, despite the mathematical integrity of string modelling, several problems do not allow this theory to satisfy the defined conditions of correspondence. First, it is necessity to use a multidimensional Universe and the corresponding problem of infinite methods of reduction (from 26 to 10) and compactification (from 10 (11) to 4) of dimensions (the so-called "landscape problem" [29]), which in turn leads to the prediction of a multiverse in which different variations of universes with different solutions of multidimensionality compactification are possible, and, accordingly, there is no full description of the mechanism of formation of the low-energy state ("vacuum state") of the observable Universe (also in this case, there are many discussions about the proposed anthropic principle [30]). Secondly, the string theory is inferior in the completeness of the nonperturbative definition to quantum modelling; thirdly, the string theory has no empirical confirmation yet, and the recorded quantisation scales of the gamma-ray burst GRB041219A indicate the need to revise the scale factors of the string model (the quantisation of the radiation was recorded only from the size of 10^{-48}m, which is much smaller than the predicted scale of string formations (Fig. 12)) [3].

The concept of string theory is formed by separate tertiary calculations, which are eventually combined into a generalised model, the *M*-theory [31] (Table 1).

Table 1. Generally accepted systematisation and classification of string modelling

String model type	Dimensionality of the Universe	Supersymmetric multiplicity type (*SUSY generators*)	Chirality	Open strings	Heterotic compacting	Symmetry gauge group	Solving the tachyon condensation problem	Additional info
Bosonic string theory (closed)	26	$N = 0$	–	–	–	–	–	No fermions
Bosonic string theory (open)	26	$N = 0$	–	+	–	$U(1)$	–	No fermions
I type superstring theory	10	$N = 1{,}0$	+	+	–	$SO(32)$	+	–
IIA type superstring theory	10	$N = 1.1$	–	–	–	$U(1)$	+	Massless nonchiral fermions
IIB type superstring theory	10	$N = 2.0$	+	–	–	–	+	Massless chiral fermions
Heterotic string theory *HO* type	10	$N = 1.0$	+	–	+	$SO(32)$	+	Strings differ in vibrational modes based on the clockwise direction
Heterotic string theory *HE* type	10	$N = 1.0$	+	–	+	$E_8 \times E_8$	+	Strings differ in vibrational modes based on the clockwise direction
Generalised string theory – *M*-theory	11	$N = 1.0$	–	–	–	–	+	A generalised solution of previous superstring models and contains *D*-brane

Source: [31]

The dualities allow combining not only the five main superstring models into a generalised *M*-theory (Fig. 14) but also connecting string modelling with the quantum field theory of supergravity (through the *AdS/CFT* mechanism (Maldacena duality) [32]), which at this stage allows stating the greatest unity of scientific thought in creating a complete model of the Universe (Fig. 15).

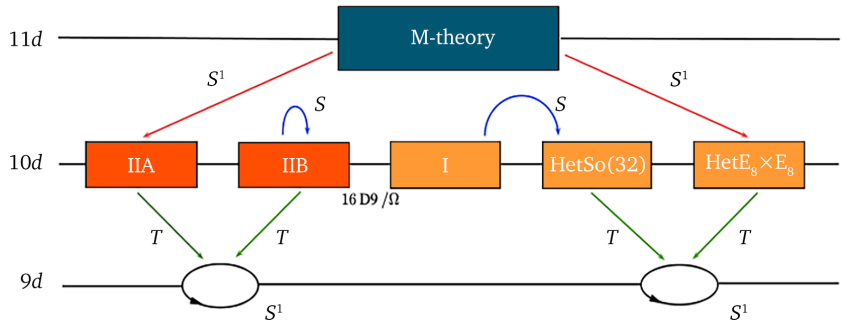

Figure 14. The generally accepted system of dual coupling of superstring models with *M*-theory
Source: [32]

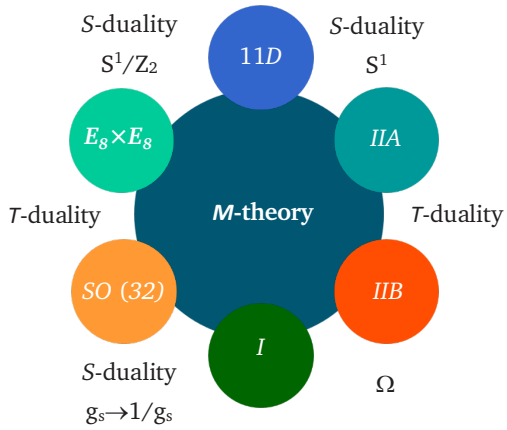

Figure 15. Generalised dual coupling system of superstring models, *M*-theory, and quantum field theory of supergravity (11*D*)
Source: [32]

Therefore, the resulting *M*-theory assumes string and brane formations of different topologies as fundamental parts [33], which can be described using the Feynman mathematical apparatus – Figure 16.

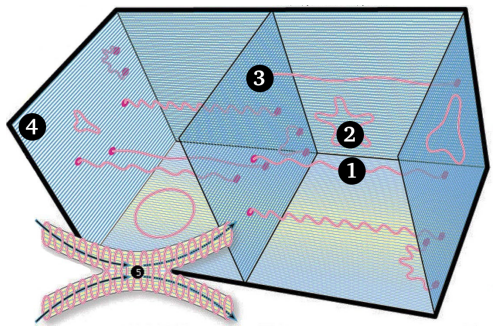

Figure 16. Abstraction of the functioning of the Universe at the level of string-brane formations and interactions within the framework of the generalised unitary *M*-theory
Note 1 – open string formations; 2 – closed string formations; 3 – fixation of open strings; 4 – D-branes; 5 – Feynman mechanism of string interaction
Source: [32]

The use of string-brane formations (Fig. 16) with the corresponding mathematical support (Table 1) and supersymmetry mechanisms allows to provide a model of the full boson-fermion unification, which is de facto the area of contact and coordination of nuclear physics, GR, quantum mechanics and cosmogony of the observable Universe.

Thus, the unitary theoretical positions of the crown of string modelling, the *M*-theory, despite certain contradictions and the lack of technical possibility of empirical testing, have already been successful, proving, if not the correctness of the chosen direction on the way to the theory of Everything, then at least the closeness to the above-mentioned path of development of ideas about the Universe.

After analysing the sources, the following aspects of the relevance of the scientometric landscape of string modelling in the current horizon of bibliometric analysis are stated:

- The development of the theoretical basis of *M*-theory is more intensive compared to string theory itself, but it is more vectorised with clear research directions;
- Among the identified vectors of the current scientific state of string modelling, the most prominent are the holographic principle, six-dimensional branes, brane interpretations, dualities, canonical singularity, etc;

Therefore, the resulting concept of string modelling – *M*-theory – forms the conceptual foundations that explain the functioning of spacetime at the deep Planck level and, although there is no empirical confirmation of string postulates and formulations, it is highly probable that string modelling is the model of the Universe that Einstein hoped to obtain.

Perspectives on string modelling in the quest for a unified theory of Everything

String modelling, as one of the trends in the development of physics outside the Standard Model and de facto not a proven theory, is often criticised by experts, including S.L. Glashow and R.F. Feynman. However, even though there were such prominent physicists in the camp of opponents and critics of

string theory, string modelling continued to develop and create common ground with other cosmogonic theories, with quantum adaptations of fundamental interactions and Einstein's principles of relativity.

The paradigm of critical thought regarding the string theory paradigm as a theory of Everything is the thesis that string modelling is only a rough assumption (zero iteration) of quantum adaptation of gravitational interaction to unify it in the Standard Model (as A. Einstein assumed), and not a full-fledged fundamental theory that can explain cosmogony and the existence of the observable Universe (Fig. 7) [2].

In particular, it is worth highlighting the following critical opinions and formulations regarding the relevance of string modelling [34]-[36]:

- based on string theory, it is not possible to obtain a prediction of physical phenomena and processes that could be further tested, and, accordingly, could be either proved or disproved;
- the basic principles of string modelling are not sufficiently clear and fundamental, and do not contain clearly defined criteria, which leads to the generation of sometimes absurd ideas that can be included in the theoretical background;
- there is a significant influence on the development of the theoretical foundations of the opinions and formulations of string physicists-influencers, as opposed to conducting real research;
- string theorists have a significant influence on the social sphere, cultivating ideas about the significant achievement of string modelling, which is not always true since string theory is currently purely conceptual;
- string modelling is quite popular (as mentioned above), which leads to a redistribution of financial flows and academic support to this sector of physics rather than to other theoretical approaches;
- string theory uses complex concepts and mechanisms that not only do not fully (and sometimes not at all) describe the observable universe, but also question recognised physical phenomena and processes;
- the problem of the landscape and falsification of various variations of string theories, as well as numerous possible options for compactifying the multidimensionality of the Universe (it is believed that there are more than 10^{500} such options), which was established in 2003 by the integration of the observed dark energy [37; 38] into string modelling generally calls into question the theoretical basis and fundamentality of string theory, giving rise to such a controversial concept as the anthropic principle [30] (either in a strong or weak formulation), proposed by one of the string influencers L. Susskind.

The criticism of string modelling began in 1998 with the discovery of dark energy, which resulted from the fact that S. Perlmutter, B.P. Schmidt and A. Riess had found that the expansion rate of the Universe was lower earlier, i.e., the 1925 hypothesis of J. Lemaitre that the cosmogonic constant was not stable was confirmed [38].

At present, thanks to the *BOOMERanG*, *MAXIMA* experiments, the *WMAP* satellite (which observed the microwave anisotropic relic background radiation, which became a tangential proof of the inflationary model of the Universe) and the Planck telescope in the period 2009-2013, it was established that the observed Universe consists of 74% dark matter [39]. The intensity factor of criticism of string modelling was increased by the attempt to explain dark energy within the framework of string theory, which led to the above-mentioned numerous variations of compactification of the multidimensionality of the Universe (and, in fact, to the paradigm of the Multiverse) [40].

Even such ideas as the five-dimensional Randall-Sundrum [41] brane model and the integration of the positive value of the cosmological constant [42] created a perception in the scientific community that these are falsifications to keep attention on string theory. Important figures among those who criticise string theory were L. Smolin and P. Voigt, whose publications significantly intensified the criticism of string theory that spread not only in the scientific world but also publicly [43]. However, even these scientists do not completely exclude string theory, but, as it turned out, strive for a wider range of studies of the Universe, not only string modelling.

String theory, despite its well-developed mathematical formalism, teeters on the edge of science and falsification due to the lack of natural observable evidence, which has led to the formation of two critical principles described below.

Approach 1 – "String theory explains nothing". This position is based on the assertion that over the entire period of development of string modelling, no clear predictions have been made about processes and phenomena in the observable Universe that could be either confirmed or refuted (K. Popper's principle). This critical remark is made in the context of the history of fundamental particle physics, where most elements were predicted and confirmed, which created the fundamentals of nuclear physics and quantum mechanics. Although K. Popper's principle of science falsification does exist and raises the question of the scientific validity of string theory, most scientists disagree with him, because humanity does not currently operate with technologies that would allow high-energy physics experiments. Therefore, there is a high probability that such experiments will be carried out in the future.

However, in this case, the criticism concerns not only string theory in general but most string theorists, who are more interested in reconciling the provisions of string modelling with proven facts and creating interesting mathematical constructions that are largely abstract. It is this basic critical thought that has been

cultivated by all string critics from R.F. Feyman to L. Smolin, which is that string modelling has no relation to empiricism and distorts scientific fundamentalism, and most importantly, violates the established approach to research [35]-[37].

Approach 2 – "String theory explains too much". The argumentation of this critical perspective on string modelling is based on the absence of unique predictions, since many theories and mathematical apparatuses of the string landscape describe phenomena and processes with quite different results, which do not give unambiguous statements about the nature of the objects under study, on the contrary, making it impossible to verify research conclusions due to their high variability.

The rapid development of the theory with many unverified results causes the model to lose its relevance as many variations of predictions that cannot be verified significantly worsen the fundamentalism of string theory, even worse than with the first critical principle.

The second critical principle evolves from the principle of Occam's razor: string critics are understandably sceptical of new mathematical constructions and inventions, without which, following string theorists, these models are irrelevant.

One of the solutions to the variability of string modelling predictions is the anthropic principle [30], following which the observable Universe is exactly like this because there are people in it. The anthropic principle (in its strongest formulation) is defended by many factors, without which the existence of life would be impossible (the location of our planet near a single star (about half of the observed stars are binary); the small ellipticity of the orbit, which allows the planet to receive solar radiation relatively evenly; the location of the planet in the circumstellar habitable zone, which ensures the relative stability of the planet's temperature field, etc.). The weak component of the anthropic principle also includes assumptions about the anthropocentricity and creationism of the cosmogony of the observed Universe (in particular, due to its chemical composition (with a predominant amount of carbon as the basis for organic life forms), successful correlations of fundamental interactions (with the corresponding cosmological constant and other constants that are somewhat projective),), the four-dimensionality of the observed Universe (which is associated with gravitational interaction, which, with increasing dimensionality, would lead to instability of matter, which is also interpreted in the successful compactification of dimensions, according to the provisions of string modelling). All of these anthropic assumptions are a violation of the deterministic principles of science and form the opinion in the scientific community that this is a weak defence of string theory. However, considering the prediction of string modelling regarding possible 10^{500} variants of multidimensionality compactification, which leads to the concept of the Multiverse [40], on the contrary, strengthens the deterministic principle of string theory, since it turns out that our Universe is not a unique phenomenon, but only one of many possible variants in which humanity is lucky enough to appear.

Criticism and constant verification of theoretical models and assumptions form the true fundamentalism that is at the heart of civilisational development. Therefore, a critical look at string modelling, which not only sought to rid quantum mechanics of renormalisation methods but also offered potential solutions to quantum gravity in combination with other competing ideas and theories, such as L. Smolin's [44] loop quantum gravity, will allow to form a true model of the universe.

At present, string theory has an elegant mathematical apparatus based on which software and numerical models are possible, but they will still be somewhat abstract, but the expectation of confirmation of supersymmetric partners [27] and gravitational waves [45-47] will significantly strengthen the fundamental nature of string modelling.

Conclusions

Based on the aforesaid, the following conclusions can be drawn. String theory/*M*-theory (in all its variations) is a formalised concept of a model of the Universe with a developed mathematical apparatus that is in dire need of empirical confirmation and fundamental findings to get as close as possible (or refute) to the paradigm of the theory of Everything. The history of the development of string modelling has been going on for more than 50 years (and, considering the first concepts, more than 100 years), but string theory has not come close to the goal of explaining the observable Universe in all its manifestations and interactions. Moreover, the predictions of string modelling have led to the formation of the hypothesis of the Multiverse, in which our Universe is not a unique phenomenon, which, in contrast to the anthropic principle cultivated by the research thought of string theorists, on the contrary, significantly strengthens the deterministic approach to understanding the real picture of the world.

The expected results of high-energy physics experiments to produce supersymmetric boson-fermion partners and detect gravitational waves (*LIGO* and VIRGO detectors) can either refute or confirm the relevance of string modelling. However, while waiting for the empirical data, string theorists have not stood still: as this review shows, the string hypothesis and string mathematics are constantly evolving, focusing on such areas as the holographic principle, six-dimensional branes, brane interpretations, dualities, the canonical singularity, etc.

It is possible that string modelling will prove to be a crude assumption of gravitational interaction quantum adaptation, but this hypothesis has pointed to the possibility of obtaining a generalised Einstein theory of

everything. Further research should be accompanied by the study of the mathematical structures of string theory and their reflection on physical phenomena, which can lead to the discovery of new physical laws that will expand the understanding of the Universe.

Acknowledgements

None.

Conflict of Interest

None.

References

[1] Raczynski S. Models for research and understanding: Exploring dynamic systems, unconventional approaches, and applications. Berlin: Springer Nature; 2023. DOI: 10.1007/978-3-031-11926-2.
[2] van Biezen AF. Top-Down cosmology and model-dependent realism: A philosophical study of the cosmology of Stephen Hawking and Thomas Hertog. Bruxelles: VUBPress; 2022.
[3] Parekh S. Introduction to String Theory [Internet]. January 16, 2022. Available at: https://ssrn.com/abstract=4009963.
[4] Mohaupt T. Short introduction to String Theory. Cambridge: Cambridge University Press; 2022. DOI: 10.1017/9781108611619.
[5] Gomis J, Guerra IV A, Román-Roy N. Multisymplectic constraint analysis of scalar field theories, Chern-Simons gravity, and bosonic string theory. *Nucl Phys B*. 2023;116069. DOI: 10.1016/j.nuclphysb.2022.116069.
[6] De Alwis SP. Wilsonian effective field theory and string theory. In: Suranyi P, editor. 87th birthday festschrift a life in quantum field theory. Singapore: World Scientific Publishing Company; 2023: 127-147. DOI: 10.1142/9789811262357_0008.
[7] Raucci S. On new vacua of non-supersymmetric strings. *Phys Lett B*. 2023;837:137663. DOI: 10.1016/j.physletb.2022.137663.
[8] Brahma S, Brandenberger R, Laliberte S. BFSS matrix model cosmology: Progress and challenges. *Phys*. 2023;5(1):1–10. DOI: 10.3390/physics5010001.
[9] Fumeron S, Berche B, Moraes F. Geometric theory of topological defects: methodological developments and new trends. *Liq Cryst Rev*. 2023;9(2):85–110. DOI: 10.1080/21680396.2022.2163515.
[10] Kunisch S, Denyer D, Bartunek J, Menz M, Cardinal L. Review research as scientific inquiry. *Organ Res Methods*. 2023;26:3–45. DOI: 10.1177/10944281221127292.
[11] Ma T, Shu J, Xiao ML. Standard Model effective field theory from on-shell amplitudes. *Chin Phys C*. 2023;47(2):023105. DOI: 10.1088/1674-1137/aca200.
[12] Gadja MEA, Khodja L, Delenda Y. Higgs p_t distribution in Higgs + jet production at hadron colliders within the noncommutative effective standard model. *Mod Phys Lett A*. 2023;38(06):2350038. DOI: 10.1142/S0217732323500384.
[13] Klco N, Roggero A, Savage MJ. Standard model physics and the digital quantum revolution: thoughts about the interface. *Rep Prog Phys*. 2022;85:064301. DOI: 10.1088/1361-6633/ac58a4.
[14] Freese A, Metz A, Pasquini B, Rodini S. The gravitational form factors of the electron in quantum electrodynamics. *Phys Lett B*. 2023;839:137768. DOI: 10.1016/j.physletb.2023.137768.
[15] Shaikh RA, Gogioso S. Categorical semantics for Feynman diagrams. *Quantum Phys*. 2022. DOI: 10.48550/arXiv.2205.00466.
[16] Di Mauro M, Esposito S, Naddeo A. A glimpse of Feynman's contributions to the debate on the foundations of quantum mechanics. In: The Sixteenth Marcel Grossmann Meeting; 2023. P. 3657–70. Singapore: World Scientific. DOI: 10.1142/9789811269776_0302.
[17] Yokota T, Masuki K, Ashida Y. Functional renormalization group approach to circuit quantum electrodynamics. *Phys Rev A*. 2022;107:043709. DOI: 10.1103/PhysRevA.107.043709.
[18] Carmesin HO. The electroweak interaction explained by and derived from gravity and relativity. Berlin: Verlag Dr. Köster; 2022. 168 p.
[19] Schiller C. Testing a conjecture on quantum chromodynamics. *Int J Geom Methods Mod Phys*. 2023;20(06):2350095. DOI: 10.1142/S0219887823500950.
[20] He M, van Hees H, Rapp R. Heavy-quark diffusion in the quark-gluon plasma. *Prog Part Nucl Phys*. 2023;130:10402. .
[21] Frison J. Towards fully Bayesian analyses in Lattice QCD. *arXiv preprint*. 2023. DOI: 10.48550/arXiv.2302.06550.
[22] Di Mauro M, Esposito S, Naddeo A. Teaching quantum physics in the footsteps of Einstein. *J Phys: Conf Ser*. 2022;2297(1):012036. DOI: 10.1088/1742-6596/2297/1/012036.
[23] Döner MK, Großardt A. Is gravitational entanglement evidence for the quantization of spacetime? *Found Phys*. 2022;52(5):101. DOI: 10.1007/s10701-022-00619-0.

[24] Agrawal P, Nee M, Reig M. Axion couplings in grand unified theories. *J High Energy Phys*. 2022;2022:141. DOI: 10.1007/JHEP10(2022)141.
[25] Strocchi, F. (2023). Local Gauss law and local gauge symmetries in QFT. *arXiv preprint*. 2023. DOI: 10.48550/arXiv.2301.06543.
[26] Gouttenoire Y. Beyond the standard model cocktail: A modern and comprehensive review of the major open puzzles in theoretical particle physics and cosmology with a focus on heavy dark matter. Berlin: Springer; 2023. DOI: 10.1007/978-3-031-11862-3.
[27] Dreiner HK, Haber HE, Martin SP. From spinors to supersymmetry. Cambridge: Cambridge University Press; 2023. 1025 p. DOI: 10.1017/9781139049740.
[28] García-Valdecasas, E. Non-invertible symmetries in supergravity. *J. High Energ. Phys*. 2023,2023:102. DOI: 10.1007/JHEP04(2023)102.
[29] Baer H, Barger V, Salam S, Sengupta D. Mini-review: Expectations for supersymmetry from the string landscape. *Proc US Community Study Future Part. Phys*. 2022. DOI: 10.48550/arXiv.2202.11578.
[30] Walsh A. The anthropic principle: A Universe built for man. Wilmington: Vernon Press; 2023. 180 p.
[31] Asano Y. Numerical development of the matrix model for non-perturbative formulation of M-theory. *Eur Phys J Spec Top*. 2023;232:321–31. DOI: 10.1140/epjs/s11734-022-00718-z.
[32] Zhang, Z. (2023). A study of BPS and near-BPS black holes via AdS/CFT [PhD thesis]. Trieste: Scuola Internazionale Superiore di Studi Avanzati.
[33] De Boer J, Llabrés E, Pedraza JF, Vegh D. Chaotic strings in AdS/CFT. *Phys Rev Lett*. 2018;120:201604.
[34] The Lens. Serves global patent and scholarly knowledge as a public resource to make science- and technology-enabled problem solving more effective, efficient and inclusive [Internet]. 2022 [cited 2023 Aug 01]. Available from: lens.org.
[35] Constantin, A. (2022). Intelligent Explorations of the String Theory Landscape. *arXiv preprint arXiv:2204.08073*. DOI: 10.48550/arXiv.2204.08073.
[36] Papavergou I, Vourliotis E. Search for physics beyond the standard model in final states with two or three soft leptons and missing transverse momentum in proton-proton collisions at √s=13 TeV. *J Phys: Conf Ser*. 2021;2105:012012. DOI: 10.1088/1742-6596/2105/1/012012.
[37] Baer H, Barger V, Sengupta D. Landscape solution to the SUSY flavor and *CP* problems. *Phys Rev Res*. 2019;1:033179.
[38] Rudelius T. Constraints on early dark energy from the axion weak gravity conjecture. J *Cosmol Astropart Phys*. 2023;2023(01):014. DOI: 10.1088/1475-7516/2023/01/014.
[39] Zu L, Feng L, Yuan Q, Fan Y-Z. Stringent constraints on the light boson model with supermassive black hole spin measurements. *Eur Phys J Plus*. 2020;135:709. DOI: 10.1140/epjp/s13360-020-00734-9.
[40] Yadav, G. (2023). Multiverse in Karch-Randall Braneworld. *J High Energ Phys*. 2023;103:103. DOI: 10.1007/JHEP03(2023)103.
[41] Akshay A, Arun MT. Flavor-violating charged lepton decays in the little Randall-Sundrum model. *Phys Rev D*. 2023;107(1):015013. DOI: 10.1103/PhysRevD.107.015013.
[42] Antoniadis I, Chen Y, Leontaris GK. Perturbative moduli stabilization in type IIB/F-theory framework. *Eur Phys J C*. 2018;78:766. DOI: 10.1140/epjc/s10052-018-6248-4.
[43] Kluso J. Note about string theory with deformed dispersion relations. *Gen Relativ Gravit*. 2022;54(6):61. DOI: 10.1007/s10714-022-02945-0.
[44] Araújo Filho AA. Particles in loop quantum gravity formalism: A thermodynamical description. *Ann Phys*. 2022;534(12):2200383. DOI: 10.1002/andp.202200383.
[45] Spanos VC, Stamou ID. Gravitational waves from no-scale supergravity. *Eur Phys J C*. 2023;83:4. DOI: 10.1140/epjc/s10052-022-11142-x.
[46] Hrechko Y, Sereda I, Babenko Ie, Azarenkov M. Thermionic coating method with preliminary ion bombardment. *Sci Herald Uzhhorod Univ Ser Phys*. 2023;53:9–8. DOI: 10.54919/physics/53.2023.09.
[47] Shynkariuk IM. Alternative representation of space and time: Geometric solution of problems of relativity theory. *Sci Herald Uzhhorod Univ Ser Phys*. 2022;(51):74–82. DOI: 10.54919/2415-8038.2022.51.74-82.

Теорія струн та теорія Всього: огляд досліджень

Абдіміталіп Сатибалдиєв

Кандидат фізико-математичних наук
Харківський національний університет імені В.Н. Каразіна
61022, майдан Свободи, 4, м. Харків, Україна
https://orcid.org/0009-0006-2226-069X

Сирга Бердибекова

Кандидат педагогічних наук
Ошський технологічний університет ім. М.М. Адишева
714018, вул. Ісанова 81, м. Ош, Киргизстан
https://orcid.org/0009-0004-1619-3537

Анарбек Аттокуров

Аспірант
Ошський технологічний університет ім. М.М. Адишева
714018, вул. Ісанова 81, м. Ош, Киргизстан
https://orcid.org/0009-0009-0012-2271

Жанаргул Ігамбердієва

Аспірант
Ошський технологічний університет ім. М.М. Адишева
714018, вул. Ісанова 81, м. Ош, Киргизстан
https://orcid.org/0009-0000-3795-9408

Анотація

Актуальність. Моделювання є основним інструментом для розуміння навколишнього світу, процесів і явищ. Моделі, якими використовується людство в сучасний час, фактично є фрагментарними (дискретними) із певними варіаціями корелятивних узагальнень. Тому людство постійно шукає математичні формулювання, які могли б охопити повну картину Всесвіту.

Мета. Метою дослідження є аналіз еволюції теоретичної та модельної основи фізичної картини світу з ідентифікацією перспективних дослідницьких векторів, що мають потенціал формувати широкі узагальнені моделі Всесвіту, тобто теорію Всього.

Методологія. Для досягнення мети були використані методи систематизації та узагальнення, метааналізу та метасинтезу. Оскільки це дослідження є оглядом і призначене для систематизації та поглиблення знань, воно побудоване на нетрадиційній структурі.

Результати. Описано поточну модель наукового ландшафту, на основі якої були визначені рухливі вектори розвитку теоретичної основи теорії Всесвіту, що дозволило зробити висновок про поточний стан системи фізичного моделювання як основного інструменту цивілізаційного розвитку людства. Дослідження дозволяє встановити, що на даному етапі розвитку ідей про фізичну картину світу М-теорія є потенційною моделлю теорії Всього.

Висновки. Практична значущість результатів дослідження вказує на потенційну математичну та теоретичну концепцію (серед існуючих теорій та моделей), яка є адекватною сучасним уявленням про космогонію, явища та структуру Всесвіту та дозволяє залучити більше уваги до певного напряму наукових досліджень, не лише серед професійної спільноти, але і серед загальної громадськості.

Ключові слова: стандартна модель; квантова хромодинаміка; квантова електродинаміка; квантова гравітація; велика єдина теорія; М-теорія

Scientific Herald of Uzhhorod University
Series "Physics"

Journal homepage: https://physics.uz.ua/en
Issue 54, 96-104
Received: 01.09.2023. Revised: 23.11.2023. Accepted: 18.12.2023

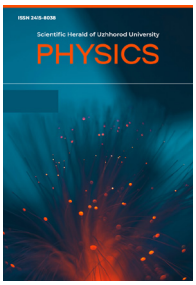

UDC 621.54
PACS 73.40. Lq, 81.05. Hd
DOI: 10.54919/physics/54.2023.96

Effect of phenol-formaldehyde resin on mechanical durability and structure of low-density polyethylene

Shucayat Aman Zeynalov
PhD in Physics, Associate Professor
Azerbaijan Technical University
AZ 1073, 25 H. Javid Ave., Baku, Azerbaijan
https://orcid.org/0000-0002-0040-6057

Farhad Shamil Kerimov
PhD in Physics, Associate Professor
Azerbaijan Technical University
AZ 1073, 25 H. Javid Ave., Baku, Azerbaijan
https://orcid.org/0009-0005-8006-5481

Sevinj Ittifaq Safarova*
PhD in Physics, Associate Professor
Azerbaijan Technical University
AZ 1073, 25 H. Javid Ave., Baku, Azerbaijan
https://orcid.org/0009-0003-5928-1177

Babakishi Garaja Garajaev
PhD in Technical Sciences, Associate Professor
Azerbaijan Technical University
AZ 1073, 25 H. Javid Ave., Baku, Azerbaijan
https://orcid.org/ 0009-0003-5927-1123

Gulshan Salman Jafarova
PhD in Physical and Mathematical Sciences, Associate Professor
Azerbaijan Technical University
AZ 1073, 25 H. Javid Ave., Baku, Azerbaijan
https://orcid.org/0009-0001-6129-877X

Abstract

Relevance. The development of technology for producing new polymer modifications with specific properties, which remain stable even when exposed to external factors, is a key area of focus for researchers in the field of high-molecular compounds.

Purpose. The purpose of this study was to create new composite materials based on low-density polyethylene.

Suggested Citation:
Zeynalov SA, Kerimov FS, Safarova SI, Garajaev BG, Jafarova GS. Effect of phenol-formaldehyde resin on mechanical durability and structure of low-density polyethylene. *Sci Herald Uzhhorod Univ Ser Phys.* 2023;(54):96–104. DOI: 10.54919/physics/54.2023.96

*Corresponding author

Methodology. The extrusion blowing method on an industrial URP 1500 unit was used for processing low-density polyethylene (LDPE) and its modified films. Electron microscopic images of the surface were captured using a S-570 scanning microscope (Japan) at X1000 magnifications.

Results. The composition and quantity of a low-molecular organic additive that alters the electrical characteristics of low-density polyethylene grade 10803-020 was ascertained. The modified low-density polyethylene is noteworthy for its minimal usage of additives and their compatibility with technology. Based on experimental data, it was found that the inclusion of 0.05 wt% phenol-formaldehyde resin in low-density polyethylene increases its mechanical strength to the highest level when compared to both the unaltered low-density polyethylene and low-density polyethylene with other additives. Furthermore, the study found that the addition of phenol-formaldehyde resin in small proportions (0.05 wt%) substantially enhances mechanical strength at varying temperatures.

Conclusions. The electrophysical characteristics of low-density polyethylene and its modified versions were comprehensively investigated. The adequately altered low-density polyethylene exhibits considerably improved mechanical durability. It was indicated that the additives used, at optimal levels, influence the physical framework of low-density polyethylene, highlighting their technological compatibility differences.

Keywords: degree of crystallinity; activation energy; lifetime, supramolecular structure; polymer; lamellas

Introduction

One of the primary obstacles confronting researchers in the field of high-molecular compounds pertains to enhancing the stability of their electrophysical and mechanical attributes. The need to cultivate new polymer adaptations with the desired features and sustained against different extraneous factors triggers the surge in polymeric materials' incorporation across multiple sectors of the national economy, instrument making and electronic industry. This is mainly because using polymers on their own lacks the necessary improvements in their electrophysical characteristics, processing techniques, stability to prolonged exposure to static and dynamic loads, as well as different radiation and climatic factors, including excessive temperatures. E.M. Godzhaev *et al.* [1] and C. Wu *et al.* [2] noted that deterioration in the mechanical properties of polymer materials occurs mainly due to ionization processes developing in air inclusions and pores inside the insulation. According to M.A. Rajab *et al.* [3], a significant breakthrough is occurring due to the new capabilities of nanotechnology, namely the ability to regulate the supramolecular structure of polymer composites.

S. Mohandesnezhad *et al.* [4] found that the most accessible methods for increasing the electrical and mechanical properties of polymers is to modify them with micro and nano additives of organic and inorganic products. The current technology used for producing polymer modifications enables the creation of mechanical and dielectric materials with diverse properties through the combination of polymers and additives. The role of micro and nano additives as crystal-forming agents, which form the fine-crystalline structure of the polymer, has also been rigorously described and studied. Sh. Zeynalov *et al.* [5] has demonstrated that the claim stating that a finely crystalline supramolecular region in polyolefins represents the most advantageous form of polymer structure, associated with a range of valuable physical and mechanical attributes, is widely held.

Extensive research has investigated changes in the mechanical strength of polymers, specifically LDPE (low-density polyethylene), with various additives. However, information regarding the influence of additives on the mechanical and electrical properties of LDPE is significantly limited. Previous studies [6] have observed changes in the mechanical strength of polymers through the introduction of fillers and additives. Thus, the strength of low-density polyethylene is enhanced to a small extent upon the addition of phthalic anhydride and orthophenylinediamine.

F. Li *et al.* [7] considered that adding phenol-formaldehyde resin sizing significantly enhances the mechanical properties of injection-molded short carbon fiber-reinforced polyethersulfone composites. This procedure leads to augmented strength, stiffness, and fracture resistance of the material. Consequently, the resulting polymer composites possess the potential for application in diverse high-tech circumstances where mechanical performance is of utmost importance. Nonetheless, this composition is deficient in mechanical strength. The mechanical strength of this composition is within 16-18 MPa [8]. Although this area has received much attention, film aging during operation is still a significant issue. The purpose of this study was to design new polymer composite materials with considerably enhanced electrical properties, as well as to minimise the rate of film aging during their operation, as well as their dependence on the supramolecular structure.

Materials and Methods

The developed modifications of LDPE were processed into films at industrial plastic processing units on the LDPE 10803-020 (Azerbaijan) grades in two stages. The proposed additives were introduced into the feedstock, granulated LDPE 15803-020 with a molecular weight of M-8.45 104 by mechanical mixing. Phenol-formaldehyde resin (PFR), chemical formula [-C6H3(OH)-CH2]n was used as an additive. The thickness of LDPE films and its compositions is 50-60 μm. Additives were introduced into LDPE by mechanical mixing. Before adding the additive to the LDPE, it was dispersed using a sieve analysis on a grain composition machine. The particle size was less than 50 μm.

The installation for sieve analysis consisted of an exhaust drive and a set of sieves. The set of sieves is selected in such a way that the entire range of grain sizes of the bulk material being tested is covered (5-6 sieves). At the very bottom there is a sieve plate to catch the last sifting. The vibration drive imparts vibration and rocking movement to the sieves installed and secured to it. The duration of sifting for coarse-grained material was 10 minutes, for fine-grained material about 20 minutes.

On a vibration drive, the time and strength of vibration were regulated by a timer. Dependency $\tau = f(\sigma)$ i.e., the time elapsed from the moment the sample was loaded until it broke, was determined using a tensile testing machine (Azerbaijan) that ensured constant mechanical stress throughout the experiment [9; 10] (Fig. 1).

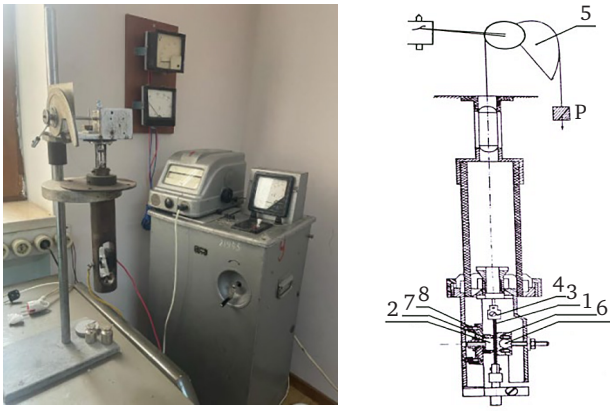

Figure 1. Installation for determining the strength of polymer film dielectrics
Note: 1, 2 – electrodes; 3 – sample; 4 — tips; 5 – lever device; 6 – ball; 7 — security ring; 8 – springs
Source: photographed by the authors of this study

LDPE and its modified variants were processed into films via extrusion blowing using an industrial unit URP-1500-2 (Russia). URP-1500-2 produces film from 30 to 150 μm, sleeve width 1500 mm (without fold), productivity ~70 kg/h, rotation unit on the head. The unit was set technological mode of processing and obtaining a film with a thickness of 20 to 50 ± 4 μm (Table 1).

Table 1. Norms of the technological mode of the unit URP-1500-2 to produce films by blowing (inflating method)

	Parameter name	Unit of measurement	The value of the measured parameter	
			Initial Raw material brand 10803-020	Raw material LDPE + 0.05 wt% PFR
1	2	3	4	5
1.	Temperature by cylinder zones	0°C		
	Zone 1	«»	110	130
	Zone 2	«»	135	150
	Zone 3	«»	140	160
	Zone 4	«»	150	170
2.	Temperature by filter zone	0°C		
	Zone 5	«»	160	170
3.	Temperature by head zones:	0°C		
	Zone 6		150	170
	Zone 7		150	170
	Zone 8		145	165

Table 1. Continued

1	2	3	4	5
4.	Auger rotation speed	rpm	20	20
5.	Load on the main motor	A	28	42
6.	Take-up roll speed	m/min.	13	13
7.	Winding roller speed	m/min.	13,5	13,5
8.	Geometric dimensions of the film:			
	• sleeve width	mm	600	600
	• film thickness	μm	20 ÷ 40 ± 4	20 ÷ 40 ± 4
9.	Performance	kg/h	25	25

Source: [11]

A qualitative assessment of the change in the structure of the LDPE film, with the introduction of small additives, was the determination of the morphology of supramolecular formations by the method of scanning electron microscopy and X-ray diffraction. Electron microscopic photographs of the surface were taken on an S-570 scanning microscope (Japan) at x1000 magnification. The samples were glued onto object machines, sprayed with a thin layer of Pt-Pd on a JB-3 installation (Japan). The morphology of supramolecular formations using scanning electron microscopy and X-ray diffraction analysis was carried out at the Azerbaijan State University.

Results and Discussion

Figures 2 and 3 illustrate the time dependences of mechanical strength for pure LDPE (3) and with additives of 0.01, 0.05, 0.7 and 0.1 wt% phenol-formaldehyde resin (4, 1, 2, 3, and 5), respectively, in semi-logarithmic coordinates $lg\tau = f(\sigma)$ and dependence $lg\tau$ on mechanical load σ at different temperatures (163, 133, 103K) for the original LDPE and for its optimum modification LDPE + 0.05 wt% PFR (Fig. 3).

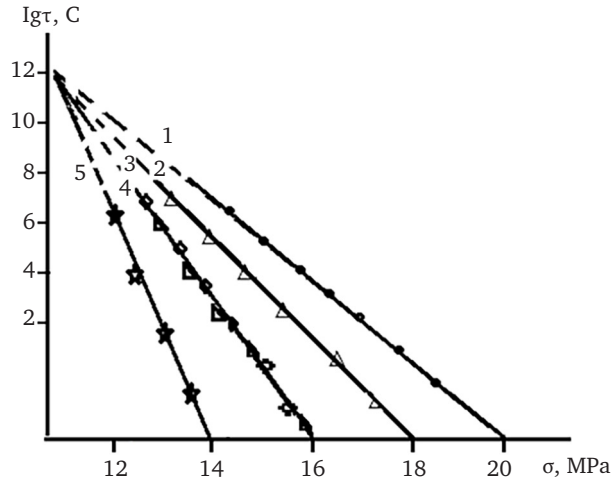

Figure 2. Dependence of the mechanical strength of LDPE (3) and its composition with additives 0.05 wt% (1), 0.07 wt% (2), 0.01 s% (3), 0.1 wt% (PFR)
Source: developed by the authors of this study

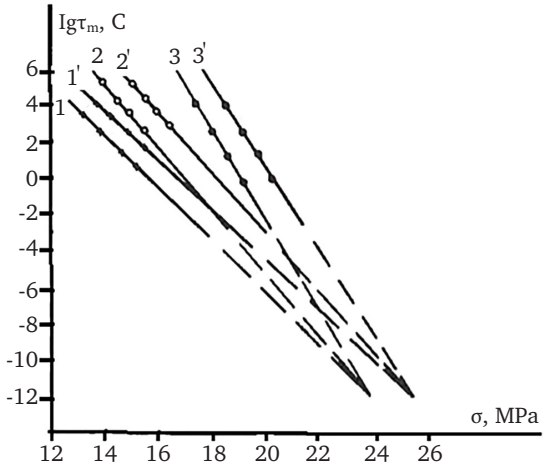

Figure 3. Force dependences of the durability of the LDPE film (1-3) and its optimal modification LDPE + 0.05 wt% PFR (1′-3′) at different temperatures (T, K); 1.1-163; 2.2-133; 3.3-103K
Source: developed by the authors of this study

The functional relationship between durability τ_m, mechanical stress σ and temperature T was obtained for a wide class of materials [12; 13].

$$\tau_\mu = \tau_0 e^{\frac{U_0 - \alpha\sigma}{KT}}, \quad (1)$$

where τ_0, U_0 and α are parameters that determine the strength properties of the material under study.

As the above dependence suggests, the durability of these samples clearly depends on the magnitude of the breaking stress σ; with a decrease in voltage, the durability τ increases greatly, i.e., the well-known equation for durability is fulfilled at $T = const$:

$$\tau = Aexp(-\alpha\sigma), \quad (2)$$

where the parameter A and α are constant coefficients that determine the dependence of durability on stress at a constant temperature at which tests are carried out. The linear dependence $lg\tau$ on σ is also justified at different temperatures (163, 133, 103K) for the original LDPE and for its optimal modification.

As Figures 2 and 3 suggest, the introduction of 0.05 wt% phenol-formaldehyde resin into LDPE leads to a significant increase in the mechanical strength of the polymer composition by more than 20%. The calculated values of the parameters of the LDPE film and its optimum modification are presented in Table 2.

Table 2. Values σ_0, U_0, α for LDPE and its optimal modification

Material	σ_0, C	$U_0 \frac{\text{kcal}}{mole}$	$\alpha, \frac{\text{kcal}}{mole} \mu P\alpha$	σ, $\mu P\alpha$ 163K
LDPE (no additive)	10^{-12}	21	0,073	16,2
LDPE + 0.05 wt.% phenol-formaldehyde resin	10^{-12}	21	0,061	20

Source: developed by the authors of this study

From the data of the tables obtained as a result of testing the LDPE film and its optimal modification at a constant temperature (133K) and a constant rupture time ($\tau = 1c$), it can be seen that the coefficients U_0 and τ_0 are constant for samples from the LDPE film and its optimal modification. The proposed additive leads to a decrease in the α coefficient and a significant increase in mechanical strength (from 16.2 for the original LDPE to 20 MPa for the modified one). The constancy of the values and activation energy U_0 of the original LDPE and its improved modification is mainly due to the same chemical bonds U_0 [14; 15]. The mechanical strength of the LDPE film noticeably increases when 0.05 wt% PFR is included in its composition. This can be attributed to the supramolecular fine spherulite structure that forms within the LDPE. The investigation into LDPE with the use of scanning electron microscopy allowed for a greater comprehension of the supramolecular arrangement of the examined specimens. Figures 4 and 5 display micrographs of the primary PE (polyethylene) and PE with the inclusion of phenol-formaldehyde resin.

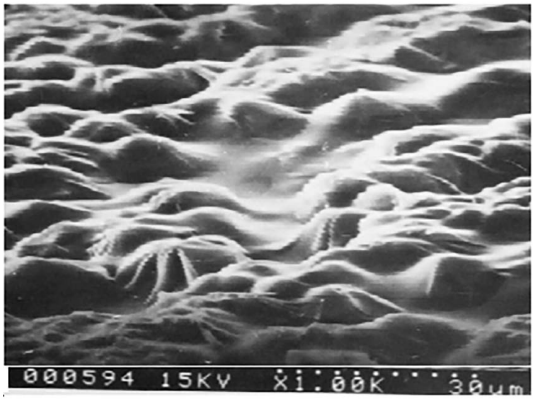

Figure 4. Micrographs of LDPE film
Source: developed by the authors of this study

Figure 5. Micrographs of LDPE film with the content of the modifying additive (PFR) 0.05 wt%
Source: developed by the authors of this study

Observations reveal that the introduction of additives into LDPE at a concentration of 0.05 wt% PFR leads to the growth of larger structural formations, resulting in an enhanced continuity or packing organization. The resulting structural elements are in the nature of lamellas intertwined within a certain polymer microvolume and at the same time passing in the form of an intrusion into neighbouring structural elements similar in structure. H. Hamadache *et al.* [16] noted that to acquire a three-dimensional image of the surface, a scanning electron microscope is utilised by employing electrons that are either scattered or emitted by the sample's surface. In this case, the sample is fixed, dried, and coated with a thin film of heavy metal, and then scanned with a narrow beam of electrons. R. Hsissou *et al.* [17] discussed the different types of polymer composites, including polymer-matrix composites (PMCs), metal-matrix composites (MMCs), and ceramic-matrix composites (CMCs). Each type had unique properties and applications. It explored the various reinforcement materials used in polymer composites, such as carbon fibres, glass fibres, and nanoparticles. Additionally, the choice of polymer matrix, such as epoxy, polyester, or thermoplastics, was discussed in detail. This review covered common manufacturing processes for polymer composites, including methods like hand layup, filament winding, and resin transfer moulding (RTM). Each process is explained, along with its advantages and limitations. V. Biziks *et al.* [18] focused on evaluating the changes in the mechanical properties of LDPE when it is combined with phenol-formaldehyde resin. Mechanical

properties include attributes like tensile strength, impact resistance, and elasticity. The study aimed to determine whether the addition of phenol-formaldehyde (PF) resin enhances or alters these properties. To mechanical testing, the study conducted a structural analysis of LDPE after the introduction of phenol-formaldehyde resin. This analysis involved techniques such as microscopy or spectroscopy to examine changes in the molecular and crystalline structure of the material. Understanding how PF resin affected LDPE's mechanical properties and structure is relevant to industries that utilize LDPE in composite materials.

In the unaltered polyethylene, the nature of structure concentrators is similar to those of the modified samples, but with the difference that they often represent separate, unconnected islands. Based on microphotography data and a comparative analysis, we can assert that PFR microadditives can accelerate the process of structure formation on the supramolecular surface. These microadditives penetrate mainly into the amorphous phase of the polymer, creating centres for structure formation. The elements of these centres then intertwine with polymer crystallites, forming a single, ordered structure with a high degree of packing. It is evident that PFR microadditives have a significant impact on structure formation. The polymer's structure does not take the form of spherulitic formations, as many researchers believe. Instead, it has a lamellar structure. The added additive accelerates the polymer's crystallization and creates larger structural elements composed of lamellas bound in various directions, irrespective of the film's orientation. E.U. Van Velzen *et al.* [19] researched that Recycled polyethylene (PE) is widely used in various applications, including packaging, construction, and automotive industries. During recycling processes, impurities such as contaminants, additives, or residues from previous use may be introduced into the recycled material. The mechanical properties of PE, including tensile strength, elongation, impact resistance, and stiffness, are critical for determining its suitability for specific applications. Understanding how impurities influence these properties is essential for ensuring the quality and performance of recycled PE products. Impurities in recycled PE can be diverse and include foreign particles, residues of other polymers, pigments, additives, and degradation products. Each type of impurity may have a different effect on the mechanical properties of the material. Y. Hiejima *et al.* [20] and N. Darie-Niţă *et al.* [21] noted that LDPE is a widely used polymer in various applications, including packaging materials. However, when exposed to environmental factors such as UV radiation, LDPE can undergo photodegradation, leading to changes in its chemical and structural properties. The study delves into the subtle structural modifications that occur at a microscopic level within LDPE when subjected to photodegradation. These changes may not be visible to the naked eye but can significantly affect the material's properties [22].

An improved organisation of the polymer surface should lead to an increase in the degree of crystallinity. Nevertheless, according to the experiment, the degree of crystallinity barely changes. This is also supported by the X-ray diffraction experimental results outlined in Table 3.

Table 3. Size and degree of crystallinity of LDPE and its optimum modifications

Material	Crystal size	Degree of crystallinity %
LDPE 10803-020 (original)	126	41
LDPE 10803-020 + 0.05 wt% PFR	130	40

Source: developed by the authors of this study

The obtained data enable a scientific approach to explaining experimental results, establishing the correlation between polymer product structure and properties, and conducting a focused search for the optimal alloying additives that can enhance the physical, mechanical, and technological characteristics of the polymer [23]. Consequently, through comprehensive analysis of modified low-density polyethylene samples with the inclusion of phenol-formaldehyde resin, we found the connection between the supramolecular structure type and the physicochemical, strength, and technological attributes of polymer products. This study investigated the temperature-time dependence of the mechanical strength of LDPE (low-density polyethylene) polymer films and its modifications under the simultaneous action of a mechanical load on them. The mechanical load value was selected to prevent any stretching or rupture of the test specimens caused by orientation.

Conclusions

Polymer composite materials based on low-density polyethylene grade 10803-020 containing a significantly small amount of the organic additive phenol-formaldehyde resin were obtained. It was revealed that compositions with additives of 0.05 wt% phenol-formaldehyde resin significantly improve the physical, mechanical, and technological properties of the polymer, and the mechanical strength of the material increases significantly. In addition, it was found that phenol-formaldehyde resin in a small amount (0.05 wt%) significantly increases mechanical strength at various temperatures.

The study showed that a change in the properties of LDPE when modified by the addition of phenol-formaldehyde resin (0.05 wt%) is reflected in changes in the structure-sensitive coefficient α alone (and an increase in strength properties corresponds to a decrease in α, and their decrease-increase in α). When adding phenol-formaldehyde resin additives to LDPE, a decrease in local stresses occurs (a decrease in the coefficient α), then according to the proposed mechanism, the probability of perturbation of chemical bonds decreases, as a result of which the mechanical strength increases.

The microstructures of low-density polyethylene, which were modified with phenol-formaldehyde resin, underwent analysis through the use of electron scanning microscopy and x-ray diffraction techniques. Based on microphotography data and a comparative analysis of the structure, we can confidently state that microadditives of phenol-formaldehyde resin can accelerate structure formation on a low-molecular-weight surface. By primarily introducing these additives into the amorphous phase of the polymer, they create formation centres. The resulting elements interweave with the polymer's crystallites, culminating in a solitary ordered structure with a superior degree of packaging. The polymer's structure deviates from spherulitic formations, once believed by most researchers, and instead exhibits a lamellar structure. The added additive's capacity to hasten polymer crystallization generates larger structural components consisting of lamellae that are interwoven in different directions, irrespective of the film's orientation.

Thus, as a result of comprehensive studies of samples of modified low-density polyethylene phenol-formaldehyde resin in the optimal amount (0.05 wt%) according to the physicochemical, strength and technological characteristics of film samples, we have established the relationship between the type of supramolecular structure and the properties of polymer products. The ability of the organic additive phenol-formaldehyde resin to act as a structure former has been shown. It has been established that the specified organic additive is an effective lamellar structure former. It has been shown that this type of structure contributes to the production of a new polymer composition with specified physical, mechanical, electrophysical and technological properties.

To determine the most suitable conditions for processing and operating polymers, one must have a comprehensive understanding of their behaviour in the crystalline glassy and viscous-flow states, as well as the corresponding transition patterns between these states. In this respect, it is intriguing to assess the impact of precise minor additives on the speed and procedure of polyethylene crystallization. The study examined dielectric properties, such as specific volumetric electrical resistance, dielectric losses, and the dielectric constant of the polymer composition under review.

Further investigation into the physical and chemical properties of these materials could involve examining their interactions and the impact these interactions have on the mechanical strength of LDPE.

Acknowledgements
None.

Conflict of Interest
The authors of this study declare no conflict of interest.

References
[4] Gojaev EM, Alesgerova DM. Mechanical strength of polymer composites LDPE + X Vol% $BiSb_3Te_6$ and Nanocomposites LDPE + X Vol% $BiSb_3Te_6$ + Y Vol% Fe. *J Multidiscip Eng Sci Technol.* 2019;6(3):9612–4.
[2] Wu C, Xu F, Wang H, Liu H, Yan F, Ma C. Manufacturing technologies of polymer composites – a review. *Polym*. 2023;15(3):712. DOI: 10.3390/polym15030712.
[3] Rajab MA, Kader EI, Hammod AA, Hameed AHI. Mechanical properties (Tensile, Hardness and Shock resistance) for the phenol formaldehyde resin with Epoxy resin. *Diyala Diyala J Eng Sci*. 2019;12(2):35-43. DOI: 10.26367/DJES/VOL.12/NO.2/3.
[4] Mohandesnezhad S, Etminanfar M, Mahdavi S, Safavi MS. Enhanced bioactivity of 316L stainless steel with deposition of polypyrrole/hydroxyapatite layered hybrid coating: Orthopedic applications. *Surf Interfaces*. 2022;28:101604. DOI: 10.1016/j.surfin.2021.101604.
[5] Zeynalov Sh, Garacayev B, Khalilov S, Kerimov F, Alekperov A. Study of the mechanical durability of a high-pressure polyethylene film and its composition at various temperatures. *Norwegian J Dev Int Sci*. 2022;(86):53–6. DOI: 10.5281/zenodo.6654091.
[6] Guliyev MA, Sadigova AR, Hadiyeva AA, Asilbeyli PB, Hadiyli AA, Mamedov NC, Safiyeva ES. Changes occurring in structure of polyethylene + nanoclay nanocomposites after influence of an electric field. *Int J Tech Phys Probl Eng*. 2023;13(4):40–4.
[7] Li F, Hua Y, Qu C-B, Ji J-H, Li Y-Q, Hu N, et al. Effectively enhanced mechanical properties of injection molded short carbon fiber reinforced polyethersulfone composites by phenol-formaldehyde resin sizing. *Compos Part B Eng*. 2018;139:216–26. DOI: 10.1016/J.Compositesb.2017.11.033.

[8] Kumar V, Gulati K, Lal S, Arora S. Effect of gamma irradiation on tensile and thermal properties of poplar wood flour-linear low density polyethylene composites. *Radiat Phys Chem*. 2020;174:108922. DOI: 10.1016/j.radphyschem.2020.108922.
[9] Godzhaev E, Zeynalov Sh, Kerimov F, Suleimanova A. Temperature-time dependence of the electrical strength of a polyethylene film and its composition at different temperatures. *Dan Sci J*. 2022;(60):61–4. DOI: 10.5281/zenodo.6606629.
[10] Kim S-Y, Choi E-J, Lee S-J, Kim HB, Oh S-H, Jeong YG. Roles of modified polyethylene addition and electron beam treatment on the interfacial, thermal, mechanical, and electrical properties of polyethylene/short carbon fiber composites. *Compos Part A: Appl Sci Manuf*. 2023;165:107350. DOI: 10.1016/j.compositesa.2022.107350.
[11] Mashprom Group. [Internet]. N.D. Avaliable from https://www.mashprom-zvd.ru/.
[12] Hajiyeva FV, Ramazanov MA, di Palma L, Bracciale MP. Structure and thermal properties of copper-polypropylene based nanocomposites. *J Thermoplast Compos Mater*. 2023;36(6):2332–49. DOI: 10.1177/08927057221094987.
[13] Arman Alim AA, Baharum A, Mohammad Shirajuddin SS, Anuar FH. Blending of low-density polyethylene and poly(butylene succinate) (LDPE/PBS) with polyethylene-graft-maleic anhydride (PE-g-MA) as a compatibilizer on the phase morphology, mechanical and thermal properties. *Polym*. 2023;15(2):261. DOI: 10.3390%2Fpolym15020261.
[14] Slimani F, Hedir A, Moudoud M, Durmuş A, Amir M, Megherbi M. Prediction of long-term physical properties of low-density polyethylene (LDPE) cable insulation materials by artificial neural network modeling approach under environmental constraints. *Turk J Electr Eng Comput Sci*. 2021;29(5):12. DOI: 10.3906/elk-2105-27.
[15] Hedir A, Slimani F, Moudoud M, Bellabas F, Loucif A. Impact of thermal constraint on the low-density polyethylene (LDPE) properties. In: Németh B, eds. Proceedings of the 21st International Symposium on High Voltage Engineering. ISH 2019. Lecture notes in electrical engineering. Cham: Springer; 2020. Vol. 599. DOI: 10.1007/978-3-030-31680-8_92.
[16] Hamadache H, Djidjelli H, Boukerrou A, Kaci M, Jofre-Reche JA, Martín-Martínez JM. Different compatibility approaches to improve the thermal and mechanical properties of EVA/starch composites. *Polym Compos*. 2019;40:3242–53. DOI: 10.1002/pc.25179.
[17] Hsissou R, Seghiri R, Benzekri Z, Hilali M, Rafik M, Elharfi A. Polymer composite materials: A comprehensive review. *Composite Struct*. 2021;262:113640. DOI: 10.1016/j.compstruct.2021.113640.
[18] Biziks V, Bicke S, Militz H. Penetration depth of phenol-formaldehyde (PF) resin into beech wood studied by light microscopy. *Wood Sci Technol*. 2019;53:165–76. DOI: 10.1007/s00226-018-1058-2.
[19] Van Velzen EU, Chu S, Chacon FA, Brouwer MT, Molenveld K. The impact of impurities on the mechanical properties of recycled polyethylene. *Packag Technol Sci*. 2020;34(4):219–28. DOI: 10.1002/pts.2551.
[20] Hiejima Y, Kida T, Takeda K, Igarashi T, Nitta KH. Microscopic structural changes during photodegradation of low-density polyethylene detected by Raman spectroscopy. *Polym Degrad Stab*. 2018;150:67–72. DOI: 10.1016/j.polymdegradstab.2018.02.010.
[21] Darie-Niță N, Vasile C, Stoleru E, Pamfil D, Zaharescu T, Tarțău L, *et al*. Evaluation of the rosemary extract effect on the properties of polylactic acid-based materials. *Mater*. 2018;11:1825. DOI: 10.3390/ma11101825.
[22] Parlag OO, Maslyuk VT, Oleynikov EV, Pylypchynets I, Lengye AI. Structure of mass-yield distributions of ^{232}Th photofission product by bremsstrahlung at energy 17.5 MeV. *Sci Herald Uzhhorod Univ Ser Phys*. 2021;49:54–60.
[23] Bence N, Lengyel A, Tarics Z. A simple model for describing the minimum differential cross-section of elastic proton scattering on protons at high energies. *Sci Herald Uzhhorod Univ Ser Phys*. 2022;51:30–38. DOI: 10.54919/2415-8038.2022.51.30-38.

Вплив фенолформальдегідної смоли на механічну міцність і структуру поліетилену низької щільності

Шукаят Аман Зейналов

Кандидат фізико-математичних наук, доцент
Азербайджанський технічний університет
AZ 1073, проспект Г. Джавіда, 25, м. Баку, Азербайджан
https://orcid.org/0000-0002-0040-6057

Фархад Шаміль Керімов

Кандидат фізико-математичних наук, доцент
Азербайджанський технічний університет
AZ 1073, проспект Г. Джавіда, 25, м. Баку, Азербайджан
https://orcid.org/0009-0005-8006-5481

Севінь Іттіфак Сафарова

Кандидат фізико-математичних наук, доцент
Азербайджанський технічний університет
AZ 1073, проспект Г. Джавіда, 25, м. Баку, Азербайджан
https://orcid.org/0009-0003-5928-1177

Бабакіші Гараджа Гараджаєв

Кандидат технічних наук, доцент
Азербайджанський технічний університет
AZ 1073, просп. Г. Джавіда, 25, м. Баку, Азербайджан
https://orcid.org/ 0009-0003-5927-1123

Гюльшан Салман Джафарова

Кандидат фізико-математичних наук, доцент
Азербайджанський технічний університет
AZ 1073, просп. Г. Джавіда, 25, м. Баку, Азербайджан
https://orcid.org/0009-0001-6129-877X

Анотація

Актуальність. Одним з основних актуальних завдань, що стоять перед дослідниками, які працюють у галузі високомолекулярних сполук, є розробка технології одержання нових модифікацій полімерів із заданим комплексом властивостей та відносно стабільних по відношенню до впливу зовнішніх чинників.

Мета. Метою науково-дослідної роботи було створення нових композиційних матеріалів на основі поліетилену низької густини.

Методологія. Переробку поліетилену низької щільності та його розроблену модифікацію в плівки здійснювали методом екструзійного роздування на промисловій установці марки URP 1500. Електронно-мікроскопічні фотографії поверхні виконували на скануючому мікроскопі S-570 (Японія) при збільшенні X1000.

Результати. Визначено склад та кількість низькомолекулярної органічної добавки, що модифікує електричні властивості поліетилену низької густини марки 10803-020. Розроблена модифікація поліетилену низької густини відрізняється значно меншою кількістю використаних добавок та їх технологічною сумісністю. На основі експериментальних даних визначено, що за вмісту 0,05 мас. % фенолформальдегідної смоли в поліетилені низької густини його механічна міцність досягає максимального значення порівняно як з вихідним поліетиленом низької густини, так і з поліетилену низької густини з іншим вмістом добавок. Встановлено, що фенолформальдегідна смола в невеликій кількості (0,05 мас. %) суттєво підвищує механічну міцність за різних температур.

Висновки. Проведено систематичне дослідження електрофізичних властивостей ПНГ та його розроблених модифікацій. Оптимально модифікований поліетилен низької густини має суттєво підвищену механічну міцність. Показано, що використані добавки в оптимальному вмісті впливають на фізичну структуру поліетилену низької густини, тобто відрізняються технологічною сумісністю.

Ключові слова: іступінь кристалічності; енергія активації; час життя; надмолекулярна структура; полімер; ламелі

НАУКОВИЙ ВІСНИК
УЖГОРОДСЬКОГО УНІВЕРСИТЕТУ
СЕРІЯ «ФІЗИКА»

Науковий журнал

Випуск 54. 2023

Заснований у 1997 р. Виходить двічі на рік

Оригінал-макет видання виготовлено
у редакційно-видавничому відділі Ужгородського національного університету

Відповідальний редактор:
Г. Івченко

Редагування англомовних текстів:
С. Воровський, К. Касьянов

Комп'ютерна верстка:
О. Глінченко

Підписано до друку 18.12.2023 р. Формат 60*84/8
Умовн. друк. арк. 12,4
Наклад 300 примірників

Адреса видавництва:
ДВНЗ «Ужгородський національний університет»
88000, вул. Університетська, 54, м. Ужгород
Закарпатська область, Україна
тел/факс: (03122) 3-20-24
E-mail: info@physics.uz.ua
www: https://physics.uz.ua/uk

SCIENTIFIC HERALD
OF UZHHOROD UNIVERSITY
SERIES "PHYSICS"

Scientific Journal

Issue 54. 2023

Founded in 1997. Published two times per year

The original layout of the publication is made
in the publishing department of Uzhhorod National University

Managing editor:
H. Ivchenko

Editing English-language texts:
S. Vorovsky, K. Kasianov

Desktop publishing:
O. Glinchenko

Signed for print 18.12.2023. Format 60*84/8
Conventional printed pages 12.4
Circulation 300 copies

Publishing Address:
Uzhhorod National University
88000, 14 Universytetska Str., Uzhhorod
Transcarpathian region, Ukraine
Tel./fax: (03122) 3-20-24
E-mail: info@physics.uz.ua
www: https://physics.uz.ua/en